LONGITUDINAL SHEAR AND THERMAL RESISTANCE OF NOVEL AND CONVENTIONAL TIES IN CAVITY WALLS

by

Ambar Lennon Baron Bello

A thesis submitted in partial fulfillment of the requirements for the degree of

Master of Science

in

STRUCTURAL ENGINEERING

Department of Civil and Environmental Engineering
University of Alberta

ABSTRACT

Double wythe masonry cavity walls consist of two masonry wythes, an exterior layer typically made of clay-backed or ceramic bricks (veneer) and the inner layer composed of concrete masonry units (CMU), which serves as a structural backup. In typical cavity wall design, the two wythes are assumed to share in resisting out-of-plane loads with the use of ties that resist the axial load. Cavity walls are subjected to vertical slip between the wythes producing longitudinal shear stresses in the ties. Literature shows that ties with the capacity to resist shear allow wythes to work together (i.e., composite action), leading to enhanced flexural stiffness and out-of-plane resistance of the wall (Mullins and O'Connor, 1987; Pacholok et al., 1989; Williams and Hamid, 2005). However, the Canadian standard for the design of masonry CSA A304-14 (2014a) does not have provisions for composite action in cavity walls.

Considering composite action enables the possibility of designing wider cavities between the wythes to accommodate thicker insulation thickness. This is an approach to meet the growing energy efficiency standards outlined in the National Energy Code of Canada for Buildings (NECB, 2022), particularly in cold-weather regions. In such wide cavities, characterizing the strength and stiffness of such ties becomes important. Additionally, the thermal resistance of these wider cavity walls and the thermal bridging effects produced when using steel ties need to be investigated.

A tie that consists of a truss geometry was developed to achieve larger shear strength and flexural stiffness compared with conventional ties. Longitudinal shear tests were conducted using 37 small-scale cavity walls to determine the shear strength and flexural

stiffness of three tie configurations: horizontally placed conventional (HC), vertically placed conventional (VC), and a novel tie (NC). The variables considered were the veneer brick type (clay and concrete) and the embedment length of the round bent bars attached to the ties and embedded within the veneer wythe (45, 60, and 75 mm). Results showed that the novel ties demonstrated larger flexural stiffness and peak load than conventional plate ties due a better material utilization (truss action). On average, the peak load for the HC, VC, and NC ties was 0.64, 1.74, and 4.32 kN and the flexural stiffness was 0.34, 0.47, and 0.71 kN/mm, respectively. Earlier crack propagation was observed in samples with clay bricks, while specimens with concrete bricks reached a larger peak load. Specimens with an embedment length of 75 mm reached the largest peak load. The larger strength of the novel tie enables it to be used with wider spacing in full walls. Since the novel tie is stiffer than other connectors, expansion joints should be provided to mitigate the effect of shrinkage in the inner and outer wythe.

A Finite Element (FE) model was developed in the 3D FE software ANSYS to determine the thermal resistance (R-value) of wider cavity wall assemblies using both conventional and novel ties. The variables considered were the tie configuration (no tie, conventional tie, and novel tie), insulation thickness (100, 125, and 150 mm), and tie material (steel, stainless steel, and GFRP). Results showed that increasing the insulation thickness resulted in a larger R-value. The assemblies with novel and conventional ties reached similar R-values, this is explained as both ties have the same height and cross-sectional area and similar volume. The GFRP exhibited the largest R-value among the materials compared, this is due to the low thermal conductivity of the material.

PREFACE

A large element of Chapter 4 was published as A. Baron Bello, B. Egbon, C. Cruz-Noguez, and D. Tomlinson, "Longitudinal Shear Resistance of Steel Plate Connectors in Masonry Cavity Walls," in proceedings of the 14th North American Masonry Conference in Omaha, Nebraska, USA, 2023. B. Egbon and I were responsible for the manuscript composition and the experiments performed. C. Cruz-Noguez and D. Tomlinson were the supervisor authors and were involved in the concept formation and manuscript composition.

Some of the work conducted for this thesis forms part of a research collaboration led by Professor Carlos Cruz-Noguez and Professor Douglas Tomlinson at the University of Alberta. The experimental tests referred to in Chapter 4 were performed with Benedict Egbon. The literature review in Chapter 2, the design background review in Chapter 3 and the computer simulations performed in Chapter 5 are my original work.

DEDICATION

Para mi amada familia, a mis padres Enrique y Martha, mis tíos, primos, abuelos y amigos.

Gracias por el apoyo incondicional que me han brindado, gracias a ustedes he llegado hasta este momento.

The greatest glory in living lies not in never falling, but in rising every time we fall.

-Nelson Mandela

ACKNOWLEDGEMENTS

I would like the thank my supervisors, Dr. Lobo and Dr. Tomlinson, whose support and continuous guidance were very important in this research project.

A special thanks to the University of Alberta lab technicians Greg Miller and Cameron West, whose help in the Structural Lab was invaluable throughout the project. We extend our gratitude to Innotech for generously providing the laboratory space to conduct the experimental work.

Some of the research conducted for this thesis is part of a research collaboration with Benedict Egbon. The novel connector discussed in this thesis was designed by Danny Romero, who also designed the technical apparatus referred to in Chapter 3 and then was modified by Mr. Egbon and the author. The experimental testing in Chapter 3 was conducted by Mr. Egbon and the author at the University of Alberta. The literature review presented in Chapter 2, the design implication discussed in Chapter 3, the data analysis outlined in Chapter 4, and the thermal analysis exhibited in Chapter 5 are all the original work of the author.

I was responsible for composing this manuscript. Dr. Carlos Cruz Noguez and Dr. Douglas Tomlinson contributed to manuscript revisions and conceptual framework. The study was funded by NSERC through the Alliance grant program, within the "Robotic Wall Construction Using Innovative Building Blocks and Processes for Enhanced Productivity, Safety, and Sustainability" project.

TABLE OF CONTENTS

LIST OF TABLES

LIST OF FIGURES

1 INTRODUCTION

1.1 Background

Masonry cavity walls are an efficient way to create durable and thermally efficient building envelopes. Masonry cavity walls usually comprise an exterior wythe known as a veneer and an interior wythe that serves as a structural backup. The veneer is usually made of clay or concrete brick, while the backup is built with concrete masonry units (CMUs). The veneer's primary function is to serve as an architectural façade and provide protection against water penetration.

The veneer is generally carried by the CMU using shelf angles, and out-of-plane loads applied to it are transferred to the backup wythe through steel connectors (Papanikolas, 1990). The cavity between the two layers is used for hygro-thermal and sound control, accommodating thermal insulation, moisture barriers, and a drainage path for the water that penetrates the veneer (Rocky Mountain Masonry Institute, 2019; Brzev, 2018). The cavity width is typically between 25 to 114 mm wide (NCMA, 2020). However, modern building codes (NEBC, 2020) have increasingly stringent energy requirements that necessitate larger thermal resistances in building envelopes. This is to reduce the energy use of space heating of buildings and increase energy efficiency. Additionally, historical evidence shows that the thickness of the insulation has increased as energy codes get more stringent (Bennett et al., 2017).

In the context of this work, connectors include all components used to join multi-wythe masonry walls including anchors, fasteners, and ties. The term "tie" is specifically used to describe elements linking the masonry veneer to the block backup. Various types of ties exist. Traditionally they were designed to transfer only axial load (tension and compression) though others, known as shear ties, can handle both axial and shear loads. Ties in a masonry cavity wall are typically made of galvanized or stainless steel to prevent corrosion (Drysdale and Banting, 2020).

Typically, the CMU backup wall independently withstands all the gravity loads, including the weight of the veneer through shelf angles. Both wythes resist together the out-of-plane loads. Those traditional cavity walls use ties that transfer only axial loads, there is no composite action in such cases. However, utilizing shear ties enables the

transfer of shear loads between the wythes, theoretically allowing for some level of composite action. If composite action is achieved, the strength and stiffness of the wall is increased.

Nevertheless, opting for high levels of composite action may not be the optimal choice for every design scenario. As high composite action increases the stiffness of the connection, this can induce cracks in the exterior wythe. This is particularly relevant when both wythes are exposed to distinct types of movements, such as expansion or contraction resulting from temperature or humidity fluctuations, dynamic loads, or differential vertical slip between wythes. Consequently, it becomes important to determine the appropriate degree of composite action according to the specific requirements and conditions of each design.

Despite the existence of ties developed to resist shear (Mullins and O'Connor, 1987; Pacholok et al., 1988, Papanikolas et al., 1990), the current Canadian masonry standard (CSA 304-14) does not consider composite action in cavity wall design. This is likely due to the scarcity of test data and the lack of standardized designs. There is still a need to characterize the shear strength of tie systems, designed using rational methods, so that composite action in cavity masonry walls is developed in a similar way that multi-wythe, reinforced-concrete (RC) systems. In RC systems, there is a variety of connections with the capacity to resist shear (Woltman et al., 2013; Arevalo and Tomlinson, 2020; Egbon and Tomlinson, 2021;). These ties allow the concrete wythes to act together to resist the lateral loads, increasing the resistance of the wall system against lateral loads. As a result, thinner wythes can be used, leading to more cost-effective systems.

1.2 Problem Statement

Cavity walls in modern construction have significant durability and structural and thermal benefits (Arslan et al., 2021). There is a need to optimize the quantity of materials used in a cavity wall to retain the competitive edge of masonry systems. Additionally, it is necessary to understand the behaviour of ties in wider cavities due to the increasing energy requirements.

The current masonry design standard (CSA S304-14) does not consider the composite capacity of cavity walls, resulting in an underestimation of the significance of ties in

enhancing the out-of-plane strength and flexural stiffness of the wall. Higher degrees of composite action may result in stronger and stiffer cavity walls, while lower levels may lead to more ductile but weaker wall systems. The degree of composite action depends on the characteristics of the connection system between the wythes, where tie properties such as location, material, angle about the load, thickness, and geometry play a fundamental role.

In Canada, the NECB (NECB, 2022) specifies minimum thermal resistance for different climate zones in the country. Additionally, there is evidence of historical increment in the energy requirements for buildings (Bennett et al., 2017; Luebke et al., 2023). Therefore, the minimum thermal resistance (R-value) for envelope elements is expected to increase. The R-value of a wall envelope is determined by the thermal conductivity of the materials comprising the wall. The insulation layer provides a thermal break that reduces the heat flow from the inside to the outside of the building. The presence of the metal ties piercing the insulation material reduces the efficiency of the insulation due to thermal bridge effects. This is due to the high thermal conductivity of the steel ties.

An approach to address the increasing energy requirements is to design wider cavities between the wythes to accommodate thicker insulation material improving the R-value of the wall. However, the mechanical and thermal behaviour of these larger ties required to connect the wythes in those wider cavities needs to be investigated. Danny and Tomlinson (2022) introduced a novel tie for wider cavity walls (175 mm) that exhibited larger tension and compression strength compared with a conventional steel plate tie. The shear strength and thermal resistance of that novel tie are compared in this study.

1.3 Objectives, Methods, and Scope

The objective of this thesis is to compare the shear resistance of a novel shear tie and a conventional tie in wider cavities (cavity width 175 mm) and their influence on the thermal resistance of such wider cavity walls.

To test this assumption, this project provides experimental evidence on the use of ties with the capacity to resist shear in masonry assemblies that simulate large cavities in double-wythe masonry cavity walls. Two types of ties were compared: a conventional tie

and a novel tie designed as part of this project. Additionally, the thermal resistance (R-value) of wall assemblies with the two connectors was compared through finite element model analysis.

The following tasks have been identified to achieve this objective:

- **Task 1:** Conduct a literature review on cavity walls, connectors, composite action, and thermal modelling on ties in wall systems.
- **Task 2:** Review and organize information on the design procedures for masonry ties in cavity walls.
- **Task 3:** Conduct an experimental investigation on the longitudinal shear strength of both novel and conventional ties within large (175 mm width) cavities.
    - ***Task 3.1:*** Investigate the response of masonry wall test specimens with novel and conventional ties under shear load in wall assemblies designed according to current design provisions commonly used in the Canadian industry,
    - ***Task 3.2:*** Evaluate the experimental results in terms of load-displacement, shear strength and stiffness, and failure modes.
- **Task 4:** Development of finite element models to assess the thermal resistance (R-value) of cavity wall assemblies with both conventional and novel ties.
    - ***Task 4.1:*** Conduct steady-state finite element thermal analysis simulations on cavity wall models to calculate their R-value using both the conventional and novel ties.
    - ***Task 4.2:*** Evaluate the effect of the insulation thickness and tie material on the R-value of the wall assemblies with the two types of ties.

1.4 Scope

The experimental study focused on small-scale (400 × 400 mm) cavity wallets. The ties investigated are composed of two components (a steel plate and a round bent bar inserted in the plate). Both components were embedded into a mortar joint of the veneer wythe. To replicate realistic conditions of the ties in the field, the tests were conducted on wall sub-assemblies where all components (CMU, brick, connectors) interact as they do in practice. Full-scale walls were not part of this project. The ties were subjected to longitudinal shear load causing slip between wythes. This slip is analogous to what

experienced walls under out-of-plane loading. This uniform pressure caused a bowing deformation in the wall, leading to vertical slip between the wythes and generating the shear load on the ties. It is worth noting that tension and compression tests were not conducted on the connectors, those specific tests were performed at the University of Alberta, in the same novel and conventional ties by Romero and Tomlinson (2023).

The testing procedure involved a custom steel frame designed to securely hold specimens during testing. The key considerations in designing the steel frame were its ability to perform the shear test, measure the vertical slip between the wythes and the corresponding load, and enable observation of tie deformation. To measure the vertical slip, the backup wythe was restrained to the frame, while the veneer wythe was allowed to move freely in the vertical direction as the load was applied.

In previous studies on shear tests in ties, Williams and Hamid (2005) encountered challenges when loading the veneer, as it tended to swing in various directions. To address this issue, the authors restrained the lateral movement and rotation of the veneer wythe, allowing only its vertical displacement. Building on this prior experience, the current project used a spacer between the wythes to restrict lateral movements and rotation of the veneer. It is worth noting that in future studies, the effect of boundary conditions in full-scale scenarios should be taken into consideration.

The thermal resistance (R-value) of three wider wall assemblies (no tie, conventional tie, and novel tie) using a cavity width of 175 mm was compared by 3D simulations in the finite element software ANSYS. The three assemblies were compared and the parameters studied were the effect of the type of tie, the insulation thickness (100, 125, 150 mm), and the tie material (steel, stainless steel, and GFRP). The material properties and method were used according to ASHRAE (ASHRAE, 2017).

1.5 Organization of Thesis

The thesis is structured into six chapters:

- **Chapter 1**: Introduces the problem statement and provides a discussion on the objectives, methodology, and scope.

- **Chapter 2**: This chapter consists of a literature review, encompassing previous tests and studies on masonry, masonry ties, and shear connections on different systems like masonry or concrete. *This chapter addresses Task 1.*
- **Chapter 3:** This chapter outlines the background of the design of ties in masonry cavity walls. *This chapter addresses Task 2.*
- **Chapter 4**: This chapter explains the experimental methodology used in the study. This includes details on specimen specifications, materials used, test setup, and loading protocol, as well as the presentation and discussion of the experimental results. *This chapter addresses Task 3.*
- **Chapter 5**: Outlines the development of a FE model to calculate the thermal resistance (R-value) of cavity wall assemblies using both the conventional and novel ties. The influence of the type of tie, insulation thickness, and tie material on the R-value of the wall assembly is investigated. The chapter covers the theoretical framework, methodology, and validation of the model. *This chapter addresses Task 4.*
- **Chapter 6**: of the thesis presents the conclusions derived from the study and recommendations for future research endeavors in the field.

2 LITERATURE REVIEW

2.1 Introduction

Masonry is one of the oldest building materials and is known for its durability and architectural aesthetic as evidenced by many masonry monuments and structures around the world. Until the early 1900s, brick was one of the primary building materials but it was replaced by materials such as structural steel and reinforced concrete (Anand and Rahman, 1989). Due to its durability, strength, and fire resistance, however, masonry construction remains a competitive option for buildings that are to remain in serviceable condition in post-disaster events (e.g., hospitals and fire stations), as discussed by Bennett et al. (2017a).

Ancient masonry buildings relied on the weight of the walls and floors to avoid tensile stresses; achieving lateral stability through gravity-controlled designs led to massive walls that made walls uneconomical in practice (Drysdale and Banting, 2022). This type of construction is called unreinforced masonry (URM) or "plain" masonry and was used in low to mid-rise structures situated in areas with low seismic activity (Drysdale and Banting, 2022). Reinforced masonry emerged primarily for application in earthquake-prone regions like India, Japan, and the United States in the 1930s. Presently, it is extensively utilized in numerous countries worldwide (Drysdale and Banting, 2022). Reinforced masonry consists in incorporating steel reinforcement into the masonry elements to resist tensile and shear stresses, promoting ductile behaviour.

To protect against moisture and offer thermal protection in hot/cold climates, masonry wall systems featuring separate layers were developed (Rocky Mountain Masonry Institute, 2019). A notable example of this type of construction is the cavity wall, used widely in Canada and the U.S. This chapter provides a literature review focusing on the behaviour of cavity walls. It includes an exploration of composite action and the connectors. The chapter also discusses the factors that influence the overall thermal performance of masonry walls, encompassing various methods used for estimating and measuring thermal resistance. Lastly, the review highlights the gaps identified within the existing literature.

2.2 Types of Masonry Walls Used in Current Construction

Exterior walls are part of the building envelope, or building enclosure, which consists of a combination of materials, components, and assemblies that act as a physical barrier between the inside and outside of a building. This environmental barrier must regulate the flow of heat, air, water (both in liquid and vapour), and other elements. Additionally, the building enclosure provides support against various physical loads, such as air pressure, gravity loads, impact, and earthquakes. It should also have an aesthetical interior and exterior finish and facilitate the distribution of utilities throughout the building. When designed appropriately, the building enclosure can enhance a building's serviceability, comfort, durability, and energy efficiency for heating and cooling (Rocky Mountain Masonry Institute, 2019). Modern types of masonry walls can be comprised of a single wythe or multiple wythes, as described in the following section.

2.2.1 Single-Wythe Walls

Single-wythe walls have a thickness equivalent to that of the masonry unit used and can be built using hollow, cored, or solid masonry units. These walls can be reinforced or unreinforced and serve for both loadbearing and non-loadbearing functions. Envelope masonry walls may feature additional functions to solve environmental concerns, such as thermal insulation, and water and moisture penetration protection.

2.2.2 Multi-wythe Walls

Multi-wythe walls are a construction system consisting of multiple layers that make up the masonry wall assembly. This approach was embraced to create thinner walls that work together to efficiently fulfill their structural and thermal functions. Various examples of multi-wythe masonry walls include solid or composite walls, cavity walls, and veneer walls, as described below.

2.2.2.1 Solid and Composite Walls

Two types of multi-wythe masonry walls are the “composite wall” and the "cavity wall”. The solid or composite walls can be single or multi-wythe. Multi-wythe solid walls are comprised of layers connected with masonry headers or steel connectors and the cavity

between the wythes is filled with mortar or grouting. The use of mortar or grouting in the cavity allows the solid wall to develop composite action (CSA, 2014a).

Composite action refers to the capability of a system made up of different elements to withstand external forces as a unified and cohesive unit. The composite action of cavity walls is discussed in Section 2.2. When various wythes are used, they can be linked together by headers, ties, or wire. Wythes separated 10 to 20 mm are filled with mortar or grout in the space between, forming a collar joint. The shear resistance in the plane of the cavity is increased by the use of headers, joint reinforcement, or ties (Drysdale and Banting, 2022).

2.2.2.2 Cavity Walls

Contemporary walls are more complex and require additional features for thermal and sound control, and to prevent rain penetration (Rocky Mountain Masonry Institute, 2019; Brzev, 2018). To address those issues, an air space or cavity was incorporated into classic masonry walls. The cavity wall is defined as a multi-wythe wall made of masonry units with a gap between the wythes (CSA, 2014a) The wythes are connected using steel ties or bonding units allowing them to work together in resisting lateral loads. For design purposes, the masonry standard doesn't account for composite action in the cavity walls. Nevertheless, it should be acknowledged that cavity walls connected with ties with the capacity to resist shear can display some degree of composite action (Drysdale and Banting, 2022; Wang et al., 1997; Page et al., 2009). Composite action in cavity walls is discussed in Section 2.2.

Figure 2-1 illustrates the components of a cavity wall system. Typical cavity walls are comprised of an interior wythe and an exterior brick veneer. The interior wythe is typically built from concrete masonry units (CMU) and serves as the structural backup of the wall. It can either be loadbearing or nonloadbearing and can be longitudinally reinforced or unreinforced. The exterior wythe known as a masonry veneer is usually made of clay or concrete brick and is a key component in modern rainscreen walls (Svetlana, 2018). The veneer's primary function is to serve as the architectural façade and provide protection against water and moisture (Papanikolas, 1990). Both wythes are connected using steel ties. The veneer is not typically considered a structural element,

and all loads applied to it are assumed to be transferred to the backup wall through the connectors (Papanikolas, 1990).

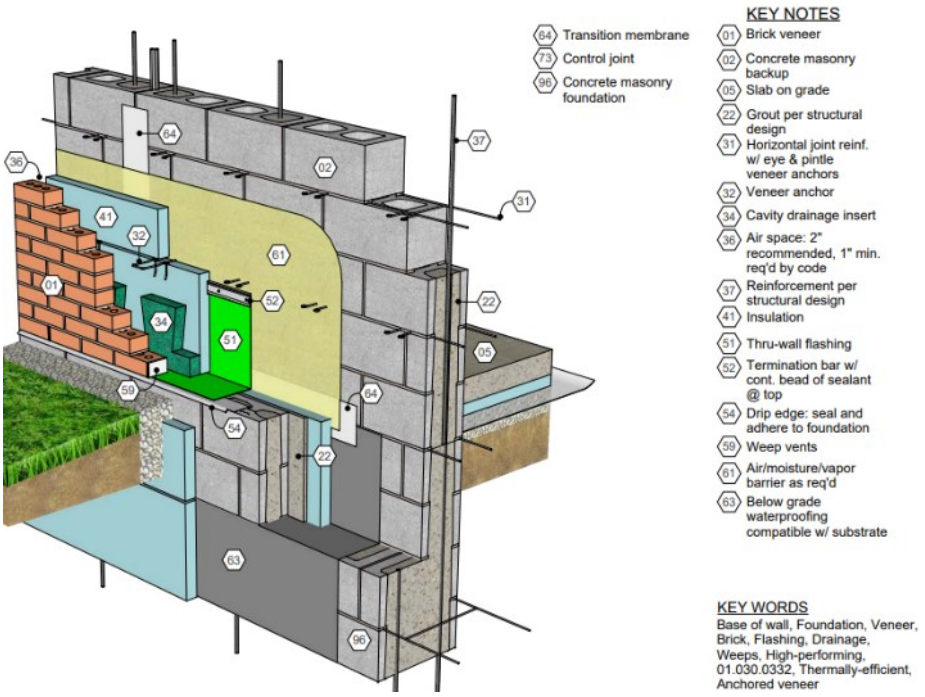

Figure 2-1. Example of a cavity wall with steel stud backup and brick veneer. (International Masonry Institute, 2019).

The connectors or ties in a cavity wall are typically made of galvanized or stainless-steel ties to prevent corrosion (Drysdale and Banting, 2020). The types of connectors are discussed in Section 2.1.2. Additionally, the cavity between the wythes is used to accommodate an insulation layer to improve the thermal behaviour of the wall, and an air/moisture/vapour barrier to prevent water penetration (Drysdale and Banting, 2022). The typical insulation layer thickness ranges between 25 to 100 mm. However, there has been a trend in previous years towards allowing the construction of wider cavities to accommodate thicker insulation material. This is to address the increasing energy requirements in buildings (Bennett et al., 2017; Luebke et al., 2023).

The vapour barrier prevents water from penetrating the CMU, so it is collected within the cavity and directed downward, ultimately being drained through the weep vents located at the bottom of the brick veneer. This drainage system offers protection to the structural elements. Moisture can have adverse effects on structural and insulation

components and it is important to have water vapour and liquid water barriers along with drainage systems in place to safeguard these components (Rocky Mountain Masonry Institute, 2019).

Concrete masonry cavity walls are a solution for building enclosures, given their favourable initial and life-cycle costs (NCMA, 2020). Additionally, this wall system has been used due to its aesthetic properties, superior ability to resist moisture, fire resistance, sound transmission, and excellent thermal resistance (Papanikolas 1990). Anchored veneer systems with CMU backup can provide higher fire resistance than other backup materials such as steel studs and wood framed (Rocky Mountain Masonry Institute, 2019).

2.2.2.3 Veneers

The masonry veneer refers to the brick façade and is typically constructed with an interior backup wythe made of wood, concrete, steel studs, or CMU. This system was introduced in the 1780s in Britain and consists of a non-loadbearing masonry wythe attached to a structural backup wythe (Drysdale and Banting, 2020). Its main purpose is to provide an attractive and durable exterior finish, but it is not designed to withstand axial or lateral loads. The backup wall can be constructed using masonry, concrete, framed wood, or metal studs. When lateral loads, such as wind or earthquakes, are applied, the wall ties transfer these loads from the veneer to the backup system. The behaviour of the ties depends on the stiffnesses of the veneer, backup, and ties, as well as the wall support conditions and tie properties and arrangement (Svetlana, 2018).

To ensure satisfactory performance, veneers must be properly connected to the backup through the ties, allowing for the effective transfer of lateral loads. The wall ties, typically made of metal, have the needed axial stiffness and strength in tension and compression to resist these loads but have limited shear capacity. However, they assist in sharing the lateral loads from the veneer to the backup wythe, although full composite action is not achieved (Page et al., 2009). The load sharing and composite action are discussed further in Section 2.2. An interior cavity is formed between the two wythes, which commonly includes air and water vapour barriers, insulation layers, and air space. Masonry veneers

are the most prevalent wall system used in contemporary Canadian masonry construction (Drysdale and Banting, 2020).

2.3 Types of Connectors for Masonry Walls

The term "connector" encompasses all elements used to join the wythes in a masonry wall. Various types of connectors may exist within masonry wall systems with each serving different functions based on the wall system. CSA A370:14 (2014) identifies eight types of connectors, as shown in Table 2-1. Each of those types of connectors can in turn be divided into two categories according to the design requirements: prescriptive or designed according to the standard. The prescriptive connectors have been traditionally used for simple solutions and are not required to comply with the design requirements. However, their use is limited to low-rise commercial and residential construction. In contrast, the second type of connectors consists of those available in the market, and need to adhere to the requirements stated by the CSA A370:14 standard.

Table 2-1. Definition of the types of connectors according to CSA A370-14 (CSA, 2014)

Connector type	CSA A370-14 definition
Anchor	Device used to connect masonry walls at their intersections or to attach them to their supports or other structural members or systems. The term also includes any device that is used to connect stone to its structural backing or to interconnect stone and is engaged directly in the stone or the mortar joint.
Continuous ties	Configuration of continuous welded wire reinforcing for masonry, normally in a ladder or truss pattern, that connects two or more wythes.
Drilled-in fasteners	Fastener that is placed in a drilled hole and depends on mechanical or adhesive action, or friction, to develop its strength.
Fasteners	Device used to mechanically join separate parts of ties or anchors, or affix ties and anchors to structural elements.
Power-driven fasteners	Fastener driven into a holding medium by a device activated by an explosive charge or compressed air. This type of fastener depends on both displacement and friction to develop its strength.
Prescriptive connectors	Connector that satisfies the requirements of Clause 10. Prescriptive connectors are recognized by this Standard as deemed-to-comply solutions to the design requirements in Clauses 4, 6, 7, 8, and 9. Specific restrictions apply to their use.
Repair connectors	Connector used to restore or improve masonry wall systems.
Ties	Device for connecting two or more wythes, or for connecting masonry veneer to its structural backing.

Masonry ties play a crucial role in transferring horizontal tensile or compressive forces, such as those caused by wind and earthquakes, through the cavity of a wall. Ties must be anchored at both ends. The insulation offers resistance to prevent tie buckling to some

extent, but this contribution is difficult to calculate, and it is difficult to guarantee its mechanical properties over time. Therefore, designers assume that the insulation does not provide support to prevent the buckling of the ties.

2.4 Masonry Ties

Masonry ties serve the purpose of connecting the brick veneer to the CMU backup within cavity walls. Their primary role is to transfer out-of-plane loads across the wythes, accomplishing this by working in both tension and compression. When cavity walls are subjected to lateral out-of-plane loads, they undergo a bowing deformation, as depicted in Fig. 2-2. Additionally, fluctuations in temperature and humidity on the interior and exterior surfaces of the wall contribute to this bowing deformation. As a result of this bowing deformation, a vertical displacement occurs between the two wythes. These differential vertical deformations that occur can induce shear stresses in the ties, as the ties restrict these movements (Fig. 2-2b) (Papanikolas 1990). The magnitude and similarity of curvature in the bowing deformation between the wythes are also influenced by the flexural stiffness of the ties.

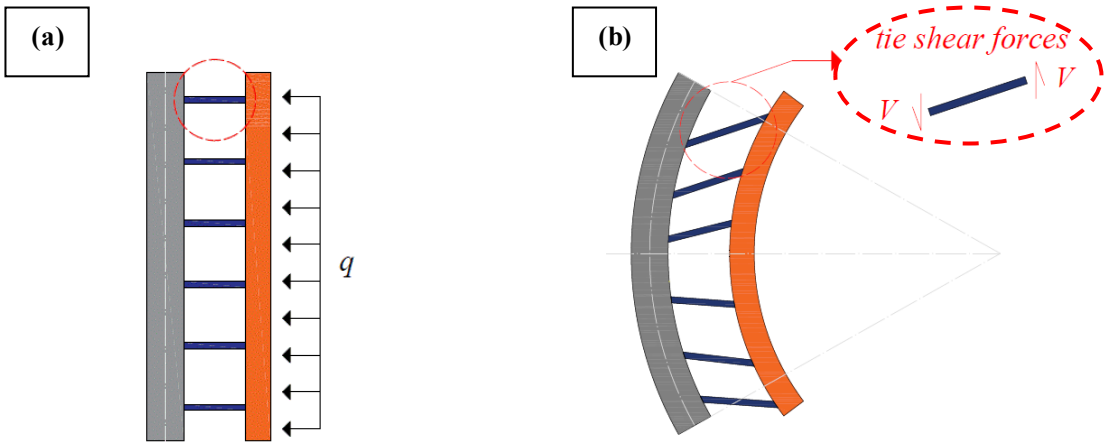

Figure 2-2. Internal stresses of a masonry tie in a cavity wall. (a) wall subjected to wind after deformation. (b) deformed shape due to wind pressure.

Masonry ties can be categorized based on either their design requirements or their ability to accommodate vertical movement between the two wythes. In terms of design specifications, masonry ties fall into two groups: prescriptive ties and those designed in compliance with the CSA standard, as discussed earlier. Regarding their capacity to allow

vertical displacement between the wythes, ties can be further classified into three types: adjustable, flexible, or shear ties. Adjustable ties feature a mechanism that permits the vertical slip between the wythes, preventing shear stresses in the tie. Flexible ties exhibit low flexural stiffness, resulting in low resistance to vertical slip between the wythes and negligible induced stresses in the tie. Conversely, shear ties possess high flexural stiffness, restricting vertical slip between the wythes and generating significant shear stresses within the tie. Examples of the types of ties according to CSA A370-14 (CSA, 2014) are presented in Table 2-2.

Table 2-2. Types of ties according to CSA A370-14 (CSA, 2014)

Tie	Description	Type of tie		
		Type	Shear	Slip
Corrugated strip tie (Fig. 2-3a)	Typically utilized to fasten the masonry veneer to the structural backing. These ties have relatively low compressive strength and are suitable for smaller cavity widths and low-rise walls.	Prescriptive	Negligible	Flexible
Z-wire and rectangular wire ties (Fig. 2-3b)	Commonly used to connect multiple layers in multi-wythe walls.		Negligible	No slip between wythes
Dovetail tie and corrugated dovetail tie (Fig. 2-3c)	Used with concrete or concrete masonry backup and allows for vertical slip between the wythes.		Negligible	Flexible
Prescriptive continuous-welded ties (Fig. 2-4)	They are known for enhancing the lateral strength of cavity walls. However, they restrict horizontal movement caused by moisture or temperature variations, which leads to internal stresses that facilitate the formation of cracks (CSA, 2014).		Shear resistant	Flexible
Adjustable tie (Fig. 2-5ab)	These ties allow for vertical, horizontal, or combined displacements by incorporating components that facilitate relative movement while maintaining the connection between the wythes.	Non-prescriptive	No shear resistant	Adjustable
Adjustable dovetail tie (Fig. 2-5c)	Typically utilized to fasten the masonry veneer to a concrete backing. This system enables vertical adjustment to be achieved.		No shear resistant	Adjustable

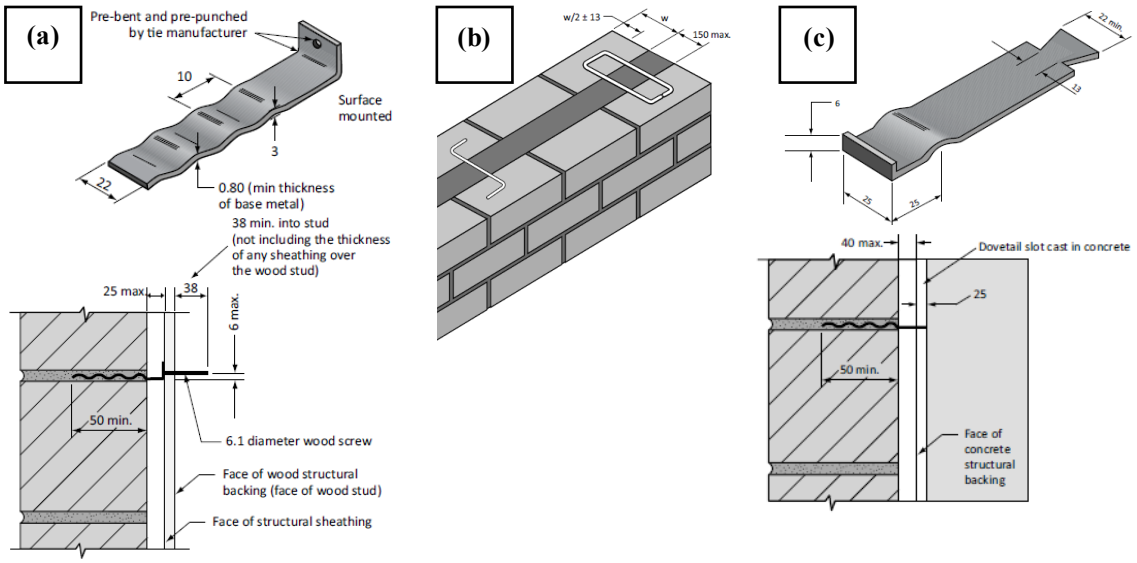

Figure 2-3. Examples of prescriptive ties: (a) corrugated strip ties, (b) z-wire tie and rectangular wire tie, and (c) dovetail tie or prescriptive corrugated dovetail tie. (CSA A370-14, 2014)

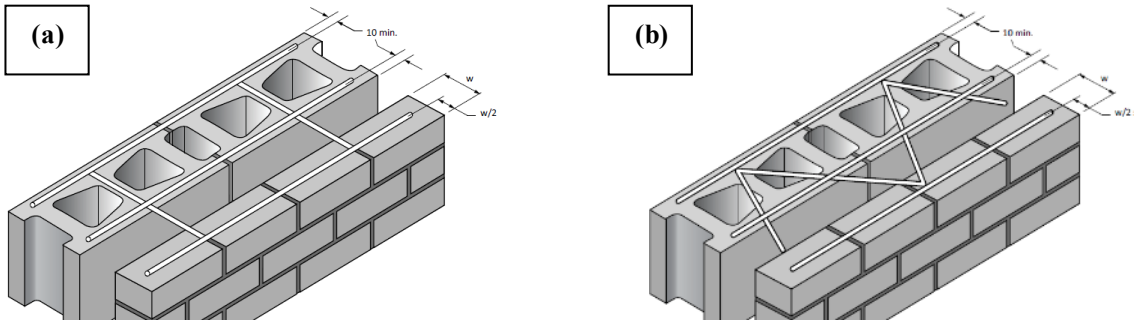

Figure 2-4. Examples of prescriptive continuous ties: (a) continuous ladder tie/reinforcing, and (b) continuous truss tie/reinforcing. (CSA A370-14, 2014)

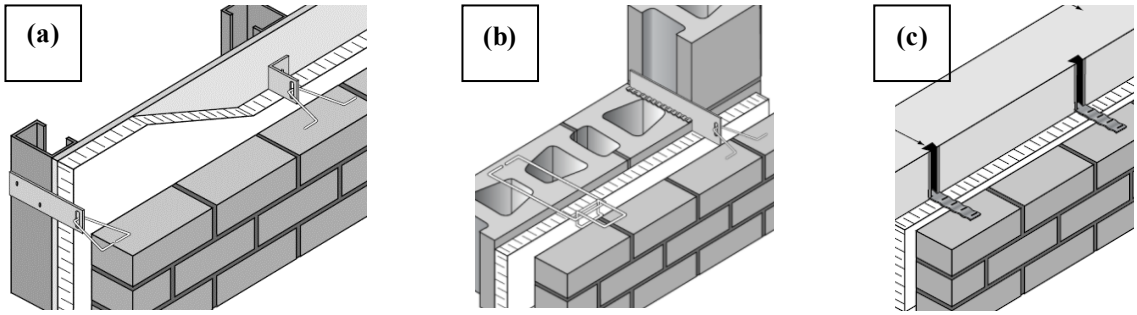

Figure 2-5. Examples of non-prescriptive ties: (a) adjustable tie with steel stud, (b) adjustable tie, (c) adjustable tie, and (d) adjustable dovetail tie. (CSA A370-14, 2014).

2.5 Composite Action

This section explains the load distribution and composite action within a cavity wall. It provides an overview of the loads affecting a cavity wall system, including external loads and environmental effects. The loads produce stresses on the ties, and depending on the characteristics of the ties, the wall will exhibit some degree of composite action.

2.5.1 Loads on a Cavity Wall

Various types of loads act upon cavity walls. These loads consist of external loads and environmental factors. Among the external loads, we find gravity loads such as live and dead loads, as well as lateral loads such as wind and earthquake forces. Lateral loads can be categorized as in-plane (Fig. 2-6c) or out-of-plane (Fig. 2-6b), leading to shear or pressure/suction loads on the surface of the wall, respectively. The out-of-plane loads cause the wall to deform in a bowing shape as shown in Fig. 2-6b. The outer veneer wythe is typically suspended from the CMU using shelf angles (Fig. 2-7).

Environmental factors, such as temperature and humidity fluctuations, produce expansion and contraction in the wythes. Materials within the wall are affected by environmental loads in distinct ways. For example, mortar, grout, and concrete blocks shrink as the material dries after initial hydration, while fired clay bricks expand when they absorb moisture during service. Furthermore, distinct temperatures within each layer also lead to additional differential vertical slips between the wythes. The interior wythe maintains an indoor temperature, whereas the outer temperature fluctuates depending on the exterior temperature and sunlight exposure. Those environmental effects contribute to the bowing deformation of the wall. Although volumetric strains resulting from the previously mentioned environmental effects are typically minor, they can accumulate over a significant distance (Lohonyai et al., 2015). For instance, the coefficients of thermal expansion for clay brick are 0.005-0.006 mm/m/ °C in the horizontal direction and 0.007-0.009 mm/m/ °C in the vertical direction according to CSA S304 (CSA, 2014a).

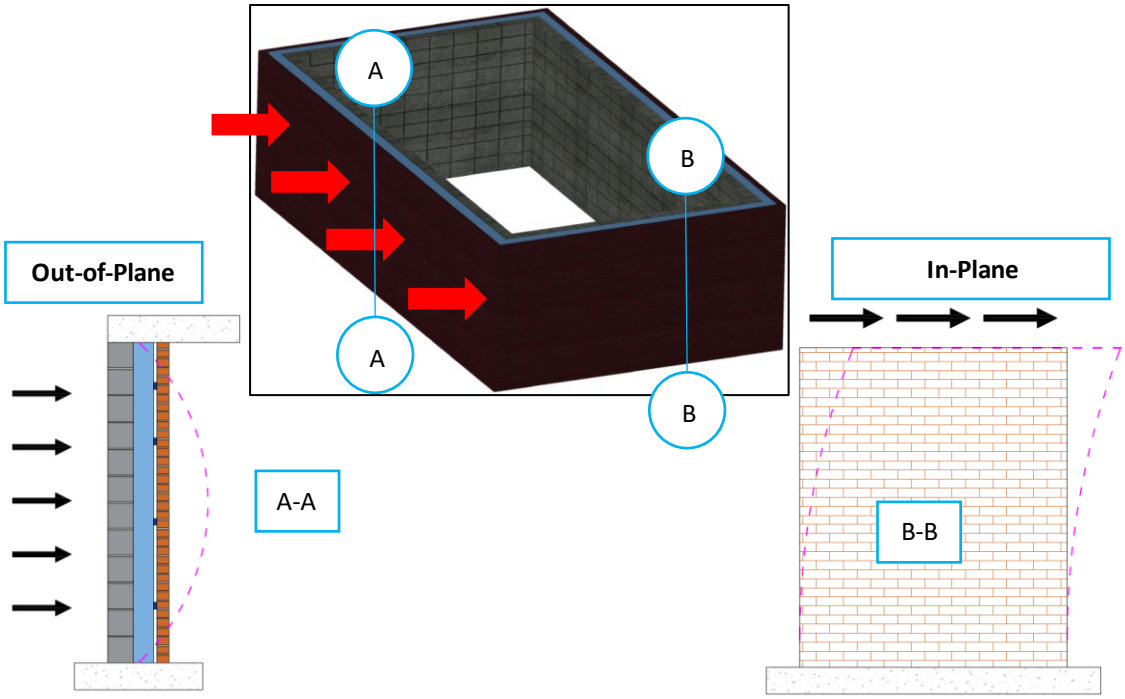

Figure 2-6. External loads on a cavity wall: (a) out-of-plane load and deflected shape, and (b) in-plane load and deflected shape.

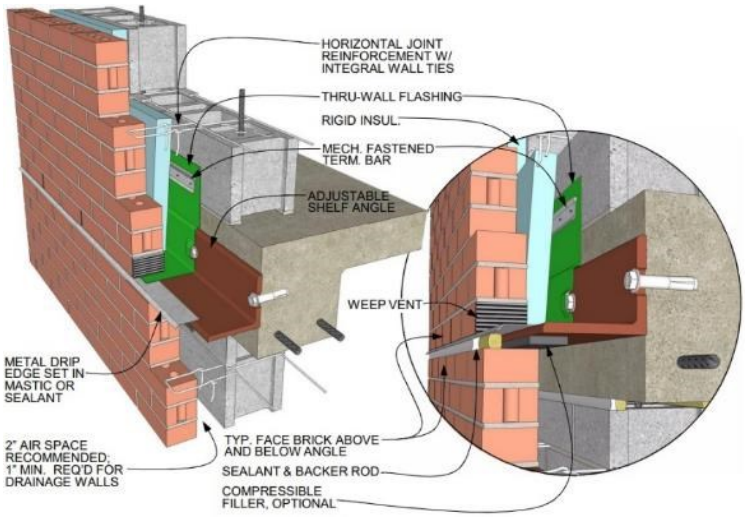

Figure 2-7. Shelf angle detail in cavity wall (International Masonry Institute).

When the wythes are subjected to out-of-plane lateral loads, pressure or suction acting on the wall produces tension and compression loads on the ties, respectively. Ties are principally designed to resist axial loads and transmit out-of-plane loads between the wythes. However, ties are also subjected to shear stress. The presence of out-of-plane

lateral loads and environmental factors induce bowing deformation on the wythes (Fig. 2-8b). In addition to bowing deformations, due to the distance between the layers and the curvature of the deformation, the wythes experience a differential vertical displacement (Fig. 2-8b). This differential vertical displacement induces shear stress on the ties. Depending on the shear strength and flexural stiffness of the ties, ties can allow or restrict that differential vertical displacement (Sakr and Neis, 2001; Wang et al., 1997). The degree of composite action in the wall system is determined by the shear strength and flexural stiffness of the connection between the ties (Papanikolas et al., 1990; Siveski, 1997; Elwi and Hatzinikolas, 1997).

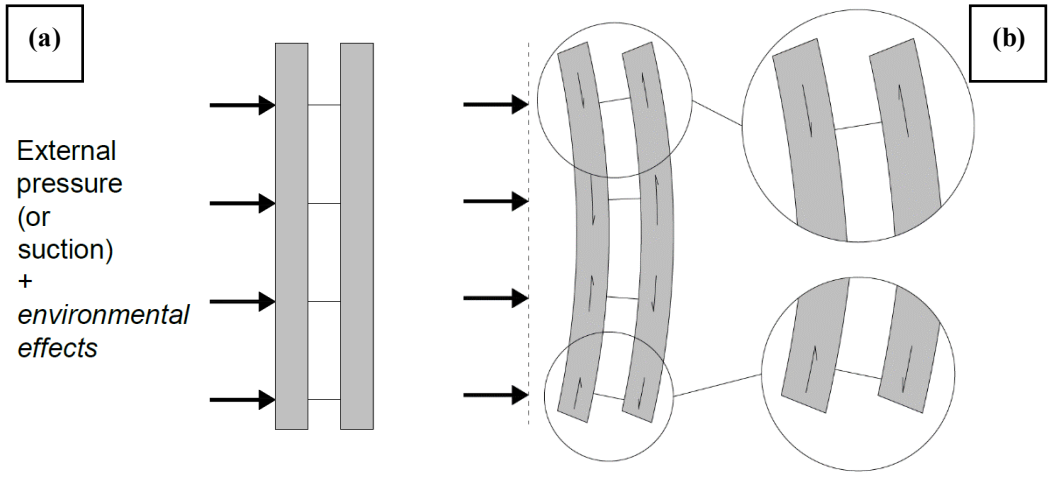

Figure 2-8. Deformation on cavity walls: a) external pressure and environmental effects acting on cavity wall, and b) bowing deformation and vertical slip between wythes.

2.5.2 Composite Cavity Wall

Composite action refers to the capacity of a system composed of multiple layers to collectively withstand external forces as a single member. This effect is achieved using a connection that facilitates the transfer of shear forces between the layers. The extent of composite action can vary and is categorized into different levels, as depicted in Fig. 2-9 for the precast concrete insulated walls (PSWP) system, and also applies to the cavity wall system.

In situations where the layers do not share shear forces (Fig. 2-9b), each layer functions independently under applied load, resulting in non-composite behaviour. In non-composite multi-wythe walls, each wythe works independently when resisting the loads. In this system only tension and compression forces are transferred between wythes, the connection system between the wythes does not allow the transfer of shear loads. An example of this connection is a flexible tie that allows the wythes to move freely vertically and horizontally between them. These characteristics lead to large shear deformation. Non-composite cavity walls have lower flexural stiffness and lateral load-carrying capacity than composite walls.

The connection system plays a vital role in achieving composite action in masonry-to-masonry wythe connection, similar to insulated concrete wall panels. To maintain the desired flexural composite action, it becomes crucial to transfer shear forces through the ties perpendicular to the direction of the load (Naito et al., 2012). In cases where the two layers can fully share the shear load (i.e., there is a linear strain profile through the cross-section) (Fig. 2-9a), it is considered to be fully composite. In fully composite cavity walls, the wythes function as a single member. The ties possess sufficient strength to facilitate the wythes functioning as a single unit. However, to achieve full composite behaviour, ties need to possess greater flexural stiffness, which can lead to increased thermal bridging effects. This ultimately leads to a decrease in the thermal resistance of the wall envelope. This thermal bridge phenomenon is elaborated on in Section 2.4.

Scenarios where some degree of shear transfer occurs (Fig. 2-9c) are classified as partially composite. Figure 2-9d is depicted as an example of the Load-deformation responses of three systems with different composite behaviour. Compared to non-composite walls, composite systems are more structurally efficient, as they can be manufactured using less material while maintaining adequate stiffness and strength (Tomlinson, 2015; Frankl et al., 2011). Partially composite walls feature ties that transfer a portion of the longitudinal shear required for complete composite action. All cavity wall systems with ties will inevitably display some level of partial composite behaviour. Precisely calculating the response of partially composite walls is challenging. Tomlinson (2015) highlighted this complexity in partially composite precast concrete insulated

panels, due to the influence of both flexural deformations within the wythes and shear deformations within the insulation. Additionally, they note an ongoing debate among designers regarding the most effective approach to predict the response of partially composite panels according to the shear strength or the stiffness of the connection.

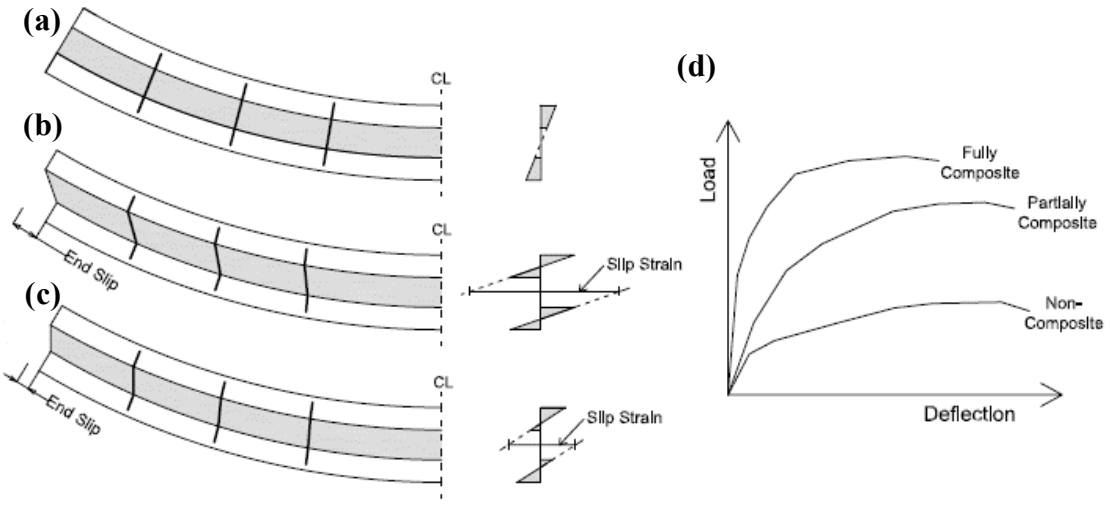

Figure 2-9. Composite action in PSWP system: (a) fully composite, (b) non-composite, (c) partially composite, and (d) respective Load-deflection responses (Tomlinson, 2015).

Since shear transfer through the ties is crucial for achieving composite action, it becomes necessary to understand and predict the behaviour of cavity walls exhibiting composite action. It is also important to establish a relationship between the shear strength of the ties and the composite action of the wall, to quantify the composite action of different cavity wall systems.

Furthermore, it is necessary to establish the level of composite action in the wall assembly based on the specific characteristics and demands of each project. It is not always necessary to incorporate the highest level of composite action in the wall design, as high levels of composite action can result in cracks in the exterior wythe. These cracks stem from the large shear stiffness of the connection and the presence of differential movements between the wythes. In such instances, opting for lower levels of composite action allows the wythes to accommodate movements without generating cracks in the veneer. Other options to mitigate this situation are: using ties that allow limited movement of the external wythe, incorporating expansion joints in the veneer, or providing

longitudinal reinforcement in the external wythe are potential strategies to mitigate this issue.

2.6 Shear Ties

2.6.1 Shear Ties in Reinforced Concrete Systems

In the 1960s, wall panels emerged as double tee sandwich panels that achieved full composite action by using solid concrete zones. Over time, metal trusses were used to connect wythes, enhancing thermal resistance while maintaining fully composite properties. In the 1980s, non-composite panels were introduced that featured non-metallic ties. Initially, these panels had larger thermal resistance but were structurally weaker. However, advancements were made to enhance their structural capacity.

Currently, the materials utilized for shear connectors typically consist of steel, fibre-reinforced polymers (FRP), and plastic. Steel connectors are preferred due to their exceptional mechanical properties (Tawil et al., 2022). FRP connectors using basalt, glass, or carbon fibres provide a blend of mechanical and thermal properties. Plastic connectors exhibit low thermal conductivity but are not as mechanically efficient (Tawil et al., 2022). The use of solid concrete as a shear connector between the wythes results in low thermal resistance and moisture issues in the wall panels. Different types of ties are available for sandwich panels, and their configuration can significantly influence their deformation response. For instance, an FRP truss tie exhibits a stiff and brittle response, while a thin steel rod produces a more flexible response with higher ductility (Naito et al., 2012). The level of composite action achieved is directly influenced by the type and effectiveness of the connections between the wythes. To illustrate the shear response of PCSW ties, the shear response of five types of ties used in Gombeda et al. (2017) is shown in Fig. 2-10.

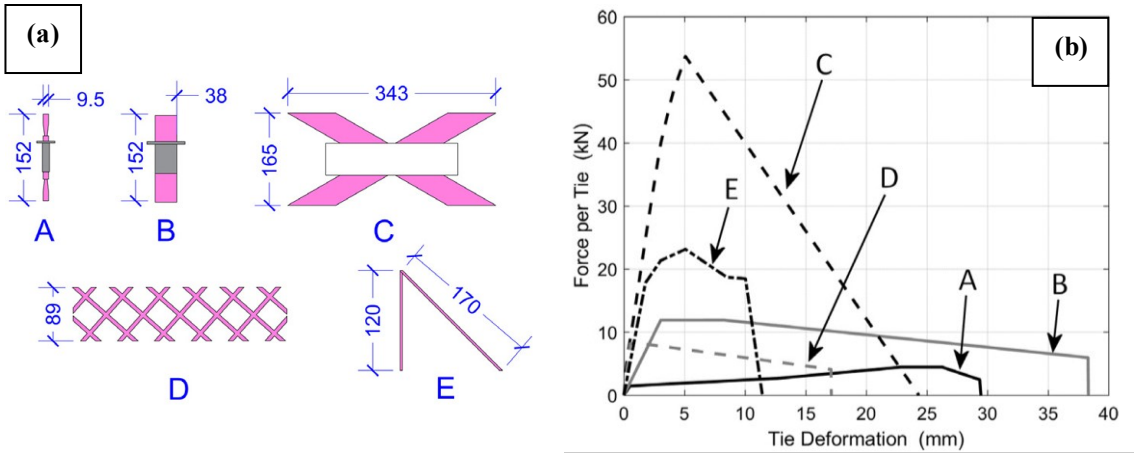

Figure 2-10. Ties and force-deformation relationship used in Gombeda et al. (2017): a) dimensions of shear ties, and b) force-deformation of shear ties.

Previous studies have been performed on PCSW panels using ties that allow shear between the wythes. The tests consisted of small-scale and full-scale specimens. These studies proved that the shear ties provide composite action to the system. Additionally, these studies concluded the following: the geometry of the ties influences the flexural stiffness of the ties, where truss ties provided higher initial flexural stiffness than pin ties (Naito et al., 2012). Increasing the diameter of the ties increased their shear strength and flexural stiffness of them (Tomlinson et al., 2016). The location of the ties influences the flexural ductility and stiffness of the panels while maintaining the same strength under lateral loads. Moreover, the ductility of the ties directly impacts the deformation capacity of the panel, for instance, ties with low ductility exhibit early strength degradation, leading to reduced composite action, overall deformation capacity, and strength of the panel (Gombeda et al., 2017; Tomlinson and Fam, 2016). Regarding the material of the ties, FRP bar ties exhibit inferior shear strength than conventional steel connectors (Woltman et al., 2013). Additionally, the in-plane shear behaviour of the wall panels is notably influenced by the interfacial bond strength between the concrete wythes and the insulation. The shear flow capacity tends to decrease as the thickness of the insulation wythe increases (Choi et al., 2019).

2.6.2 Shear Ties in Reinforced Masonry Systems

Numerous research studies have been conducted to examine the axial behaviour of ties in various wall systems. However, limited studies exist regarding the shear behaviour of ties in masonry walls. Is fundamental to understand the factors influencing the shear response to understand their performance in cavity walls. Recent research has emphasized the need for further investigation into the shear strength of ties (Arslan et al., 2020; Romero and Tomlinson, 2023).

The existing Canadian design standard for masonry buildings, CSA S304-14 (CSA S304-14 2014), does not account for the out-of-plane load resistance of the veneer. It assumes that all loads acting on the wall assembly are solely resisted by the CMU backup wythe. However, researchers (Mullins and O'Connor, 1987; Pacholok et al., 1989; Williams and Hamid, 2005) have demonstrated that cavity walls using ties capable of transferring shear load from the veneer to the CMU, exhibit composite behaviour. This composite behaviour allows the veneer wythe to contribute to the out-of-plane resistance, thereby enhancing the overall out-of-plane resistance compared with walls with conventional ties. Below is presented an overview of previous research studies that investigated the influence of shear ties in cavity walls. Table 2-3 summarizes the characteristics of relevant studies in masonry cavity wall shear ties.

Table 2-3. Summary of previous research in shear ties in masonry cavity walls.

Author	Type of tie	Specimen	Cavity width *mm*	Loading	Conclusions
Pacholok et al., 1989	Introduced a novel shear tie (fig. 2-11a)	Full-scale	70 and 100	Positive lateral pressure	Shear ties enhanced the out-of-plane strength of the walls and reduced lateral defection. Increasing the cavity width increased the out-of-plane strength of the shear-connected cavity walls.
(Papanikolas et al., 1990)	Introduced a novel shear tie (fig. 2-11b)	Full-scale	25, 50 and 100	Lateral pressure and outdoor conditions	Composite action was achieved using shear ties. Flexural strength and out-of-plane strength increased with larger concrete block size, vertical reinforcement, and wider cavity width when subjected to lateral loads.
Goyal et al., 1993	Shear tie	Full-scale	75 and 100	Vertical loads with different eccentricities	Shear ties enhanced the stiffness and ultimate load-carrying capacity of the walls under eccentric vertical loads and deflection was reduced. Increasing the cavity width improved the stiffness of the shear-connected cavity walls.
Choi and LaFave, 2004	Conventional corrugated metal tie	Small-scale	25	Lateral load in-plane and out-of-plane	The tie thickness and eccentricity affected the tension stiffness. Increasing the embedment length increased the tension and strength of the specimens.
Williams and Hamid, 2005	Adjustable ties (Fig. 2-11c)	Small-scale	100	Shear	Developed a practical testing method to assess the in-plane lateral stiffness of masonry ties. Higher shear stiffness leads to a more effective transfer of in-plane shear from the veneer to the CMU.
Zisi and Bennett, 2011	Conventional corrugated metal ties	Small-scale	25	Monolithic and cyclic shear (In-plane load)	Tie geometry and bend eccentricity were the most important factors. The location of the ties in the bed joint, the fastener type, and the quantity were less significant.
Messali et al., 2017	Conventional L-shape tie (wire)	Small-scale	80	Axial and shear loads, monotonic and cyclic	Clay brick specimens presented more brittle behaviour and higher peak load. The performed tests should not be used to evaluate directly the interaction between the axial and shear forces.
Arslan et al., 2021	Conventional wire ties	Small-scale	80	Tension and compression	Embedment length and tie geometry affected significantly the axial resistance. The authors recommended shear tests on traditional metal ties.
Romero and Tomlinson, 2023	Novel shear tie (same used in Chapter 4) and conventional ties	Small-scale	176	Tension	The tensile strength of novel ties was larger than conventional ties. Increasing the embedment length and using concrete bricks instead of clay bricks increased the axial strength of the specimens.

In prior research (Zisi and Bennett, 2011; Messali et al., 2017), the shear strength of traditional ties in masonry cavity walls was investigated. The studies revealed a low shear strength for conventional ties, approximately 0.1 kN, the authors recommended neglecting it in the design (Messali et al., 2017). The tie geometry and bend eccentricity were identified as the most influential factors, whereas the placement of ties in the bed joint, and the type and quantity of fasteners were comparatively less significant (Zisi and Bennett, 2011). Other findings included the lack of influence of brick type on shear

strength and the identification of the failure mechanism primarily being governed by plastic deformation of the tie and the crushing of the surrounding mortar (Messali et al., 2017).

Previous studies involved both small-scale and full-scale cavity wall specimens subjected to out-of-plane loads and using shear ties. These studies have demonstrated that these ties enhance the out-of-plane resistance of walls and exhibit reduced lateral deflection compared to walls with conventional ties (Mullins and O'Connor, 1987; McGinley et al., 1989; Pacholok et al., 1989; Papanikolas et al., 1990). This indicates that the inclusion of shear ties in cavity walls provides a certain level of composite action to the wall system. Other findings include the observation that both flexural strength and out-of-plane strength increase with larger concrete block sizes and vertical reinforcement when subjected to lateral loads (Papanikolas et al., 1990). Additionally, augmenting the embedment length of ties in the veneer enhances the out-of-plane resistance of the specimens (Choi and LaFave, 2004).

Previous studies determined that the cavity width influences the axial and out-of-plane resistance of cavity walls (Pacholok et al., 1989; Goyal et al., 1993; Sakr and Neis, 2001). Pacholok et al. (1989) found that in the shear-connected cavity walls they examined, increasing the cavity width significantly enhanced the out-of-plane capacity of the walls. The cavity width of the specimens investigated in the previous studies varied from 25 to 100 mm. Studies are scarce on cavity walls with thicker cavities.

Other studies (Goyal et al., 1993) tested shear-connected full-scale cavity walls subjected to eccentric vertical loads. The researchers concluded that incorporating shear ties improved the stiffness and ultimate load-carrying capacity of the walls when subjected to eccentric vertical loads, resulting in reduced deflection. It was also observed that increasing the cavity width enhanced the stiffness of the shear-connected cavity walls, and an increase in load eccentricity amplified the contribution of the veneer wythe.

Williams C. and Hamid A. (2005) developed a testing approach to evaluate the in-plane lateral stiffness of three adjustable masonry ties (Fig. 2-11c). To test the ties in a manner consistent with their behaviour in an actual cavity wall, a customized testing frame was constructed (Fig. 2-11d). This testing frame served as a reference for designing

the testing frame used in Chapter 4 of the present study. The authors determined the flexural stiffness of the ties in the serviceability limit state, specifically focusing on the initial, linear elastic response. They concluded that higher flexural stiffness indicates a more efficient transfer of in-plane shear from the veneer to the CMU.

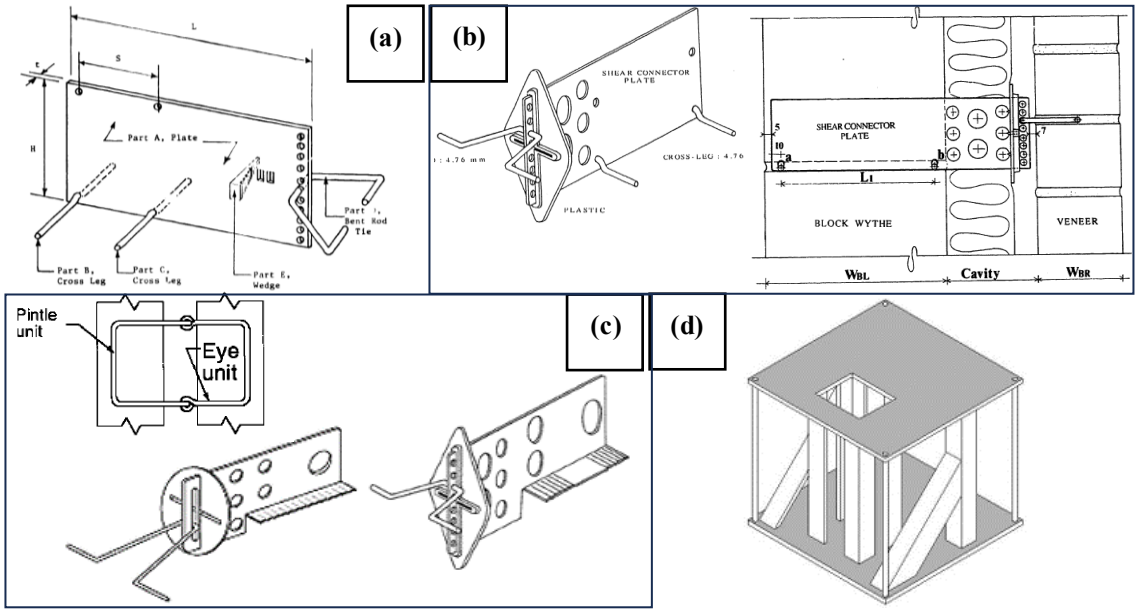

Figure 2-11. Shear ties in previous studies: (a) shear tie by Pacholok et al. (1989), (b) shear tie by Papanikolas et al. (1990), (c) ties, and test frame by Williams and Hamid (2005).

Romero and Tomlinson (2023) evaluated the tensile strength of a novel tie, the same one used in Chapter 4 of this project. The researchers compared the novel tie with conventional ties in small-scale cavity wall specimens featuring a thicker cavity width of 176 mm. The findings indicated that the tensile strength of specimens using the novel tie surpassed those with conventional ties. Specifically, the peak load of specimens with the novel tie was 172%, 210%, and 41% larger than those with conventional z-tie, rectangular ties, and plate ties, respectively. Furthermore, enhancing the embedment length of ties into the mortar joint and using concrete bricks instead of clay bricks for the veneer contributed to an increase in the axial strength of the specimens.

2.6.3 Dowel and Truss Action in Shear Ties

Previous studies tested shear ties subjected to shear load in both masonry and concrete systems evaluating different factors that impact the shear response. These factors include

geometry, thickness, material, angle of the load, location, and embedment length into the wythes, as discussed in the previous sections. For instance, Naito et al., (2012) found that truss ties exhibited higher initial flexural stiffness compared with pin ties horizontally placed. The mechanics of both truss and horizontal ties can be analyzed to observe the advantages of the truss geometry.

Figure 2-12 illustrates a tie example consisting of two components: a horizontally placed top member and an inclined bottom member. Dowel action is observed in horizontally placed ties subjected to shear (Fig. 2-12c), while truss action occurs in inclined members subjected to shear (Fig. 2-12d). Tomlinson (2016) tested ties comprised of these two members in Concrete Sandwich Wall Panels to analyze the contribution of truss and dowel action to resist shear load. The results indicated that the contribution of the horizontal member (dowel action) to shear resistance was minimal, ranging between 2% and 15% of the total shear resistance for all specimens. In contrast, inclined members with truss action demonstrated much greater effectiveness in resisting loads compared to members exhibiting only dowel action. Additionally, the authors found that the contribution increased with the diameter.

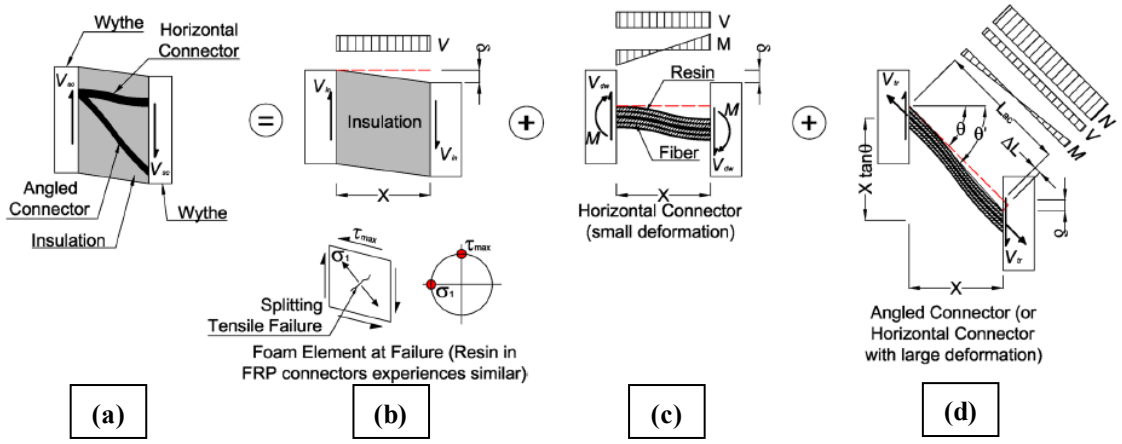

Figure 2-12. Diagrams of shear-resisting components in PCSW (a) overall resistance, (b) insulation resistance, (c) dowel action resistance, and (d) truss action resistance (Tomlinson et al., 2016).

2.7 Thermal Behaviour of Cavity Walls

2.7.1 Introduction

Global energy consumption is on the rise, with approximately 40% of this energy being consumed by buildings (Zhang et al., 2022). Specifically, about 60% of the energy used in buildings is attributed to space heating and cooling (Zhang et al., 2022). The efficiency of buildings in terms of energy consumption is heavily influenced by the components of their structural envelope, which are directly exposed to external factors like solar radiation and climate fluctuations. The heat transfer through this envelope accounts for a significant portion, ranging from 20% to 50%, of the heating and cooling loads in the building (Zhang et al., 2022). As a result, it is important to understand the thermal performance of envelope walls and explore effective solutions to reduce energy consumption while maintaining indoor thermal comfort.

The thermal performance of wall envelopes is predominantly determined by the materials used in the cavity wall. The thermal conductivity of elements like mortar, grouting, CMUs, bricks, and insulation plays a key role in determining the thermal resistance (R-value) of the wall assembly. Calculating the R-value can be accomplished through either theoretical calculations or experimental tests on actual assemblies. However, when highly conductive components penetrate the insulation layer, it can reduce the R-value and complicate its calculation process.

This section will start with an explanation of key thermal concepts, followed by an overview of the Canadian energy requirements and the impact of the different materials on the thermal performance of the cavity walls. Finally, methods to estimate the R-value of wall assemblies are presented.

2.7.2 Definition of Thermal Factors

The thermal conductivity (k) is a material property that represents the ability of the material to conduct heat, expressed as energy per unit area per unit thickness for each degree of temperature difference (W/mK) (Hershfield, 2022). Thermal conductivity occurs by molecular agitation and contact, involving the transfer of heat without the physical movement of the solid material (Nave, 2000). The direction of heat flow follows the temperature gradient, moving from regions of higher temperature and molecular

energy to those with lower temperature and energy. This heat transfer occurs until thermal equilibrium is achieved. The heat transfer is influenced by the magnitude of the temperature gradient and the intrinsic thermal properties of the material. For instance, at high temperatures, molecules exhibit increased movement, leading to a higher rate of heat transfer through the material. Consequently, the thermal conductivity of the identical sample can change drastically with temperature fluctuations.

The heat flow (Q) represents the amount of energy per unit of time that passes through an assembly under a specific temperature.

The thermal transmission coefficient or U-value is defined as the heat flow per unit of time through a unit area of an assembly per temperature degree difference. It can be expressed in W/$m^2°K$, which is the inverse of the effective RSI, or in the imperial units (BTU/h $ft^2°F$). The convention is to include the impact of air films.

The thermal resistance or R-value is the inverse of the U-value and represents the measure of a material to resist the flow of heat. It is expressed in RSI ($m^2°K/W$) if the international system is used or in the imperial units (h $ft^2°F/BTU$).

Thermal bridging is defined as a building envelope component where the uniform thermal resistance is altered due to complete or partial penetration of thermal insulation by materials with lower thermal conductivities, and/or when there are variations between the interior and exterior areas of the envelope. This situation commonly arises at parapets and corners (Morrison Hershfield, 2022).

2.7.3 Energy Code Requirements for Walls

In Canada, the regulations governing energy efficiency in new construction are primarily outlined in two national codes: the National Building Code of Canada (NBC) and the National Energy Code for Buildings (NECB). The NBC, Part 9, is responsible for ensuring compliance with thermal performance requirements for small buildings like single-family homes and low-rise structures, while the NECB, Part 3, addresses the thermal performance requirements for larger buildings, such as commercial or institutional structures. The American Society of Heating, Refrigerating, and Air-Conditioning Engineers (ASHRAE) introduced its first building energy standard, ASHRAE Standard 90.1 in 1975. In contrast, the first version of Canada's NECB was

introduced in 1997. Various provinces and territories across Canada have adopted these national codes, often incorporating modifications to suit their specific needs. For instance, Ontario has the Supplementary Standard SB-10, Quebec follows the Regulation Respecting Energy Conservation in New Buildings Act, and Alberta has Section 9.36 of the Alberta Building Code (ABC) to guide building designers in complying with energy standards. Chapter 5 in this study presents minimum values of U-value for envelope elements based on the type of element and the geographic location of the building according to the NECB (NECB, 2022).

The National Energy Code of Canada for Buildings (NECB, 2022) has been imposing stricter requirements on buildings to enhance energy efficiency and reduce energy consumption. To meet these demands in masonry buildings, a potential solution is to increase the thermal resistance (R-value) of the wall envelope. However, this comes with challenges such as thermal bridging that occurs when highly conductive elements penetrate the insulation. Thermal bridging is common in many building systems not only in masonry. Examples of thermal bridging sources in cavity walls are the steel ties that connect the veneer to the CMU or a shelf angle penetrating the insulation, which complicates the calculation of the R-value for the wall assembly.

The thermal properties of materials play a crucial role in determining the thermal performance of buildings. Masonry has notable thermal energy storage capacity due to its thermal mass, which in companion to high R-value insulation leads to a reduction in the heating and cooling loads on a building (Gregory, et al., 2007; Tomlinson, 2015). However, the thermal resistance is significantly influenced by various factors, including the thickness, shape, and materials of all the components within the wall assembly. Consequently, calculating the R-value in masonry walls becomes complex due to the combination of materials with varying thermal properties and configurations. Minimizing thermal bridging in designs and carefully considering its impact is crucial, as it can be a large source of thermal performance deficiencies in masonry walls.

The 2017 edition of the energy code (NECB, 2017) had significant revisions to energy regulations and guidelines. One notable change was the calculation requirements for the effective R-value. In the previous version, the majority of the structural elements and

highly conductive elements that penetrated the envelopes could be excluded from the calculation if they comprised less than 2% of the total wall area (Straube, 2017). However, new versions of the code mandate the inclusion of all elements in the effective R-value calculation. As a result, more accurate methods and tools are necessary to provide precise estimates of the effective R-value.

2.7.4 Influence of the Wall Components on the Thermal Performance

The overall thermal behaviour of cavity walls is primarily governed by the thermal characteristics of the construction materials comprising the wall assembly (e.g., concrete, clay, grout, mortar, and insulation). Additionally, the insulation layer situated within the cavity serves as a thermal barrier with low thermal conductivity, enhancing the wall's overall thermal resistance. However, structural elements such as shelf angles and ties, typically constructed from steel, pose a challenge due to their high thermal conductivity. These steel elements penetrate the insulation layer, diminishing its effectiveness and resulting in a reduction of the thermal resistance. Figure 2-13 shows the typical materials that comprise the cavity wall and detailed thermal properties provided in Table 2-4.

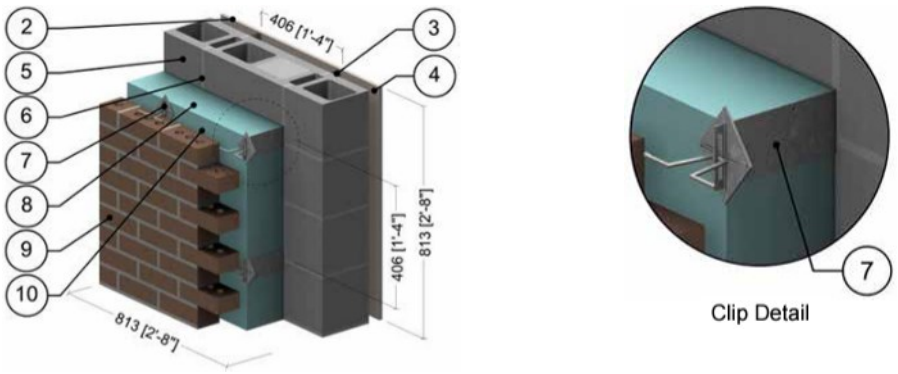

Figure 2-13. Typical cavity wall assembly components (Hershfield, 2022).

Table 2-4. Thermal properties of typical components in a cavity wall (Hershfield, 2022).

ID	Component	Thickness, mm	Conductivity, Btu in/ft²h°F (W/mK)	Thermal resistance, h ft² °F/Btu (m²K/W)	Density, kg/m³
1	Interior film	-	-	R-0.7 (0.12 RSI)	-
2	Gypsum board	13	1.1 (0.16)	R-0.5 (0.08 RSI)	800
3	Steel studs	20 gauge	430 (62)	-	7830
4	Air in the stud cavity	41	-	R-0.9 (0.16 RSI)	1.2
5	Concrete block	190	3.5 (0.5)	-	1900
6	Mortar	-	3.5 (0.5)	-	1800
7	Masonry ties	14 gauge	347 (50)	-	7830
9	Exterior insulation	varies	-	R-5 to R-35 (0.88 to 6.2 RSI)	28
9	Brick veneer	92	5/4 (0.78)	-	1920
10	Air gap	25	-	R-0.9 (0.16 RSI)	1.2
11	Exterior film	-	-	R-0.2 (0.03 RSI)	-

2.7.4.1 Concrete and clay

The thermal resistance of block and brick units is impacted by factors such as their shape, size, aggregate size, moisture content, and density. The thermal conductivity of concrete blocks or fired clay bricks primarily relies on aggregate type. For instance, the thermal conductivity of concrete often correlates with its density, which is heavily dependent on aggregate type (ESCSI, 2007). Moreover, the type and configuration of a hollow block can significantly affect the overall thermal efficiency.

Sanders et al., (2017) performed dynamic thermal resistance tests on cavity walls featuring clay brick, using an innovative hot box setup. The results indicated that the thermal mass of the clay brick veneer significantly reduced the flow of energy through the wall system when compared with the same wall systems without the clay brick veneer. This means that the clay brick veneer stores energy during temperature fluctuations, thereby minimizing the transfer of energy from the interior to the exterior of the building. However, a beneficial effect was observed only in transient state testing.

2.7.4.2 Grout and mortar

In masonry three distinct types of mortar are utilized: lime mortars, hydraulic lime mortars, and Portland cement or masonry cement lime-based mortars. These mortar

varieties have discernable characteristics like compressive strength, flexibility, water and vapor transmission rate, and frost durability.

In general, grout has a negative impact on the overall R-value of a masonry wall. This influence of grout hinges primarily on the shape and thermal resistance of the concrete block. Localized thermal bridges stemming from grout-filled CMU cores play a substantial role in impacting the thermal resistance of the system (Kosny, 1995).

Conversely, mortar joints constitute a notable portion of the wall's area (approximately 7%), yet they typically possess a distinct density compared to the CMUs. Abdou and Murali (1994) demonstrated an approximate 8% reduction in the R-value of a concrete masonry wall in the absence of mortar joints. This enhancement in thermal resistance is attributable to the air enclosed within the mortar joints.

2.7.4.3 Ties and shelf angles

Veneer ties and shelf angles play a major role in providing structural integrity to masonry walls. Nevertheless, research findings indicate that conventional steel masonry veneer ties and steel shelf angles significantly contribute to thermal bridging in these walls (Roppel et al., 2012). Essential determinants influencing the wall R-value include tie material, shape, and spacing. For example, stainless steel ties with perforations result in a thermal resistance reduction of exterior insulation ranging from 3% to 9%, whereas galvanized iron ties without holes exhibit a reduction between 8% to 25% (Wilson, 2019).

Advancements have been made in tie design, encompassing material and shape enhancements, to mitigate thermal bridging while adhering to resistance standards. For instance, adding holes to tie bodies decreases the insulation-penetrating area of the tie and lowers the thermal conductance of the element. However, introducing additional variables to the tie, such as geometry, size, material, and the other components in a cavity wall, can complicate the process of determining their thermal resistance due to the complexity of accounting for those characteristics in the calculations (Kontoleon et al., 2013).

2.7.4.4 Insulation

The insulation layer is characterized by its low thermal conductivity which increases the thermal resistance of the wall assembly. Therefore, the materials that comprise this layer

act as a barrier that diminishes the temperature variations in the direction of heat flow. There are various insulation materials, including fibreglass, rock wool, and polystyrene. The extruded polystyrene (EPS) and expanded polystyrene (XPS) foams are the most commonly used because of their high thermal performance and workability (Kim and You, 2015).

Insulation designs hinge on an economic balance between the initial cost of enhancing the envelope and the subsequent cumulative cost of operational energy for climate control. This takes into account factors like durability and maintenance expenses. The thermal efficiency of any building enclosure relies significantly on its insulation design (Schumacher et al., 2013). Various insulation design approaches have been utilized in the construction of masonry walls, depending on the specific thermal requirements, prevailing climate conditions, construction feasibility, budget considerations, and other design factors.

2.8 Calculation of Thermal Resistance

The rising energy demands necessitate more precise methods to predict and test the thermal performance of masonry wall assemblies. Both experimental and analytical methods can be performed under static or transient state. Static state calculations are easier and require less time than transient methods. However, transient methods permit the analysis of the thermal behaviour of the wall assembly under variations of temperature during the day, which is the condition in reality. Furthermore, computational simulations are gaining prominence for their ability to offer valuable insights into the behaviour of wall assemblies during the design process (Ismaiel, 2022). Thermal resistance is commonly defined as the capacity to resist heat flow.

2.8.1 Simplified Analytical Methods

This section presents an overview of various existing analytical methods used to estimate the thermal resistance or transmittance of building elements. It explores the underlying assumptions and limitations associated with each method.

2.8.1.1 Thermal resistance of concrete masonry units

The two common techniques for calculating thermal resistance are the parallel-path and the series-parallel methods. The first method is used to determine the thermal resistance

of CMUs, only for units that are not insulated (ACI, 2022). This method assumes that heat flow is transferred through the CMUs in parallel flows. When the CMU is hollow, the heat flow depends on the ratio between the web area and the core area, as indicated in Equation 2-1.

$$R_t = \frac{R_w R_c}{a_c R_w + a_w R_c} \quad \textbf{(2-1)}$$

In Eq. 2.1, a_c represents the fractional core area, which refers to the area of the specific element being studied (core or webs) divided by the total area of the block; a_w denotes the area percentage of the web; R_c stands for the thermal resistance of the cores (empty or with fillings) (m^2K/W); and R_w represents the thermal resistance of the concrete webs (m^2K/W).

The series-parallel method (or isothermal planes) is used for both insulated and uninsulated masonry units and accounts for lateral heat flow in face shells, this is because as with fluid flow and electrical currents, this method considers that heat flow follows the path of least resistance (ACI, 2002; NCMA, 2013; ASHRAE, 2019). This method divides the block into a series of thermal layers, and the overall R-value is obtained by adding up the resistance of each layer, as expressed in Equation 2-2.

$$R_T = R_i + \frac{R_f R_m}{a_f R_m + a_m R_f} + \frac{R_w R_c}{a_c R_w + a_w R_c} + R_a + R_V + R_O \quad \textbf{(2-2)}$$

In Eq. 2-2, the variables as defined as: a_c: fractional core area; a_f: fractional face shell area; a_m: fractional mortar joint area; a_w: fractional web area; R_a: thermal resistance of cavities between the veneer and backup wall, including continuous insulation (m^2K/W); R_c: thermal resistance of cores, empty or with fillings (m^2K/W); R_f: thermal resistance of both face shells (m^2K/W); R_i: thermal resistance of interior air surface films (m^2K/W); R_m: thermal resistance of mortar joints (m^2K/W); R_O: thermal resistance of exterior air surface films (m^2K/W); R_T: overall thermal resistance of the wall (m^2K/W); R_V: thermal resistance of the veneer (m^2K/W); R_w: thermal resistance of concrete webs (m^2K/W).

2.8.1.2 Series and parallel heat flow paths

The thermal resistance of wall assemblies comprised of multiple materials is determined using the Series and Parallel methods. In the Series method, heat flows sequentially through each layer of the wall assembly from the hot side, adhering to the principles of the second law of thermodynamics. The thermal resistance of each layer is calculated based on the ratio of its thickness to its thermal conductivity. Consequently, the total thermal resistance of the wall assembly, comprising different materials, is obtained by summing up the resistances of each wythe in series as shown in Equation 2-3 (ASHRAE, 2017).

$$R_{total} = R_1 + R_2 + R_3 + \cdots + R_n \qquad \text{where: } \left(R_n = \frac{t_n}{k}\right) \tag{2-3}$$

In Eq. 2-3 the variables are defined as: $R_1, R_2, R_3, \ldots, R_n$: thermal resistance of each layer (m^2K/W); R_{total}: total resistance of the wall assembly (m^2K/W); t_n: thickness of the specific layer (m); k: thermal conductivity of the corresponding material.

In the parallel path method, heat flows through various pathways and is considered to be transferred through parallel paths within the wall assembly. This method assumes one-dimensional heat transfer perpendicular to the element's surfaces and is valid when materials within the same layer have similar conductivity values. However, this assumption is not valid for assemblies with highly conductive elements (e.g., steel components) in contact with low conductive elements like insulation, due to the presence of thermal bridging effects (Ismaiel, 2022). In wall assemblies where components are arranged in a manner that facilitates parallel heat flow, the average transmittance of the envelope is calculated using Equation 2-4 (ASHRAE, 2017).

$$U_{average} = aU_a + bU_b + cU_c + \cdots + nU_n \qquad \text{where: } \left(U_n = \frac{1}{R_n}\right) \tag{2-4}$$

In Eq. 2-4, the variables are defined as: $a, b, c, \ldots, n$: surface weighted path fractions for a standard basic area comprised of different paths, each with their respective transmittances $U_a, U_b, U_c, \ldots, U_n$.

Typical building assemblies are composed of multiple layers with combinations of series and parallel pathways. To address that situation, the series-parallel method is applied. In this approach, it is assumed that heat can flow laterally in any component, and the thermal resistances of adjacent components are combined in parallel, resulting in a path with series-parallel resistance combined. The total average resistance in this case is the sum of the resistances of the layers between the isothermal planes. Each layer is calculated separately, and the results are weighted by the contributing surface area.

2.8.1.3 ISO 6946 Combined Method

The ISO 6946 (ISO, 2017b) standard presents the combined method for calculating the thermal resistance of building elements, encompassing both homogeneous and inhomogeneous layers, including those with air layers up to 0.3 m thick. This method combines the results from the parallel path and isothermal plane methods. The total thermal resistance is determined by averaging the upper and lower thermal resistance limits obtained from the respective methods. However, there are certain limitations to this approach. Firstly, it can only be applied if the ratio between the upper and lower limits does not exceed 1.5. Secondly, the method is not suitable for assemblies with thermal bridging, as significant differences in thermal conductivity within the same layer may affect its validity.

2.8.1.4 ASHRAE Method

To calculate an accurate R-value for assemblies with the presence of thermal bridges, ASHRAE has proposed a modification to the parallel path method, introducing the zone method. This method is applied to assemblies with widely spaced metal elements of uniform cross-section areas and adjacent materials with notable differences in thermal conductivities, such as steel framed walls (Di Placido et al., 2019). In this method, an adjustment is made to the parallel path method. The procedure consists of dividing the wall into two sections, first containing the steel thermal bridge influence, and secondly the remaining portion of the element without the thermal bridge effect. Using factors from charts, the width of the two sections assumed is calculated based on the dimensions of the addressed thermal bridging element. The thermal resistance is calculated and then combined using the parallel path method. The factors obtained to determine the sections'

width are limited to steel studs and lightweight steel framed walls. This method is appropriate for lightweight steel framed elements due to its simple geometries and uniform thermal bridging.

However, Lee and Pessiki (2008) proposed an alternative method to the zone method, arguing that the zone method was developed for metal frame structures and is not accurate for systems with steel ties such as precast concrete sandwich wall panels (PCSW) or cavity walls. The authors found that the current zone method predicts higher R-values than the FEM R-values. Conversely, their new proposed method considers the effects of metal tie sizes and spacing, and material conductivities in the R-value calculation.

2.8.1.5 Point and Linear Transmittances

The concept of linear and point transmittances simplifies thermal bridging analysis by disregarding the area of thermal bridges. This approach involves comparing the heat flow through an assembly with the thermal bridge and without it. The difference in heat flow between the two scenarios is then related to the detail as heat flow per linear length (linear transmittance) or as a single point heat flow (point transmittance). The linear transmittance due to linear thermal bridges (e.g., shelf angle, slab edge) can be calculated as shown in Equation 2-5.

$$\Psi = \frac{Q_a - Q_b}{L} \quad \textbf{(2-5)}$$

In Eq. 2-5 the variables are defined as: Ψ: linear transmittance resulting from thermal bridges (W/mK); Q_a: heat flow of the assembly with a portion of the clear field replaced by intersections (W/K); Q_b: heat flow of the clear field; L: assembly width (m).

The point transmittance refers to point anomalies (e.g., intersections between linear elements, beam end penetrations). It is calculated as the heat difference, as shown in Equation 2-6.

$$\chi = Q_1 - Q_2 \quad \textbf{(2-6)}$$

In Eq. 2-6: Q_1: heat flow of the entire assembly unit with intersections (W/K); Q_2: heat flow of the assembly without intersections (W/K); χ: point transmittance (W/K).

To determine the overall thermal transmittance of an element, the thermal transmittance is divided into three categories: clear field transmittance (U_O), linear transmittance (Ψ), and point transmittance (χ) (Hydro, 2016). The final overall U-value is then calculated as illustrated in Equation 2-7.

$$U_T = \frac{\sum(\Psi \times L) + \sum \chi}{A_{total}} + U_O \quad \textbf{(2-7)}$$

In Eq. 2-7: U_O: clear field thermal transmittance (W/ m^{2}K); A_{total}: total area of the opaque wall (m^2); Ψ: point transmittance heat flow from the linear thermal bridge (W/mK); L: length of the linear thermal bridge (m); χ: heat flow from the point thermal bridge (W/K).

The overall U-value is determined using the point and linear transmittances method when the three thermal performance values for the clear, linear, and point fields transmittances are known. This last requires computer simulations or experimental testing.

2.8.2 Experimental Testing for R-value

Experimental testing is used to assess and enhance the accuracy and reliability of analytical and numerical calculations. Furthermore, certain unique configurations can only be adequately captured and understood through experimental methods.

2.8.2.1 Hotbox apparatus

The hot box method is widely utilized for experimental studies on the thermal performance of building assemblies. The ASTM C1363 (ASTM, 2019) standard outlines the guidelines for steady-state tests on both homogeneous and non-homogeneous specimens. There are two types of hot box apparatus available: the guarded hot box for smaller specimens and the calibrated hot box for larger ones. Data obtained from these apparatuses allow for the experimental calculation of the R-value of the elements.

Hot boxes are designed to assess the heat transfer through a specimen under constant environmental conditions on both sides, ensuring steady-state conditions. During the test, a substantial temperature gradient is applied across the specimen, allowing the measurement of the heat flow through the specimen. Finally, the R-value of the specimen is calculated as depicted in Equation 2-8.

$$R = \frac{A \times \Delta T}{Q} \quad \textbf{(2-8)}$$

In Equation 2-8: R: thermal resistance of the specimen (m^2K/W); Q: heat flow through the area of the specimen (W); A: area (m^2); ΔT: difference in temperature between the surfaces of the specimen (K).

In addition to measuring R-values under constant conditions, R-values can also be evaluated dynamically, with temperature variations. Dynamic tests are conducted using the calibrated hot box method, where the indoor air temperature remains constant while the outdoor air temperature is systematically changed based on a predetermined time-temperature relation. The energy needed to maintain a constant indoor air temperature is recorded over time (Van et al., 1982). The benefit of the dynamic tests is that account for the temperature variations to which the envelope elements are exposed throughout the day in real conditions (Sanders et al., 2017).

2.8.2.2 Thermal imaging

This method involves the capture of infrared images where long-wave radiation is converted into a colour scale on the surface of the element. The colour scale represents the temperature variation. This method permits the observation of the thermal performance permitting the identification of surface temperatures with a non-invasive detection principle. Thermographic imaging is a practical and swift method to assess improperly installed or damaged insulation.

2.8.2.3 On-site R-value measurements

Theoretical and laboratory methods used to evaluate the thermal performance of building elements may not fully consider workmanship issues, material degradation over time, and openings in the envelope elements. To obtain more precise information about existing elements, in-situ non-destructive measurements are conducted to study their thermal behaviour.

The ASTM standard C1155-95 (ASTM, 2013) outlines guidelines for conducting in-situ measurements of heat flux and temperatures to determine the thermal resistance of

building elements. The standard discusses two techniques: the summation technique and the sum of least squares technique.

The widely accepted approach for in-situ thermal characterization of building elements is the average method, as described in ISO 9869 (ISO 9869, 2014) (Deconinck and Roels, 2016). This method involves measuring the heat flow rate through the internal face of the element and obtaining surface and air temperatures of both the internal and external faces. To ensure accuracy, the averages should be taken over a sufficiently long period. Additionally, ISO 9869 provides an adjustment for storage effects, which is particularly relevant for elements with high thermal mass. This adjustment accounts for the thermal storage capacity of the element and enhances the performance of the method.

In contrast to the previous quasi-stationary methods, advanced dynamic methods have been developed to accommodate the inherent dynamic conditions in in-situ measurements. These methods take into account the fluctuations in heat flux and temperature measurements during the analysis. Moreover, they use inverse modelling techniques, wherein a model is constructed using the acquired measurements to extract information about the thermal performance of the building element.

2.8.3 Numerical simulation

Numerical simulation through computational methods offers a cost-effective and precise alternative to studying the thermal behaviour of building elements. In the thermal modelling market, various programs are available to conduct simulations in both two and three dimensions. Examples of two-dimensional simulation software include THERM, HEAT2, and Energy2D, while three-dimensional simulation programs include ANSYS, ABAQUS, HEAT3, and SIEMENS. Various researchers (del Coz Diaz et al., 2006; Norris et al., 2012; Desjarlais and McGowan, 1997) explored the precision of simulation outcomes by comparing them to experimental measurements, and the findings indicated a favourable agreement of approximately 3% between the numerical and experimental results.

Various mechanisms of heat transfer are present through the wall assembly due to the presence of airflow between the brick veneer and insulation boards and within the cores of concrete units. When conducting thermal analysis of concrete masonry cavity walls, it

is essential to account for the thermo-fluid dynamic behavior to ensure the accuracy of results (Shao, 2021). The fundamental equations governing fluid dynamics and thermal analysis consist of the continuity equations, which represent mass conservation. These governing equations are nonlinear partial differential equations that can be effectively addressed using finite element simulation software, such as ANSYS Workbench 2019 (ANSYS Inc, 2019).

2.9 Gaps in Literature Review

With the increasing emphasis on thermal efficiency, it is anticipated that standards will require thicker insulation layers, resulting in larger connectors. In this scenario, the current connectors may have reduced tension, compression, and shear strength, making them more susceptible to buckling. Pacholok et al. (1989) found that increasing the cavity width in the studied shear-connected cavity walls led to a substantial improvement in the out-of-plane resistance. The cavity width of specimens tested in previous research range between 25 to 100 mm, there are limited studies on the structural behaviour of cavity walls with wider cavities and the shear response of the larger ties. Understanding the shear response of larger ties in wider cavity walls is necessary to understand the composite behaviour of these walls. Other variables can influence the shear response of the larger ties in cavity walls such as the type of brick of the veneer, the embedment length of the ties in the veneer, or the type of tie used to connect the wythes. Additionally, there are limited studies regarding the thermal behaviour of those wider cavity walls with masonry ties.

3 DESIGN OF TIES IN CAVITY WALLS

3.1 Introduction

A typical masonry cavity wall is comprised of an interior CMU backup, an outer brick veneer, and a cavity between them. The cavity is used to accommodate insulation and a moisture barrier. The two wythes are connected using steel ties. Masonry cavity walls serve both structural and thermal purposes. Structurally, cavity walls resist gravity and lateral loads. Thermally, the insulation layer, air gap, and thermal mass provide both a thermal break and an efficient way of controlling temperatures inside the buildings. Additionally, cavity walls protect against water penetration, draining moisture that penetrates the veneer wythe through the cavity until it is expelled through the weepholes in the bottom of the veneer.

There are different types of ties (as discussed in Chapter 2) in terms of their strength against axial and shear loads, and their ability to allow or limit vertical slip between the veneer and CMU wythes. In walls incorporating ties that can resist shear, there is evidence that some degree of composite action between the two wythes could be achieved. However, the Canadian standards for the design of masonry walls, CSA A304-14 "Design of masonry structures" (CSA, 2014a) and CSA A370-14 (CSA, 2014) "Connectors for masonry" do not recognize any degree of composite action for cavity walls, and thus, this reserve of strength remains unexplored. This chapter presents an overview of the structural behaviour of cavity walls, structural design considerations for masonry ties, and the thermal considerations for building envelopes according to Canadian standards.

3.2 Structural Behaviour of Cavity Walls

In the design of cavity walls in North America, the fundamental structural design principle for cavity walls entails both wythes sharing lateral wind or seismic loads, while one or both wythes bear the vertical gravity loads.

If a single wythe sustains the applied gravity load, that specific wythe must be designed to resist the entire compressive force. The contribution of the other wythe to resist lateral loads should not be assumed. This is because the lightly loaded wythe has much less resistance to flexural cracking as the backup wall benefits from precompression caused

by the axial load. However, if it is assumed that the compressive axial load is resisted together by the two wythes, each wythe needs to be designed as an independent member subjected to the respective portion of axial load and the calculated proportion of lateral load. In that case, some degree of mutual lateral stiffening can occur. The second option (considering each wythe acting independently in cavity walls) is recommended by CSA S304-14 (CSA, 2014a). However, conventionally, cavity walls are constructed in a manner where the total superimposed gravity load is resisted by the interior CMU wythe (Drysdale and Hamid, 2005). This choice stems from the complexities of evaluating the effects of the factors affecting the distribution of load between the wythes. These factors include the different materials of the wythes, differential movements, and rotational influences from floors and beams.

Metal ties are commonly used to link the two wythes of a cavity wall. Typical ties have high axial load capacity and their shear resistance is neglected. Thus connected, the two wythes experience similar deflections and collaboratively withstand the entire lateral load. Figure 3-1a depicts a typical cavity wall experiencing both external pressure (P_o) and internal pressure (P_i). If the ties are closely spaced and the boundary conditions for both wythes are identical, the forces transmitted in the ties can be approximated as a uniformly distributed load (P_t). The loads in the external and internal wythes are $P_o - P_t$ and $P_i + P_t$, respectively (Fig. 3-1b). The presence of weep holes and vents in the outer wythe may allow the cavity pressure to equate to the external pressure (P_o). Consequently, the outer wythe carries the tie-induced load, P_t, and the inner wythe carries the load $P_o + P_i - P_t$.

In this scenario, if both wythes share the same boundary conditions and possess significant axial stiffness, their deflections in the midspan become equal ($\Delta_o = \Delta_i$). Additionally, the distribution of load resisted by each wythe is proportionate to their respective flexural stiffness, as well as the resulting maximum bending moments. This relationship is expressed in Equation 3-1 (Drysdale and Hamid, 2005).

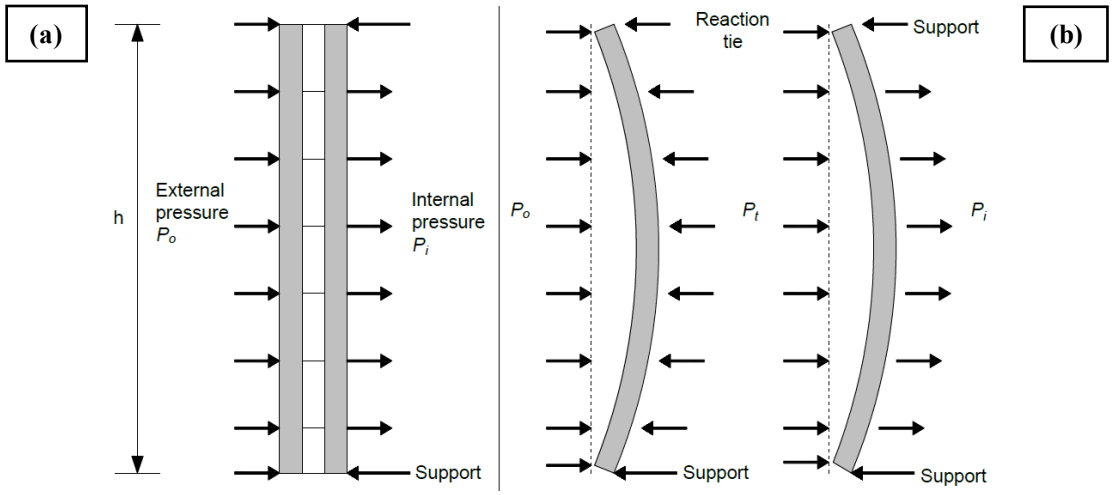

Figure 3-1. Lateral loading in a cavity wall: (a) masonry wythes with the same boundary conditions, and (b) free body diagram of each wythe (Drysdale and Hamid, 2005).

$$M_o = \left(\frac{E_o I_o}{E_o I_o + E_i I_i}\right) M_T \qquad \textbf{(3-1)}$$

$$M_i = \left(\frac{E_i I_i}{E_i I_i + E_o I_o}\right) M_T$$

Where: E_o, E_i: elastic modulus of the outer and inner wythes; I_o, I_i: moments of inertia of the outer and inner wythes; M_o, M_i: maximum bending moments in the outer and inner wythes, respectively; M_T: total bending moment.

Ties with the capacity to resist shear forces allow some degree of composite action, resulting in a stiffer and stronger wall system. Previous research has been conducted on the topic, confirming that partial composite action is achievable (Mullins and O'Connor, 1987; McGinley et al., 1989; Pacholok et al., 1989; Williams and Hamid, 2005;). Some researchers even found improvement in the vertical strength of the cavity walls under eccentric loads when using ties with shear capacity (Goyal et al., 1993).

However, CSA S304-14 (CSA S304 2014a) does not include provisions for composite action. The standard recommends for design purposes to treat the stiffness of the cavity wall as the summation of the stiffness values of the two wythes, functioning in a non-composite manner. This indicates that even though the ties impose comparable curvatures in both wythes, they do not transfer shear forces across the cavity. Therefore, both wythes

are designed to independently resist out-of-plane lateral loads without composite action (Drysdale and Hamid, 2005).

3.3 Structural Design Considerations of Cavity Wall Ties

Tie requirements are specified in CSA A370-14 (CSA, 2014). Additionally, the design philosophy for ties within cavity walls is outlined in CSA A370 (CSA, 2014) and consists of providing requirements to transmit axial load (both tension and compression) between the two wythes while preventing excessive relative displacement between the wythes.

Bowing deformation produced by the out-of-plane loads in the cavity wall (Fig. 3-1) and the presence of thermal and moisture-induced movements in the exterior wythe, can lead to vertical slip between the wythes. Commonly, designs are developed to accommodate these relative vertical movements. This design approach requires the use of ties that are flexible enough to allow relative displacements of the tie ends. In terms of flexibility, current ties can be categorized into two groups: tension-compression ties and shear ties.

Tension-compression ties are designed to withstand axial loads with little to no shear load, thus enabling vertical slip between the wythes. Within this group, two types of ties exist: flexible ties (Fig. 3-2a) and adjustable ties (Fig. 3-2b). Flexible ties have low flexural stiffness, resulting in negligible shear forces. However, adjustable ties incorporate a mechanism that facilitates vertical differential movement between wythes and, therefore has zero shear resistance. Shear ties (Fig. 3-2c) are capable of withstanding axial loads and have high shear resistance, thus restricting vertical slip between the wythes.

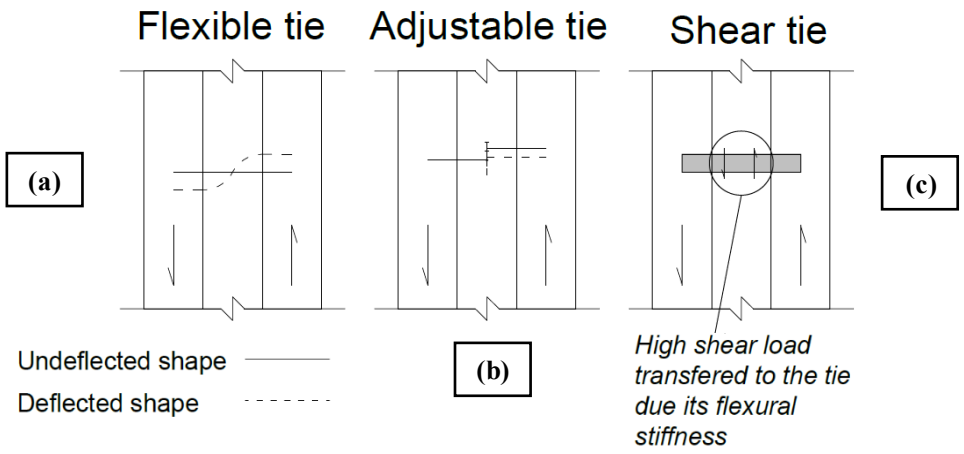

Figure 3-2. Types of ties: a) flexible tie, b) adjustable tie, and c) shear tie.

3.3.1 Corrosion Resistance

Ties and other metal elements are desirable to possess the same durability as the masonry veneer. To ensure the corrosion resistance and longevity of masonry connectors, CSA A370-14 (CSA, 2014) mandates the usage of stainless-steel connectors for masonry exceeding 13 metres in height in regions prone to high wind-driven rain. For walls under 13 metres in such areas or drier regions, hot-dipped galvanized coatings serve as the minimum acceptable corrosion protection.

Annex E of CSA A370 contains values of annual driving rain indices (aDRI) for different locations in Canada. This index is the mean annual rainfall in metres multiplied by the mean annual wind speed in metres/second. Additionally, the standard defines three levels of requirements for corrosion protection that will be used according to the use and environmental conditions outlined in Table 3-1. These corrosion protection levels encompass:

- **Level 1:** Fabricated from unprotected carbon steel or steel whose zinc coating does not meet the minimum requirements in Table 3.1.
- **Level 2:** Fabricated from carbon steel that is hot-dip galvanized after fabrication to at least the minimum requirements in Table 3-1.
- **Level 3:** Fabricated from stainless steel meeting requirements outlined in Table 3-2.

Table 3-1. Minimum level of corrosion protection for masonry connectors according to CSA A370-14 (CSA, 2014)

Connector use	Exposure environment	Type of connector	Minimum level of corrosion protection
Interior masonry	Not subject to moisture	All connectors	1
	Subject to moisture		2
Masonry below grade (in contact with ground)	Protected by waterproofing on the face in contact with the ground	All connectors	1
	Non-aggressive soils		2
	Other		3
Exterior masonry (not more than 13m above local grade)	aDRI <= 7	All connectors	2
	aDRI > 7	All connectors except anchors	2
		Anchors	2
Exterior masonry (more than 13m above local grade)	aDRI < 2.75	All connectors	2
	aDRI >= 2.75	All connectors except anchors	3
		Anchors	2

Table 3-2. Material requirements for connectors according to CSA A370-14 (CSA, 2014)

Material	Grade or type	Applicable standard
Steel wire	-	ASTM A82
Steel sheet and strip	40	ASTM A1008/A1008M, ASTM A568
Steel bars, plates, angles, etc	W	CSA G40.21
Steel bolts	A	ASTM A307
Stainless steel wire	304 or 316	ASTM A580
Stainless steel sheet	304 or 316	ASTM A240
Stainless steel sheet, strip, plate, and bar	304 or 316	ASTM A666

3.3.2 Strength and Stiffness

According to CSA A370-14, connectors should withstand loads, without allowing or restraining movement or deflection that could negatively impact the integrity or performance of the masonry. To determine the strength of the connector, an engineering analysis, testing, or a combination of both must be conducted that considers all potential

modes of failure. When accurate predictions for certain factors cannot be made, tests are required to validate the predictions.

The minimum permitted ultimate strength of a masonry tie in CSA A370-14 is 1000 N. The determination of the ultimate strength of connectors depends on whether the failure occurs in the body of the connector or the embedment, fastener, or due to buckling. For failures that occur outside the body of the connector, the strength should be considered as the minimum resistance to any of these mechanisms or a combination thereof, based on the intended service conditions.

3.3.2.1 Strength

CSA A304-14 (CSA, 2014a) specifies that the tensile and compressive strength of the ties is calculated as the lower value between the initial peak load from the load-deformation curve or the load at a 4 mm deformation of the assembly, accounting for mechanical free play. The mandated minimum strength is 1000 N, without incorporating the resistance factor.

Additionally, the application of out-of-plane lateral loads onto the cavity wall leads to tensile and compressive forces within the ties. Conventionally, tie loads have been estimated based on the tributary area around each tie, leading to predetermined restrictions on tie spacing. However, this assumption considers equal forces being resisted by all ties, which is only accurate if rigid body motion prevails within the wythes. In actual wall structures, the wythes undergo deflection, causing the force in each tie to be contingent on the stiffness and positioning of the ties and wythes.

The assumption that the force of the tie corresponds to its tributary area is applicable when dealing with backup walls that are considerably stiffer than the veneer. However, in cases where the upper portion of the veneer lacks direct support from the roof or upper floor, the top tie assumes the role of a principal support or reaction point (Drysdale and Hamid, 2005). This top tie bears a significant portion of the load carried by the external wythe. Calculations can be performed to estimate the necessary magnitude of the top tie. However, this value is influenced by factors like the height and support conditions of the wythes, the placement and strength of the top tie, its stiffness, and the level of lateral load applied directly to the backup wall. The extent of lateral load applied directly to the

backup wall hinges on the relationship between the stiffness of the backup and veneer wythes.

Drysdale and Hamid (2005) found that the distribution of the forces in the ties is highly influenced by the support conditions of the backup wall and the flexural stiffness of both the backup wall and the ties, as shown in Fig. 3-3. Results show that when ties are rigid and the backup wythe exhibits significant stiffness, the distribution of tie forces is uniform, excluding the top tie. Additionally, in scenarios where ties are more flexible, coupled with a flexible backup wythe, reduced tie stiffness results in an uneven distribution of forces, characterized by notably elevated forces in the top tie and minimal load transfer to the backup.

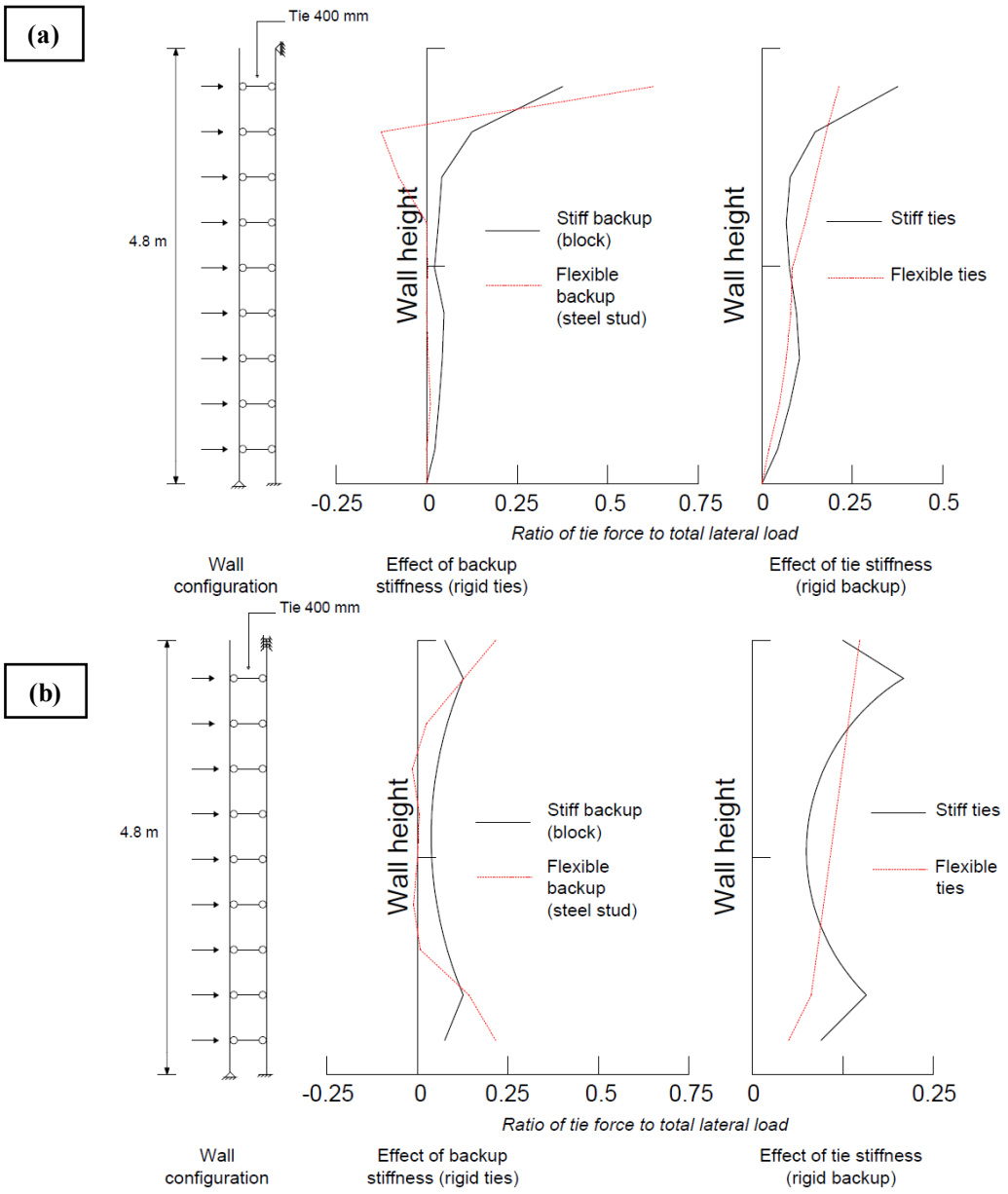

Figure 3-3. Tie forces in cavity walls for different support conditions: a) simple supported backup, and b) continuous backup (Drysdale and Hamid, 2005).

The strength of the ties must be determined by engineering analysis by testing according to CSA A370 (CSA, 2014) or a combination of both. For design, the factored resistance is defined as average strength minus 1.64 standard deviations with the result multiplied by a resistance factor ϕ applicable to the failure mode. The value of the factor for the tie's material failure is 0.9 and 0.6 for the embedment, fastener, or buckling failure. The least of these reduced capacities govern.

3.3.2.2 Stiffness

In cavity wall analysis, the assumption is made that the ties possess infinite rigidity in both tension and compression, thereby permitting the wythes to deflect uniformly (Drysdale and Hamid, 2005). This implies that the axial deformation of the ties is considerably minor in comparison to the deflection of the wythes. Nevertheless, certain flexible and adaptable ties may not adhere to this assumption.

The load distribution through the ties is heavily influenced by the support conditions of the wythes. For instance, when the wythes are independently supported at the top and bottom, the stiffness of the ties plays a significant role in load sharing. If the ties are flexible, the load transfer is minimal, whereas stiff ties enable load sharing in proportion to the stiffnesses of the wythes (Brown and Elling, 1979). Conversely, when the veneer lacks top support, the distribution of lateral load-transferring tie forces is impacted by tie stiffness, the relative stiffness of the backup wythe, and the stiffness ratio between wythes (McGinley et al., 1986).

According to CSA A370 (CSA, 2014), the mechanical play between tie assembly components must not surpass 1.2 mm and a resistance of at least 0.4 kN should be achieved within a total deformation of the tie assembly, encompassing mechanical free play, of 2 mm or less.

3.3.3 Spacing

The maximum spacing of ties within a wall is defined in both the S304-14 and A370-14 standards. For stiff backup materials like concrete and block, the feasible maximum spacing is 600 mm vertically and 820 mm horizontally. And for flexible stud backups, the typical spacing is 600 mm vertically and 410 mm horizontally. Ties are required to be positioned within 300 mm from the top of the wall and 400 mm from the base. When it comes to lateral deflection limits caused by wind load for flexible stud backups supporting veneers, the limit is span/360.

3.3.4 Thickness Requirements

The maximum thickness allowed for individual connectors is restricted by CSA (CSA, 2014) to two-thirds of the mortar joint thickness if the connector is made from round or deformed stock, or half the thickness of the mortar joint if the connector is made from

square or flat stock. Connectors with thickness exceeding these limits must be accommodated by recesses or cavities within the masonry, allowing them to be embedded in mortar or grout with sufficient coverage to achieve the required resistance.

3.3.5 Tests on Cavity Wall Ties

CSA A370-14 (CSA, 2014) proposes particular test arrangements for evaluating tension and compression resistance, as depicted in Fig. 3-4 and 3-5, respectively. The standard specifies that during the testing the materials and configuration of the specimen should be representative of the actual conditions of those that will be used in service. However, the standard does not outline a specific arrangement for conducting shear resistance tests.

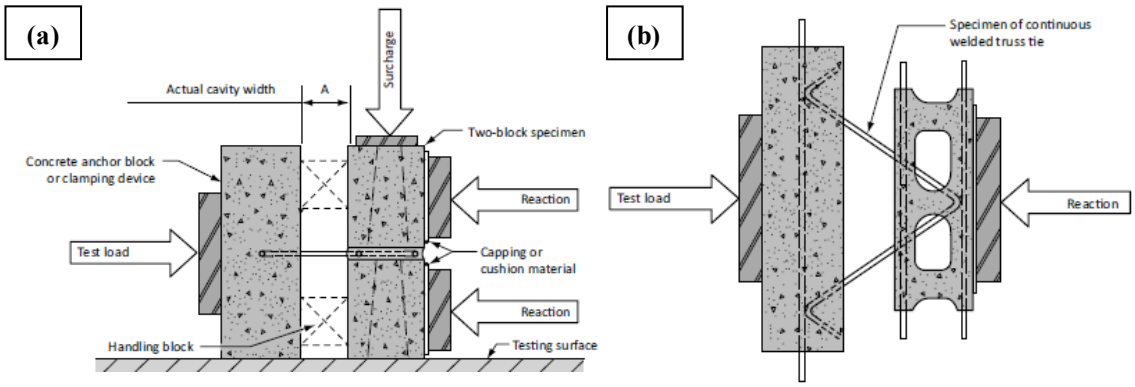

Figure 3-4. Compression tests on ties: (a) elevation view, and (b) plan view (CSA, 2014).

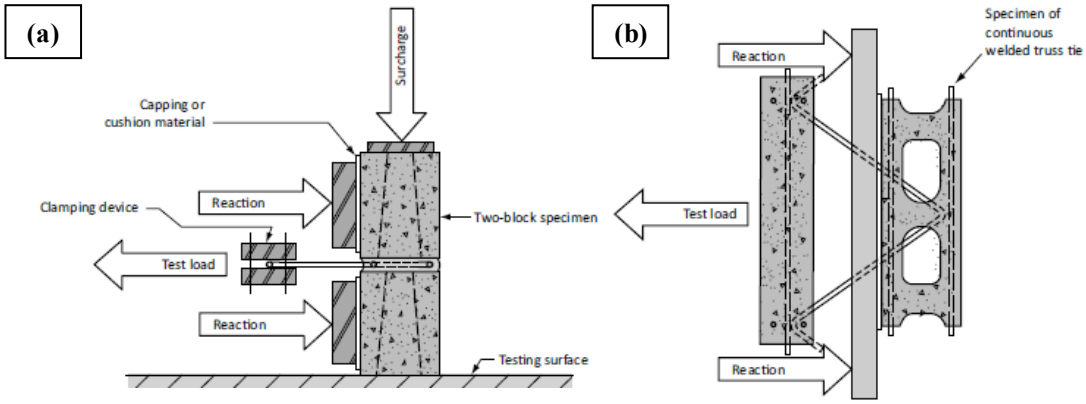

Figure 3-5. Tension test on ties: (a) elevation view, and (b) plan view. (CSA, 2014).

3.4 Thermal Considerations for Building Envelopes

The National Energy Code of Canada for Buildings (NECB, 2022) provides the energy requirements for buildings and their systems, components, and assemblies. Part 3 of the code discusses the transfer of heat and air through the building materials, components, and assemblies that comprise the building envelope. Two of the main thermal parameters of the envelope elements are the thermal transmittance (U-value) and the thermal resistance (R-value), as discussed in Chapter 2. Those parameters are calculated including insulation, sheathing, interior and exterior finish materials, and air films. Additionally, since the 2017 version of the NECB, it is required to account for the thermal bridging effect of high conductive elements that pierce the insulation layer such as masonry ties and shelf angles, that decrease the effectiveness of the insulation.

The R-value, which is the inverse of the U-value, needs to be calculated and compared with the minimum required by the standard. The code specifies the minimum U-value for building elements that comprise the building envelope based on the type of element and the geographic location. The code defines 6 zones with different values of heating degree-days (HDD). Figure 3-6 shows the map of Canada with the value of the approximate average annual heating degree-days taken at 18 °C for the different regions defined in Canada. The HDD value is used to provide the minimum U-value for the specific building according to its location. Table 3-3 shows the maximum overall thermal transmittance for the type of element (wall, floor, roof) for each climate zone.

Figure 3-6. Climate zones according to the NECB 2022 (NAIMA Canada).

Table 3-3. Overall thermal transmittance for different climate zones and types of elements according to NECB 2022. (NECB, 2022)

Above-ground opaque building assembly	Heating Degree-days of building location (°C)					
	Zone 4	Zone 5	Zone 6	Zone 7A	Zone 7B	Zone 8
	< 3000	3000 to 3900	4000 to 5999	5000 to 5999	6000 to 6999	>= 7000
	Maximum Overall Thermal Transmittance (W/m^2K)					
Walls	0.290	0.265	0.240	0.215	0.190	0.165
Roofs	0.164	0.156	0.138	0.121	0.117	0.110
Floors	0.193	0.175	0.156	0.138	0.121	0.117

The thermal resistance of the wall assembly needs to be calculated accounting for the thermal bridging, ensuring that the obtained R-value complies with the minimum required by the code. To calculate the thermal characteristics of the building envelope materials, it is necessary to evaluate them by the applicable product standards outlined in the NECB. In situations where these standards do not apply, the evaluation should follow the guidelines for steady-state measurements as stipulated in ASTM C177 or ASTM C518 standards.

The thermal properties of building assemblies, excluding fenestration and doors, should be determined through one of the following three options: theoretical calculations, 2-D or 3-D thermal modelling, or laboratory testing. The calculations should align with guidelines presented in the ASHRAE handbook (AHSRAE, 2017) or ISO 14683 (ISO, 2017a), which covers the thermal bridges, and linear thermal transmittance using the simplified methods. The laboratory testing should adhere to the specifications outlined in ASTM C1363 (ASTM, 2019) for testing the thermal performance of elements using the Hot Box apparatus. The testing conditions should include an indoor air temperature of 21±1°C and an outdoor air temperature of –18±1°C.

3.5 Conclusion

Masonry cavity walls have a dual purpose in buildings, serving to both support gravity and lateral loads and enhance thermal performance. Metal ties are commonly used to connect the wythes, which facilitate their consistent deflection and the distribution of out-

of-plane loads. These cavity wall ties are the fundamental components of these structures, and their design is governed by CSA A370-14 (CSA, 2014).

Canadian masonry standards allow for the design of cavity walls in which the wythes collaborate in resisting out-of-plane loads, but they do not consider composite action. The standard also specifies the use of ties with varying shear strength characteristics. Some ties allow for vertical displacement between the wythes and exhibit low shear strength, while others have high shear strength and restrict vertical slip between the wythes. However, all ties must possess a minimum tensile and compressive resistance of 1 kN. No minimum resistance is given for shear strength. The presence of high-shear-strength ties can impact crack propagation in the brick veneer. When vertical slip occurs, these shear ties act to restrain such movements, resulting in additional stresses within the brick veneer where the tie is embedded.

The presence of thermal bridging elements, such as masonry ties, reduces the thermal resistance (R-value) of a building envelope significantly due to the high thermal conductivity of those elements that pierce the insulation layer. Prior to the 2017 version of the NECB, the calculation of the thermal resistance of envelope walls permitted the exclusion of those structural and other thermally conductive elements that penetrated the envelopes, if they comprised less than 2% of the total wall area. However, since the 2017 version, it requires that all of these elements be included in the calculation of the R-value. The NECB code provides the minimum R-value for wall assemblies according to the geographic location of the building. The calculation of the R-value accounting for the thermal bridge effects needs to comply with these indicated by the code.

4 SHEAR RESPONSE OF INNOVATIVE AND CONVENTIONAL TIES FOR CAVITY WALL SYSTEMS

4.1 Introduction

Newer, more stringent energy regulations in Canada require more thermally resistant walls. One solution is to build wider cavities for double-wythe masonry wall systems, to accommodate thicker layers of insulation. The wider cavities require longer, specialized connectors, for which there is a scarcity of test data and design information leading to uncertainty in their structural performance, and high cost due to the desire of manufacturers to provide ample safety margins.

To understand and optimize the design of connectors for wide cavities, this chapter aims to provide experimental evidence on the longitudinal shear performance of long ties used in wider cavity walls (175 mm cavity width). Two ties are compared, a contemporary steel masonry tie and a novel tie. The novel characteristic of the latter tie is the geometry, the tie is comprised of two inclined members (Fig. 4-2). Additionally, the novel tie possesses the same thickness and material as the contemporary tie. Both ties are comprised of galvanized steel which is traditionally used in masonry ties as permitted by CSA A370-4 (2014) according to the level of exposure of the building.

The inclined connector was designed so that it would enable a larger degree of composite action between the wythes of the cavity wall than conventional connectors. Composite action, however, is not investigated in this study and remains a key topic for future studies. Composite action in cavity walls translates into the potential to reduce the thickness of the backup wythe, which may reduce wall costs significantly.

In this investigation, small-scale wall specimens were built to analyze the performance of both conventional and innovative ties, using a setup similar to previous studies in concrete and masonry systems (Naito et al., 2012; Woltman et al., 2013; Tomlinson et al., 2016; W. Choi et al., 2019; Egbon and Tomlinson, 2021; Choi and LaFave, 2004; Williams and Hamid, 2005; Zisi and Bennett, 2011; Messali et al., 2017; Arslan, O. et al., 2021; Romero and Tomlinson, 2023). The design of the conventional ties is typical of that used for wide cavities in current practice. The inclined tie is based on the tie introduced by Romero and Tomlinson (2023) in a previous investigation on tie axial

response. As discussed in Chapter 2, inclined ties achieve truss action which was found to be more efficient than only dowel action. Therefore, the novel tie used in this study is expected to achieve larger shear resistance compared with the conventional ties.

The ties were tested in 37 small-scale cavity walls under longitudinal shear. Parameters taken into account included the type of bricks used in the veneer side (clay and concrete) and the embedment length of the anchors embedded into the veneer.

4.2 Test Specimens

37 small-scale cavity wall specimens were built with nominal dimensions of $400 \times 400 \times 475$ mm (length, height, thickness) as shown in Fig. 4-1. The specimens were built by a certified mason, using two block courses in a running bond pattern for the Concrete Masonry Units (CMU) and six brick courses in a stack pattern for the veneer (Fig. 4-1a). The dimensions of the CMUs were $400 \times 200 \times 200$ mm and the dimensions of the bricks used in the veneer were $200 \times 67 \times 100$ mm. The width of the cavity between the two wythes is 175 mm, which represents 150 mm of insulation thickness and 25 mm of air gap. Typical insulation thickness ranges between 25-100 mm according to previous literature in concrete and masonry systems (Raouf and Al-Ghamdi, 2019; Luebke et al., 2023). Therefore, the cavity width of 175 mm is representative of the expected thicker insulation layer needed to meet the increasing energy requirements and to provide an investigation on the performance of the ties in these thicker cavity walls. This assembly resembles the actual construction process. No insulation was included in the specimens as it is assumed that insulation will not contribute to the lateral support as outlined in CSA A370:14 (CSA, 2014). The absence of insulation also allowed for clear observation of connector deformations. The CMU was partially grouted with coarse grout and reinforced with 1-15M (cross-sectional area of 200 mm^2) steel rebar (Fig. 4-1b), which represents the minimum reinforcement for loadbearing walls according to CSA S304-14 (CSA, 2014a). The mortar thickness in both wythes was 10 mm and made of Type S mortar. Following CSA A370-14 (CSA, 2014). A surcharge load of 500 N, representing 14 kPa was placed on top of the CMU to simulate the inner wythe carrying gravity load as specified by CSA A370-14 (CSA, 2014).

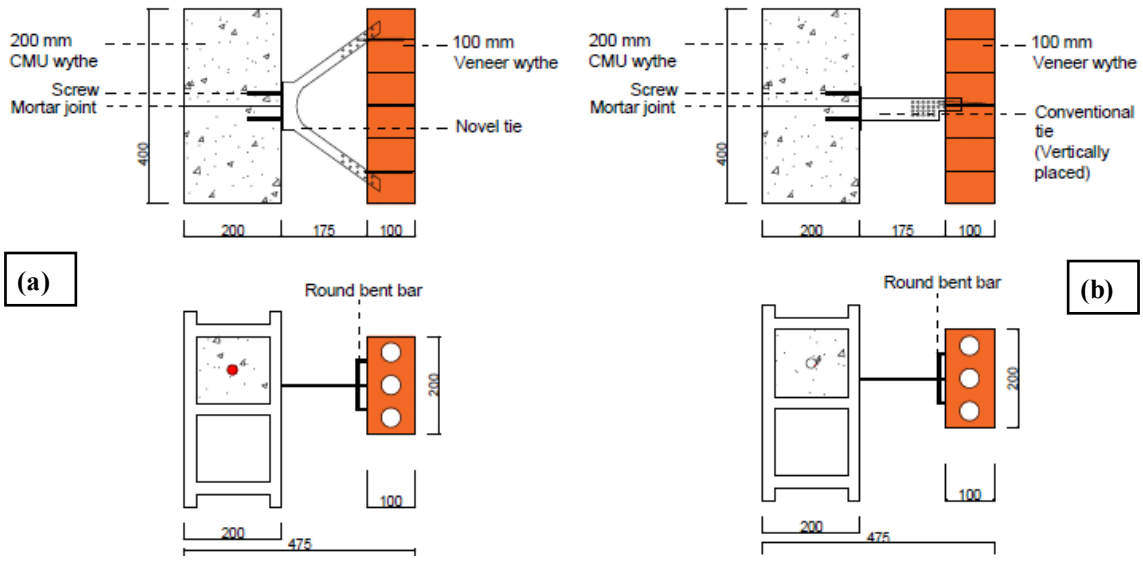

Figure 4-1. Specimen details: a) novel tie, and b) vertically placed conventional tie (dimensions in mm).

All connectors were made with a 3 mm thick, plain steel plate (Fig. 4-2). The conventional plate connectors were 50 mm wide and 229 mm long and were tested in horizontal and vertical orientations (specimens HC and VC, respectively). The width of these ties was similar to ties used in the industry (FERO, 2023). The novel connector (NC) had a V-shape and each arm was 14.7 mm wide. Figure 4-3 shows the dimensions of the embedded bent bars used in VC and NC specimens. Those bent bars were introduced in the holes in the body of the connectors and embedded in the veneer bed joints. The connectors were attached to the CMU with four Tapcon screws (Fig. 4-3b) of 69 length and 6.3 mm diameter. On the veneer side, slots were drilled to reduce the volume of material which reduces the self-weight and the thermal conductivity. Those holes also serve as an attachment point for the 4.8mm round bent bars embedded in the brick veneer (Fig. 4-4).

The vertically placed conventional ties had one round bent bar attached, the novel ties had two bent bars attached through the slots, and the HC connectors were embedded in the veneer but no embedded bars were used in these connectors for constructability reasons. The novel connector had a 36° inclination ensuring that pre-cut slots align with a mortar joint in the brick wythe.

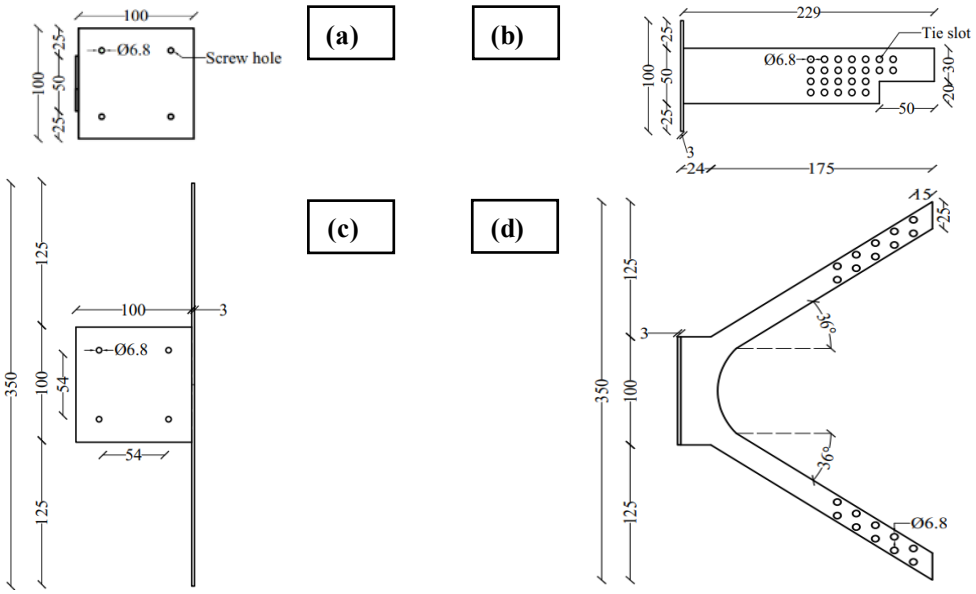

Figure 4-2. Connectors under study. Conventional Connector: a) Back view. b) Side view. Novel Connector: c) Back view. d) Side view.

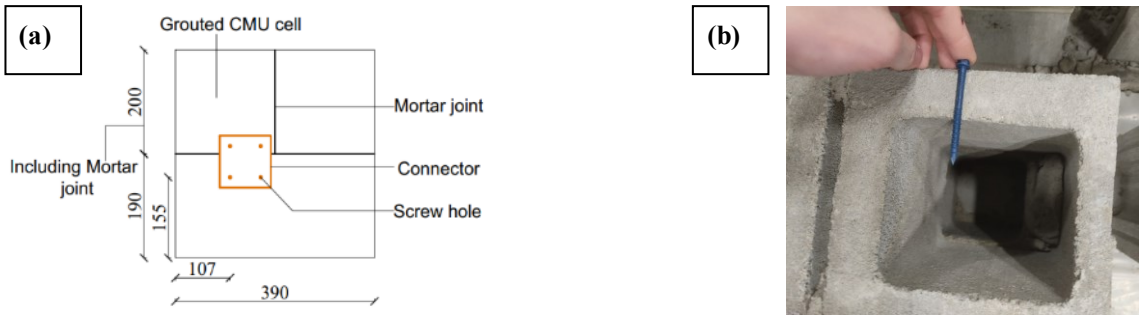

Figure 4-3. Embedded bar dimensions a) General dimensions. b) Bar sample.

Figure 4-4. Screws holding connectors to CMU. a) Specimen dimensions. b) Screw sample.

4.3 Test Matrix

Thirteen types of specimens were tested with two to four repetitions for each type, for a total of 37 specimens (Table 4-1). The specimens with the horizontal conventional connector were identified with a two-digit code, while the vertical conventional connector and the novel connector were identified using a three-digit code. The first two characters represent the type of connector of the specimen (HC: Horizontal Conventional Connector, VC: Vertical Conventional Connector, NC: Novel Connector), the third and fourth characters represent the type of brick used in the veneer of the specimen (CL: Clay brick, CN: Concrete brick), and the fifth and sixth characters represents the embedment length of the embedded bars used in each specimen (45: 45 mm of embedment length, 60: 60 mm of embedment length, 75: 75 mm of embedment length). The specimens with the HC connector did not have embedded bars, and therefore they only have the first two-digit code.

Table 4-1. Specimen configuration matrix.

Specimen	Brick	Connector type	Embedment length, mm	Number of specimens
HC-CL	Clay	Horizontal Conventional Connector	-	2
HC-CN	Concrete			2
VC-CL-45	Clay	Vertical Conventional Connector	45	3
VC-CN-45	Concrete			3
VC-CL-60	Clay		60	3
VC-CN-60	Concrete			3
VC-CL-75	Clay		75	4
VC-CN-75	Concrete			3
NC-CL-45	Clay	Novel Connector	45	3
NC-CN-45	Concrete			2
NC-CL-60	Clay		60	3
NC-CN-60	Concrete			3
NC-CL-75	Clay		75	3

4.4 Specimen construction

All the specimens were built following established masonry construction practices in Canada. Initially, the concrete masonry unit (CMU) wythes were built (see Fig. 4-5a),

and one cell within each CMU was filled with coarse grout (Fig. 4-5b). Within each grouted cell, 1-15M reinforcing steel was inserted (Fig. 4-5c). After the grout had cured, holes were pre-drilled followed by the installation of screws and connectors (Fig. 4-5de). Subsequently, the veneer wythes were built (Fig. 4-5f), and the respective round bent bars were introduced into the VC and the NC connectors, embedding them within the veneer (Fig. 4-5g). For curing, specimens were covered with polypropylene sheets, and water was applied during the initial 7 days of curing (Fig. 4-6ab). Afterward, specimens were allowed to air cure until reaching 28 days, at which point they were subjected to testing.

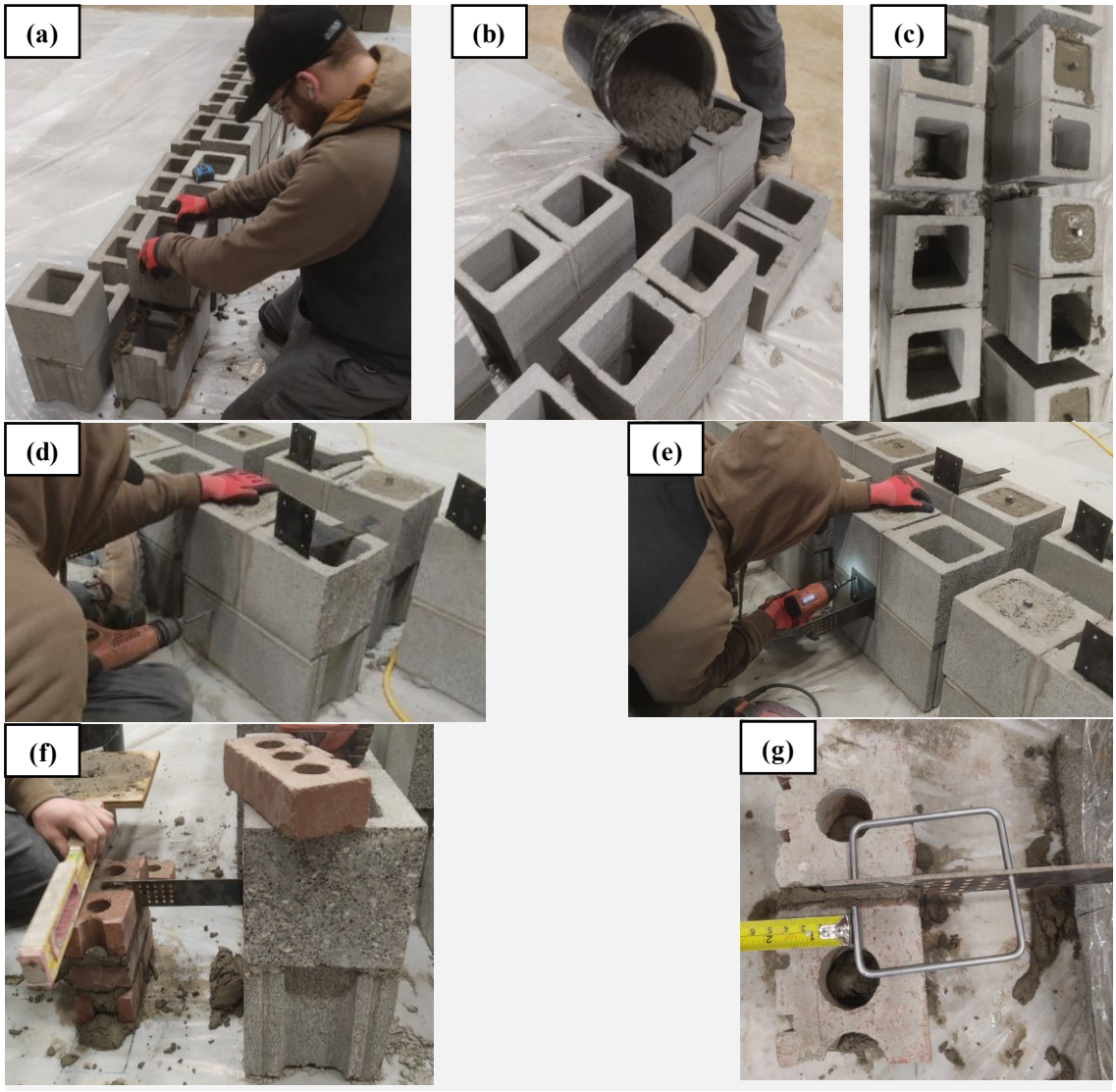

Figure 4-5. Specimen Construction: a) CMU, b) filling CMU with grout, c) longitudinal reinforcement, d) predrilling CMUs, e) screwing CMUs, f) veneer, and g) round bent bar.

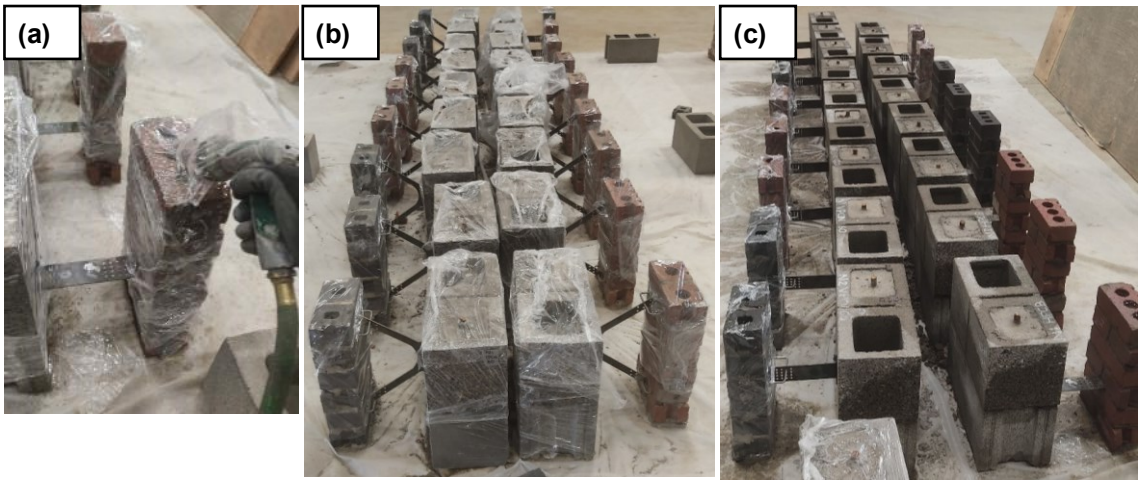

Figure 4-6. Specimen curing: a) spraying water on the veneer, b) specimens covered with polypropylene, and c) specimens after curing.

4.5 Material Properties

4.5.1 Mortar and Grout

Type S mortar was used in the construction of the wall specimens. To determine the compressive strength of the mortar, a total of six mortar cubes with dimensions $50 \times 50 \times 50$ mm, were subjected to crushing under axial load following the guidelines outlined in CSA A179-14 (CSA, 2019). The test outcomes, detailed in Table 4-2, revealed that the mean strength after 28 days was 16.8 MPa. These tests were performed by Gonzalez (2022), and the results apply to this study as the grout and mortar tested were from the same batch as the ones used in this study.

Table 4-2. Test results on mortar cubes performed by Gonzalez (2022).

ID	Peak load, kN	Strength, MPa
1	43	17.3
2	40	16.1
3	42	16.8
4	41	16.5
5	44	17.5
6	42	16.8
Average (MPa)		**16.8**
COV (%)		**2.75**

A course grout, designed to meet a specific strength requirement of 20 MPa, was used to fill the reinforced cells during wall construction and the hollow cells during prism construction. For assessment purposes, samples of the grout mixture were used to cast four cylinders measuring 200×200 mm each, and these cylinders were subjected to concentric axial loading as per CSA A179 standards. As detailed in Table 4-3, the test outcomes revealed an average compressive strength of 24.9 MPa after 28 days.

Table 4-3. Test results on grout cylinders performed by Gonzalez (2022).

ID	Peak load, kN	Strength, MPa
1	210	26.7
2	189	24
3	187	23.7
4	198	25.2
Average (MPa)		**24.9**
COV (%)		**4.72**

4.5.2 Masonry Units

Three types of masonry units were used in this project: hollow concrete blocks (Fig. 5-7a) for the construction of the CMUs, and solid clay (Fig. 5-7b) and solid concrete (Fig. 5-7c) bricks used in the construction of the veneers. The CMU used was a 20 cm block, which is common in current construction. The nominal compressive strength was 15 MPa. Concerning the concrete blocks, grouted and ungrouted prisms were tested in accordance with CSA A165.1 (CSA, 2019), and the averaged 28-day compressive strengths of 21.5 MPa and 16.6 MPa, respectively. The weight of the clay and concrete bricks were 17.0 N and 17.5 N, respectively.

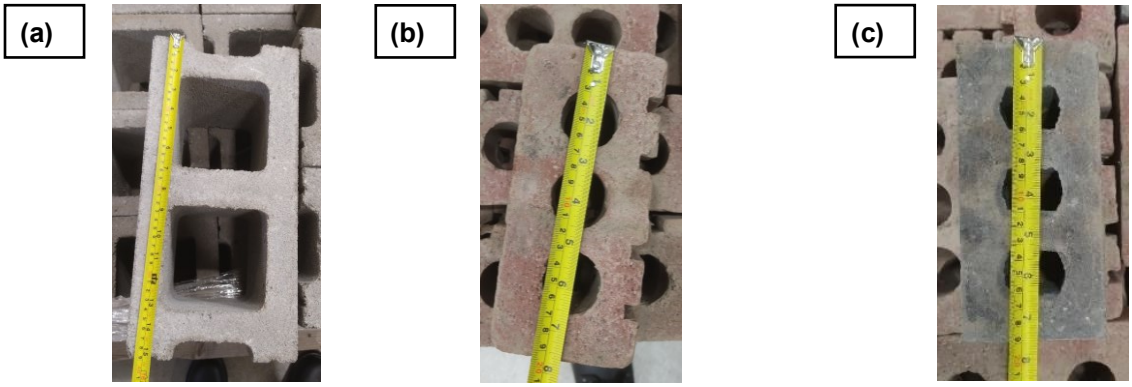

Figure 4-7. Masonry units: a) concrete masonry unit, b) clay brick, and c) concrete brick.

4.5.3 Steel

4.5.3.1 Longitudinal Steel

The vertical steel reinforcement used in the specimen construction consisted of Grade 400 bars in 15M (area of 200 mm^2) size. Three 600 mm long bar samples were subjected to tension tests, adhering to the guidelines outlined in ASTM A615. The test outcomes, as presented in Table 4-4, revealed an average yield strength (f_y) of 429 MPa and a modulus of elasticity (E_s) of 193 GPa. Tests on the longitudinal reinforcement were performed by Gonzalez (2022), and the results apply to this study since the steel used was from the same batch.

Table 4-4. Test results from steel rebar coupons performed by Gonzalez (2022).

ID	Yield Strength, MPa	Elastic Modulus, GPa
1	426.0	187.1
2	432.1	196.0
3	429.0	197.2
Average (MPa)	**429.0**	**193.4**
COV (%)	**0.6**	**2.1**

4.5.3.2 Steel of ties and bent bars

Table 4-5 shows the yield stress and elastic modulus of the steel used in the bent bars and the ties. Figure 4-8 shows the respective strain stress curves of the steel. The samples of

the steel used in the ties (Fig. 4-9a) and the steel of the bent bars (Fig. 4-9b) were tested in the setup shown in Fig. 4-10.

Table 4-5. Yield stress and elastic modulus of steel used in bent bars and ties.

	Static Yield Stress, MPa		Elastic Modulus, MPa	
ID	bent-bar	Tie	bent-bar	Tie
1	590.0	236.0	193480.0	199126.7
2	597.0	240.0	198100.0	181161.3
3	593.0	225.0	188566.7	203760.0
4	580.0	230.0	208313.3	183950.0
5	574.0	238.0	198507.1	201080.0
Avg	**586.8**	**233.8**	**197393.4**	**193815.6**
COV (%)	**8.5**	**5.5**	**6545.4**	**9352.3**

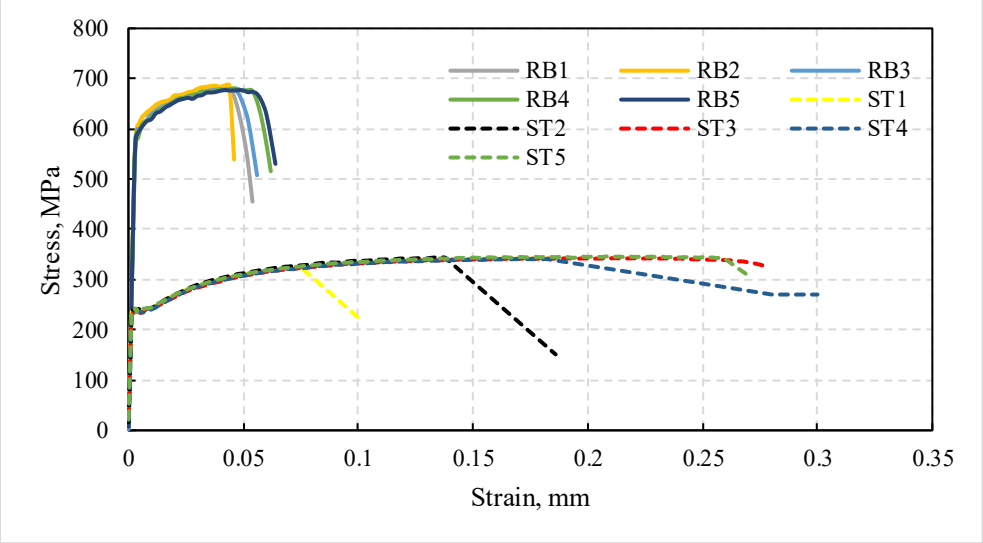

Figure 4-8. Stress-strain response of steel used in the ties (ST) and round bent bars (RB).

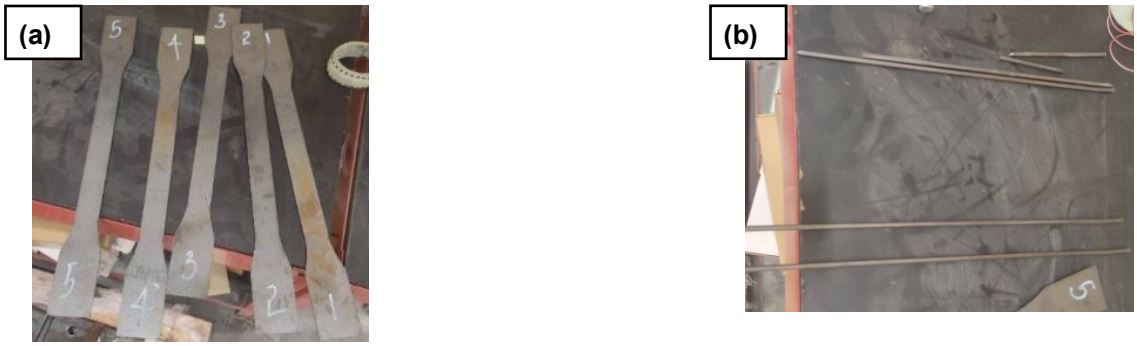

Figure 4-9. Steel samples for testing: a) steel of ties, and b) steel of round bent bars.

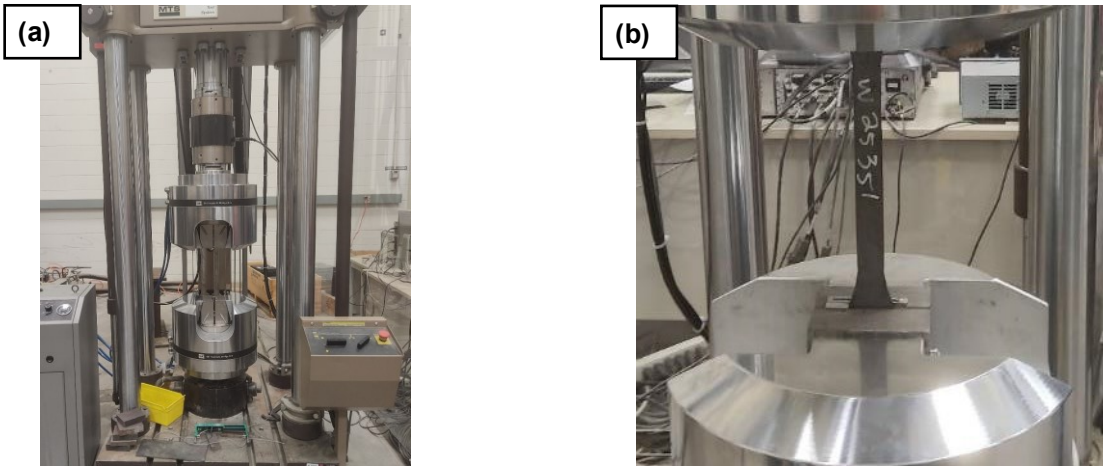

Figure 4-10. Steel testing setup: a) testing setup, and b) steel of the ties under testing.

4.6 Experimental Setup

The experimental setup used in this study is depicted in Fig. 4-10. It comprised a 529 kN hydraulic actuator used for applying pressure onto the veneer, with a wooden spreader positioned atop the veneer. The steel frame included an opening at its base to allow for vertical deflection of the veneer, and this frame was supported by two steel components, which, in turn, were situated on a steel platform. The concrete masonry unit (CMU) was positioned on a specialized steel frame designed for this purpose, and the CMU was horizontally clamped to the frame to prevent any displacement while the veneer underwent loading (Fig 4-11a).

To prevent any rotation of the veneer and replicate the shear load, two wooden blocks were inserted between the CMU and the veneer (Fig. 4-11a), similarly as in previous studies (Williams and Hamid, 2005). Preliminary testing showed rotation of the veneer during loading. To solve this, two wood spacers were included in the testing frame to confine the veneer and prevent its rotation while applying the load. Additionally, Teflon strips were placed at the contact surface between the wood spacer and the veneer to reduce friction during the application of the load. To replicate the gravity load in the CMU

backup, a surcharge load equivalent to 10 kPa, was applied on top of the blocks (Fig. 4-11a).

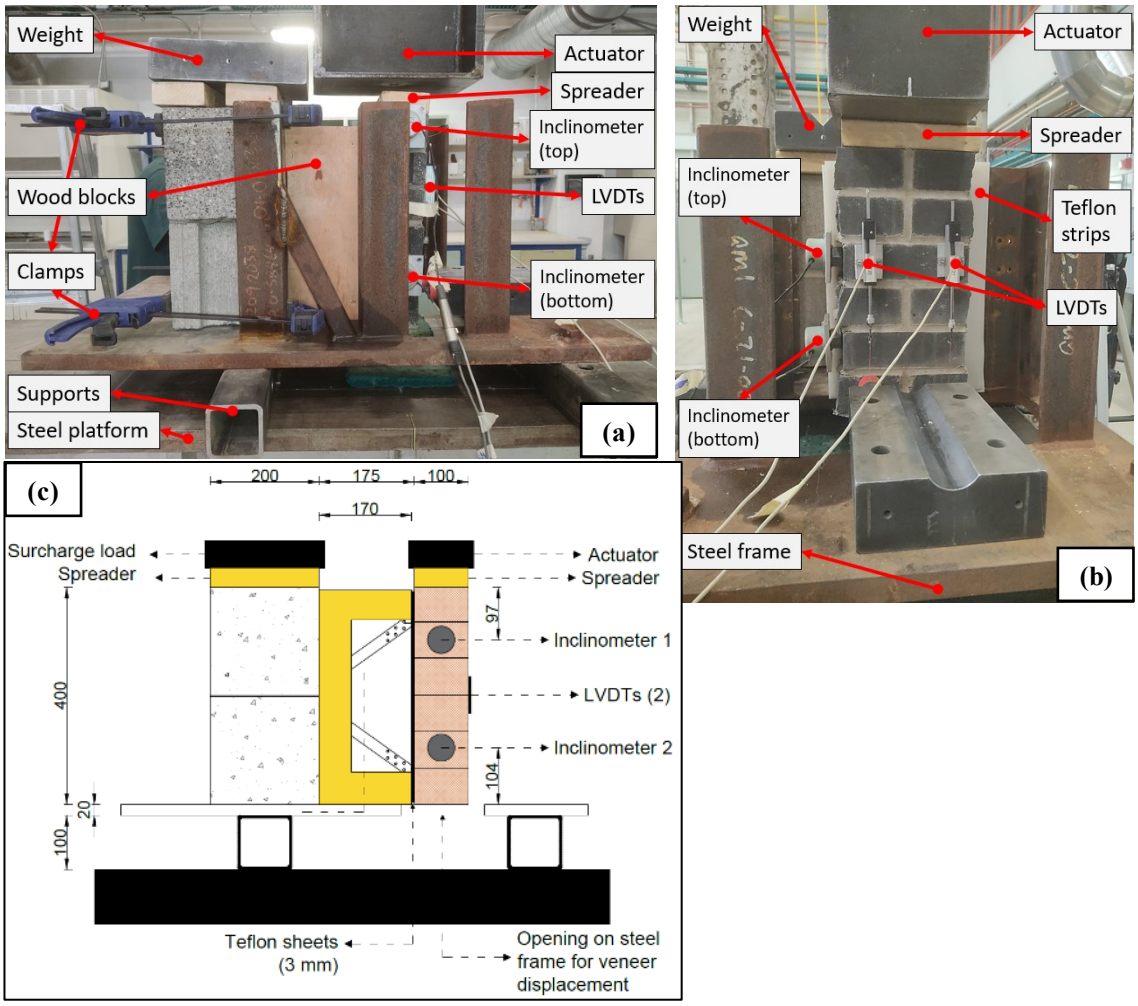

Figure 4-11. Test setup: a) side view, b) front view, and c) schematic diagram of test frame (side view).

4.7 Instrumentation

To measure the vertical displacement of the veneer, two 50 mm Linear Variable Differential Transformers (LVDT) were installed in the external face. The reported displacement measurements were obtained by taking the average of the two LVDT readings. The rotation of the veneer was measured using two inclinometers on one side

of the veneer, to measure the inclination on the top and the bottom. The location of the instrumentation in the setup is shown in Fig. 4-11.

4.8 Testing Procedure

The specimens were tested by applying the load on top of the veneer with the hydraulic press with a loading rate of 3 mm/min, until the load dropped suddenly, when the connectors deformed more than 50 mm without change in magnitude or when the specimen collapsed.

4.9 Results and Observations

The displacements and forces were obtained through the LVDTs and load cells, respectively. Rotation at the top and bottom of the veneers was obtained with inclinometers.

The load-displacement response of the specimens under the shear load is presented in Table 4-6. The table shows the summary of the average peak load from test results for each of the thirteen types of specimens, including the self-weight of the veneer (0.102 kN for clay, and 0.105 kN for concrete bricks).

The initial flexural stiffness of the tie, k, shown in Table 4-6 follows the secant method as used in previous studies (Egbon and Tomlinson, 2021). Stiffness was calculated using load and displacement values at 40 and 10% of the peak load ($P_{U40\%}$, $P_{U10\%}$, $d_{U40\%}$, $d_{U10\%}$), as shown in Equation 4-1. When $P_{U40\%}$ was greater than the proportional limit, the proportionality limit was used as the value for $P_{U40\%}$.

$$k = \frac{P_{U40\%} - P_{U10\%}}{d_{U40\%} - d_{U10\%}} \quad \textbf{(4-1)}$$

Table 4-6. Average response of the specimens at load peak.

ID	Proportional Limit (PL)				Peak Load				Initial Stiffness		
	Load, kN	Mean Load, kN	Std, kN	δ, mm	Load, kN	Mean Load, kN	Std, kN	δ, mm	Stiffness, kN/mm	Mean, kN/mm	Std, kN/mm
	-			-	-			-			
HC-CL	0.13	0.14	0.02	0.5	0.65	0.60	0.07	40.0	0.27	0.29	0.03
	0.16			0.5	0.55			42.5	0.31		
	-			-	-			-	-		
HC-CN	0.23	0.20	0.04	0.5	0.80	0.68	0.17	29.0	0.46	0.40	0.08
	0.17			0.5	0.57			48.5	0.34		
	0.35			0.5	1.59			26.0	0.71		
VC-CL-45	0.20	0.24	0.10	0.5	1.98	1.67	0.27	21.0	0.41	0.48	0.21
	0.16			0.5	1.45			24.0	0.32		
	0.22			0.5	1.75			21.0	0.45		
VC-CN-45	0.24	0.24	0.01	0.5	1.63	1.77	0.15	12.0	0.50	0.50	0.05
	0.25			0.5	1.92			29.0	0.54		
	0.18			0.5	1.59			35.5	0.40		
VC-CL-60	0.14	0.16	0.02	0.5	1.53	1.63	0.12	44.5	0.29	0.34	0.06
	0.16			0.5	1.76			46.5	0.32		
	0.27			0.5	1.74			39.0	0.59		
VC-CN-60	0.35	0.25	0.11	0.5	1.92	1.80	0.10	31.0	0.70	0.52	0.22
	0.14			0.5	1.75			15.0	0.27		
	0.39			0.5	1.81			45.0	0.78		
VC-CL-75	0.10	0.28	0.13	0.5	1.93	1.71	0.27	50.0	0.19	0.55	0.27
	0.37			0.5	1.32			23.5	0.73		
	0.25			0.5	1.80			15.5	0.51		
	0.31			0.5	1.75			46.0	0.62		
VC-CN-75	0.19	0.22	0.08	0.5	1.99	1.86	0.12	43.5	0.37	0.44	0.15
	0.16			0.5	1.85			41.5	0.33		
	1.27			1.5	4.36			23.0	0.96		
NC-CL-45	0.33	0.79	0.47	0.5	3.68	4.01	0.34	23.0	0.66	1.05	0.45
	0.77			0.5	4.00			31.0	1.54		
	0.26			0.5	5.14			33.5	0.52		
NC-CN-45	-	0.42	0.22	-	-	4.44	1.00	-	-	0.83	0.44
	0.57			0.5	3.73			24.5	1.14		
	1.11			2.5	4.21			33.0	0.47		
NC-CL-60	0.15	0.50	0.53	0.5	4.35	4.21	0.15	30.5	0.30	0.42	0.10
	0.25			0.5	4.06			31.0	0.49		
	1.96			2.0	4.67			37.0	1.12		
NC-CN-60	0.19	0.77	1.03	0.5	4.87	4.51	0.47	31.5	0.37	0.61	0.44
	0.17			0.5	3.98			29.5	0.34		
	1.63			4.0	4.97			42.0	0.45		
NC-CL-75	1.41	1.93	0.71	2.0	3.32	4.44	0.97	25.5	0.79	0.62	0.17
	2.73			4.5	5.03			21.0	0.62		

δ: displacement at the specific load. Std: Standard deviation.

Table 4-6 shows the peak load for all the specimens. The orientation of the conventional tie changes its moment of inertia about the shear load, and this influences the shear resistance of the specimens with conventional ties. The VC tie had a larger moment of inertia and the average shear strength was 1.7 times larger than the HC tie specimens. The NC tie with the largest inertia, reached 6.7 and 2.5 times the peak load of the HC and VC ties, respectively. Another reason for the larger strength of the NC connectors is the better utilization of material, as with this truss geometry it has a member that is in compression

(top plate) and the other working in tension (bottom plate) attached to embedment ties that provide additional resistance. In terms of the type of brick, the specimens with concrete brick reached 1.1, 1.1, and 1.1 times the peak load reached by those with concrete bricks for the HC, VC, and NC ties, respectively. In terms of embedment length, increasing from 60 to 75 mm increased the peak load 1.0 and 1.1 times for both VC and NC ties, respectively.

Table 4-6 also shows the initial flexural stiffness of the specimens. The average stiffness of the HC, VC, and NC ties was 0.34, 0.47 and 0.71 kN/mm, respectively. The stiffness of the NC tie was 2.05 and 1.5 times larger compared with the HC and NC ties, respectively. In terms of the type of brick, the stiffness was larger for concrete brick than those for clay brick. On average, the stiffness of the HC, VC, and NC ties with concrete brick was 1.37, 1.07, and 1.03 larger than those with clay brick. In terms of embedment length, the largest stiffness for the VC and NC ties was achieved with 75 and 45 mm of embedment length, respectively.

Variations seen in specimens of the same type were similar to those observed in previous shear tests (Martins et al., 2017, Williams and Hamid 2005), and largely attributed to material variability and construction tolerances.

4.9.1 Load-Deformation relationship

The response of all the tests was divided into three stages (Fig. 4.12). The first stage occurred between the beginning of the loading and the proportional limit, the point where the relationship between the variables becomes nonlinear. After this point, the response was nonlinear due to the development of cracks in the bed joints. The second stage occurred after the proportional limit, where the response had a lower slope, indicating a reduction in stiffness. In this stage, some load drops were observed, which can be attributed to the formation of the cracks. The third and final stage began with the attainment of the peak load, followed by a load drop until the delamination of the mortar joint of the veneer closer to the tie or in some cases until the collapse of the veneer.

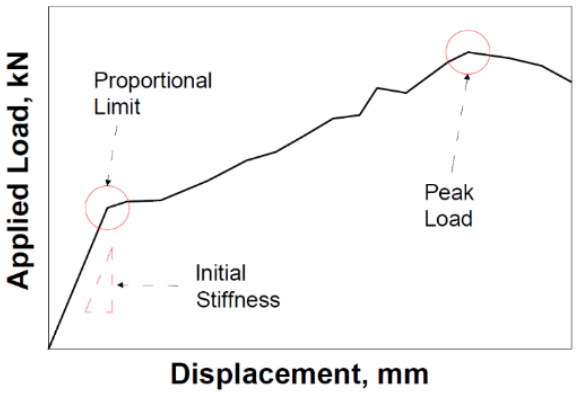

Figure 4-12. Illustration of initial stiffness, proportional limit, and peak load.

Figure 4-13 shows the average load-displacement relationship for the three ties. The displayed specific load-displacement responses of the specimens are shown separately for each tie in Fig. 4-14.

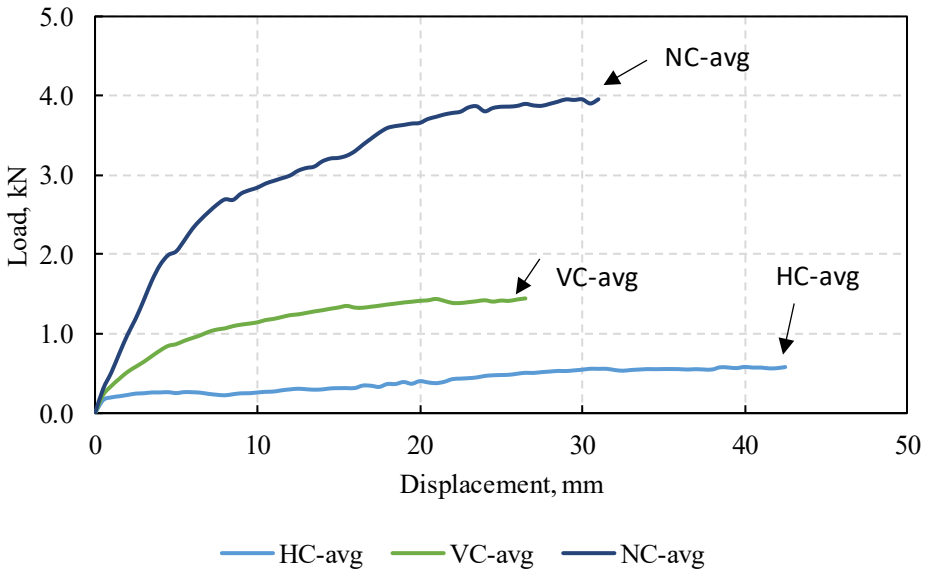

Figure 4-13. Average Load-displacement response of the studied ties under shear load.

Figure 4-14 shows the response of the horizontal conventional connector (HC) (Fig. 4.14a) for clay brick, concrete brick, and the average of the tie. Additionally, the response of the specimens with vertical conventional connector (VC) with clay (Fig. 4.14b) and concrete (Fig. 4.14c) is shown. Finally, the response of the novel connector (NC)

specimens with clay (Fig. 4.14d) and concrete bricks (Fig. 4.14e) is shown. The individual plots for tests are shown in Appendix A.

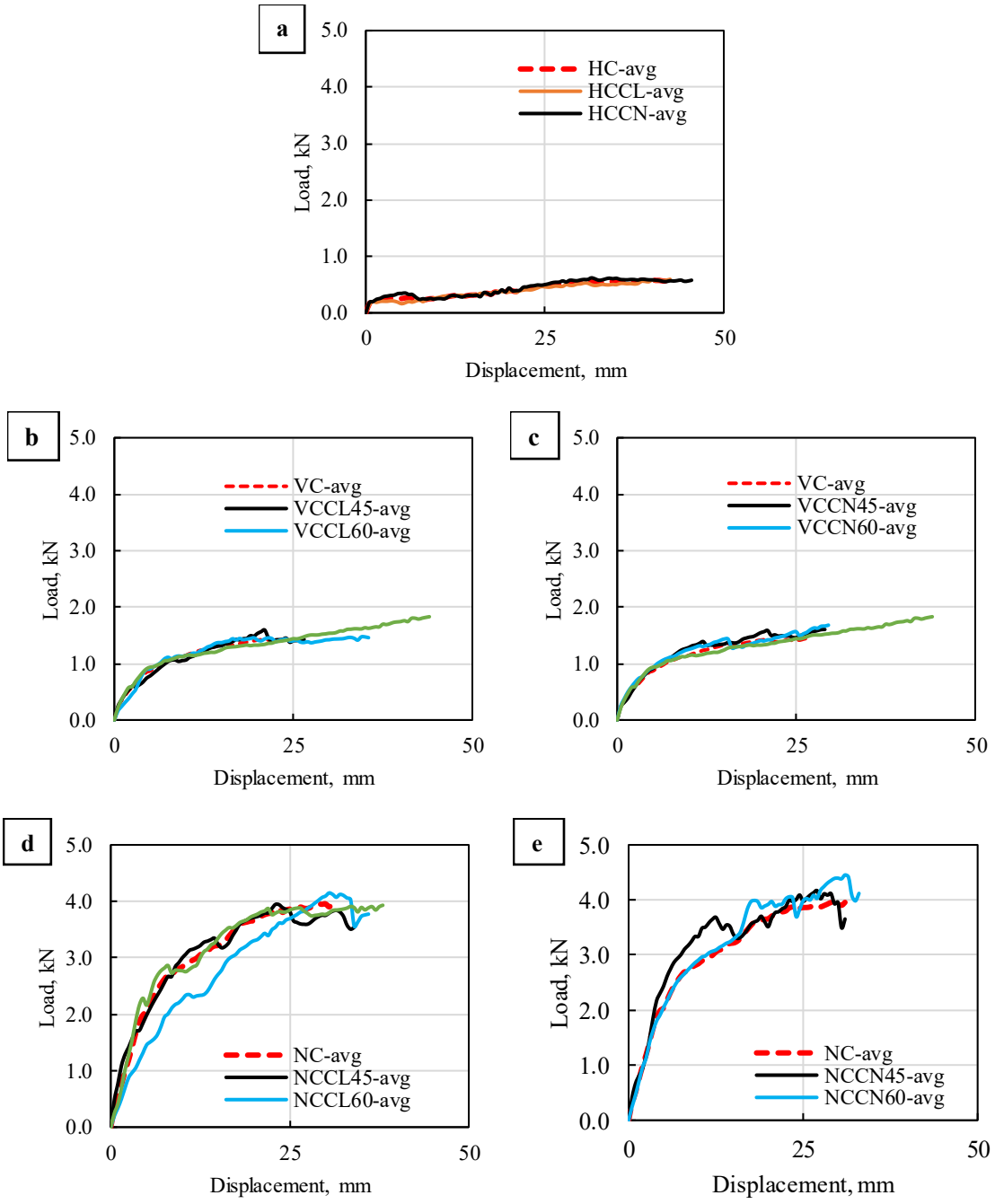

ss

Figure 4-14. Load-displacement response of ties under shear load for each tie: a) HC tie, b) VC clay brick, c) VC concrete brick, d) NC clay brick, and e) NC concrete brick.

4.9.2 Failure modes

Inspections were carried out on the specimens during and after the tests. For specimens with horizontal (HC) and vertical (VC) conventional connectors (Fig 4-15), cracks were initiated at the mortar joint of the veneer wythe hosting the connector. It then transitioned to failure of the connector due to yielding. For the NC connector (Fig. 4-16), failure was initiated by buckling of the compression member (top plate), followed by a pullout of the attached round bent bar attached to the tension member (bottom plate). The final failure for all specimens was delamination of the mortar joint in the veneer wythe and/or collapse of the veneer wythe. For specimens with concrete bricks, crack propagation from the veneer bed joint where the connector was inserted to the exterior of the veneer occurred in the later stage of testing, which may be attributed to the higher bond strength developed from the deeper and wider frogs present in the concrete veneer (Madhava et al., 1996).

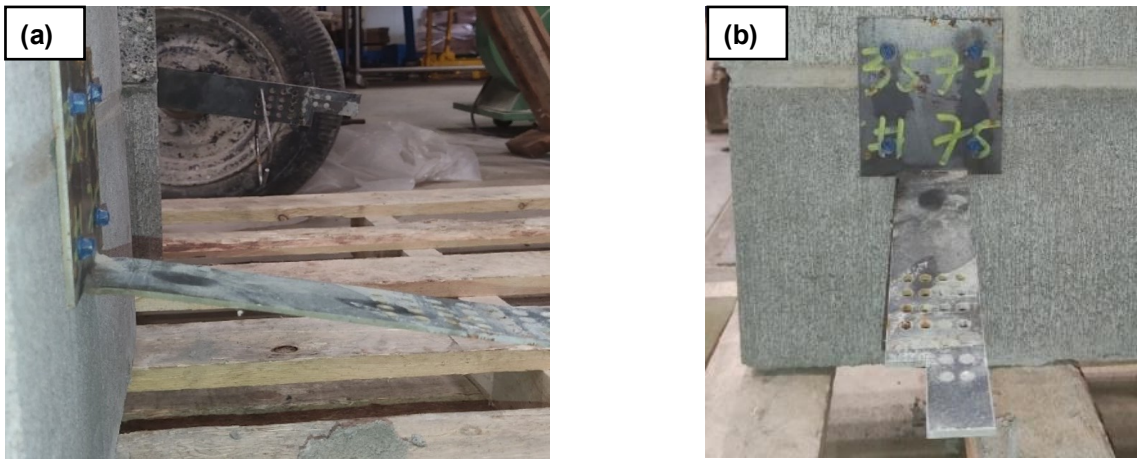

Figure 4-15. Deformed shape of the HC connector: a) Side view. b) Front view.

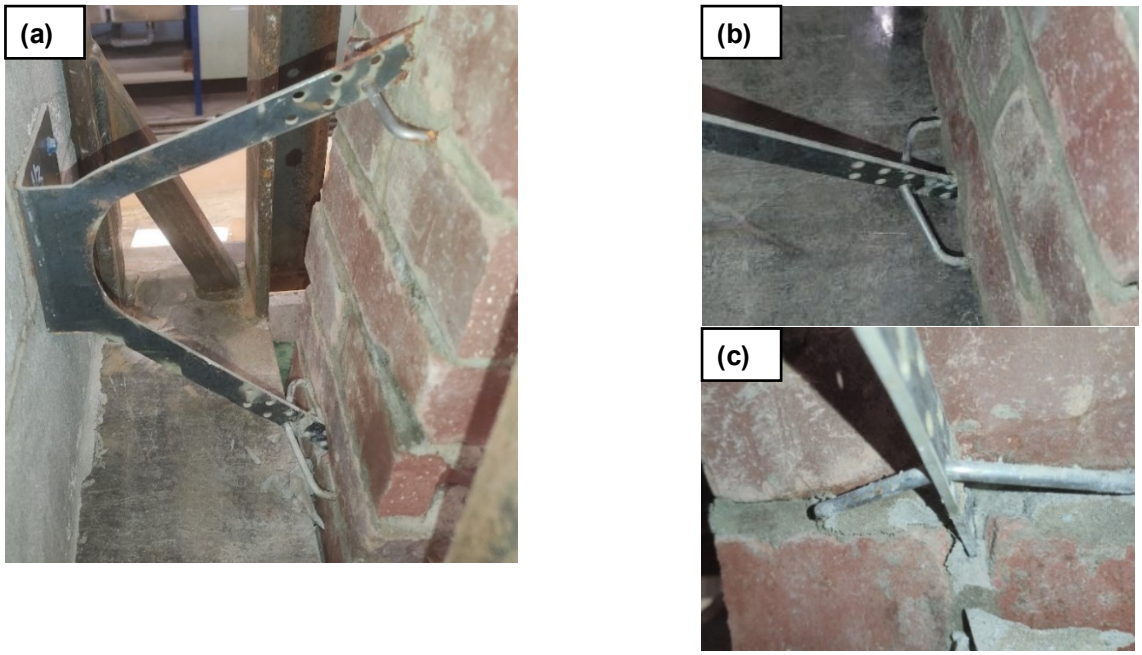

Figure 4-16.Deformation of NC connector (75 mm embedment): a) specimen before the test, b) bottom plate pull-out, and c) embedded bar.

4.9.2.1 Horizontal conventional tie

The horizontal conventional connector was tested using four specimens, two specimens with clay brick veneer and two with concrete brick veneer. In some of the specimens, cracks were formatted during the transportation process. Figure 4-17 shows the failure process of two specimens with HC tie. Figure 4-17a shows the specimen before the test, Fig. 4-17b shows the formation of cracks in the veneer during the loading, and Fig. 4-17c shows the deformation of the tie after the test.

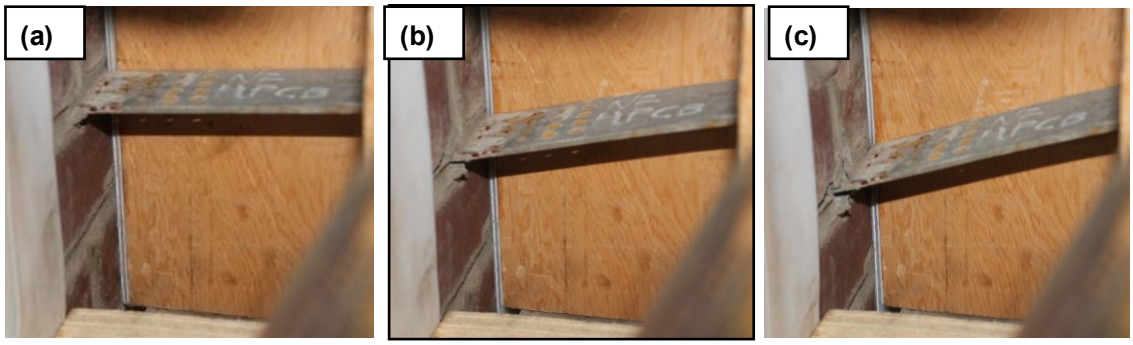

Figure 4-17. Failure process of horizontal tie specimens (clay brick): a) specimen before the test, b) formation of cracks, and c) maximum deformation of the tie.

4.9.2.2 Vertical conventional tie

The vertical conventional connector (VC) was tested using 19 specimens, 6 specimens using 45 mm embedment length and the two types of brick, 6 specimens with 60 mm embedment length and the two types of brick, and 7 specimens with 75 mm embedment length and the two types of brick.

The failure process of the specimens with VC ties consisted of the formation of cracks in the veneer and then transitioned to yielding of the connector during the loading. Additionally, in an early stage, the top corner of the plate screwed to the CMU presented a deformation (Fig. 4-18b), then the tie continued yielding until the end of the test. In some cases, until the collapse of the veneer (Fig. 4-18c).

Figure 4-19 shows the failure process of specimens with VC tie, clay brick, and 45 mm of embedment length. The specimen before the test (Fig 4-19a), the formation of cracks during the test (Fig. 4-19b), and the deformed tie after the test (Fig. 4-19c) are shown.

Figure 4-20 shows the exterior face of the veneer before the test (Fig. 4-19a) and after the test (Fig. 4-20b) exhibiting the cracks in the bed joints close to the tie, after the test. Additionally, Fig. 4-21 shows the VC tie in the area of the plate screwed to the CMU, before (Fig. 4-21a) and the deformation after the test (Fig. 4-21b).

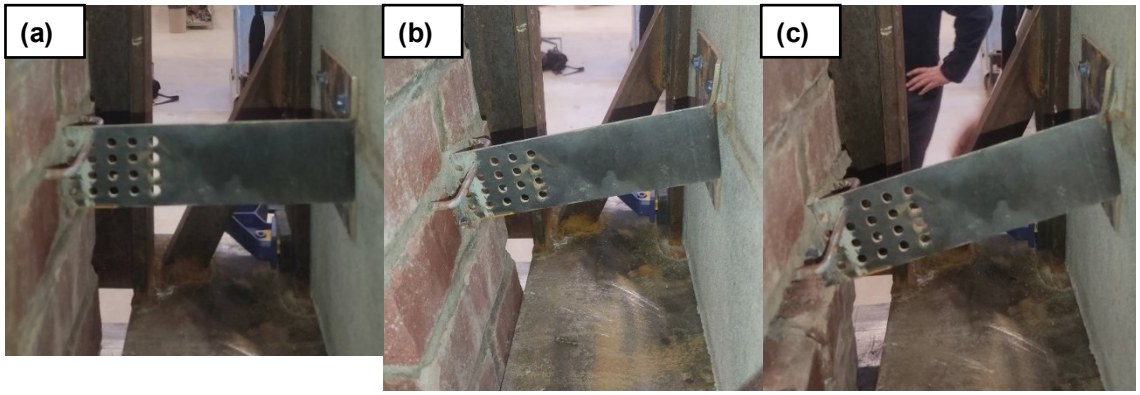

Figure 4-18. Failure of VC tie (75 mm embedment): a) specimen before test, b) deformation of tie, and d) collapse of veneer.

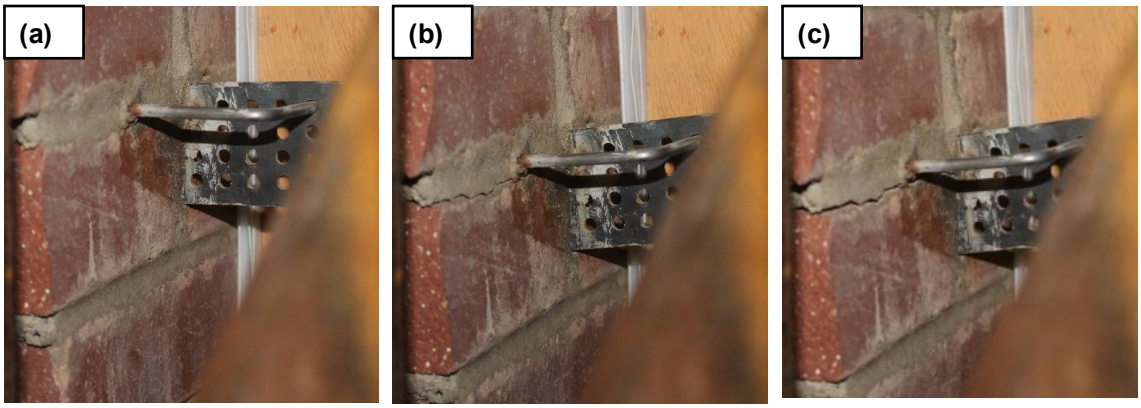

Figure 4-19. Failure process of a vertical tie (45 mm embedment length): a) connector before the test, b) formation of cracks, and c) maximum deformation of the connector.

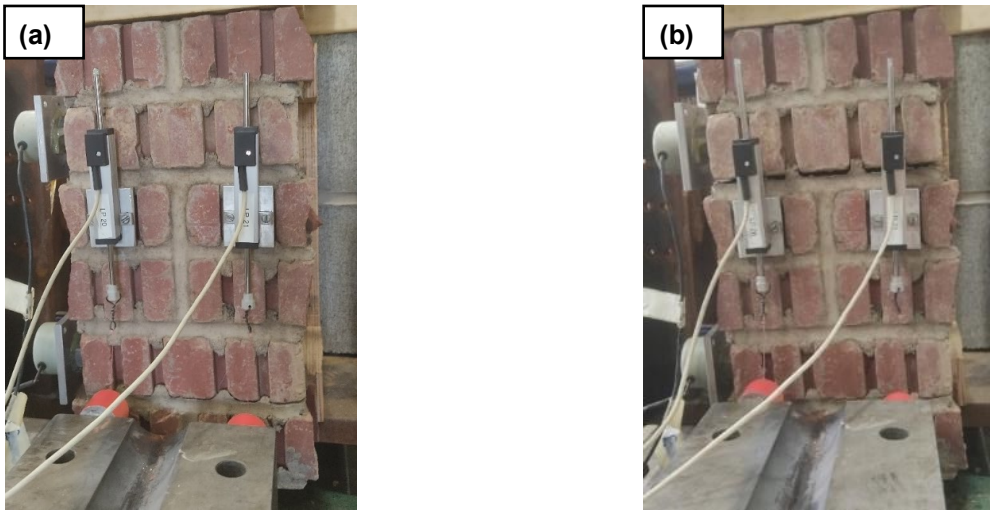

Figure 4-20. External face of veneer (VC tie) (45 mm embedment): a) early stage of test, and b) cracks on the specimen after the test.

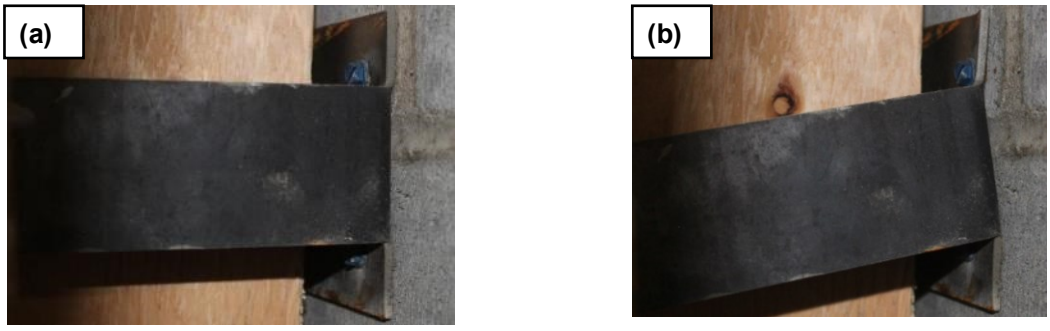

Figure 4-21. Deformation of plate screwed to CMU (VC tie) (45 mm embedment): a) tie before the test, and b) connector after the test.

4.9.2.3 Novel tie

The novel connector (VC) was tested using 14 specimens: six specimens using 45 mm embedment length and the two types of brick, six specimens with 60 mm embedment length and the two types of brick, and three specimens with 75 mm embedment length and the two types of brick.

The deformation of the NC tie specimens was characterized by the compression of the top member of the tie (Fig. 4-22), then it transitioned to pull out of the round bent bar attached to the bottom member from the veneer (Fig. 4-23) until the end of the test.

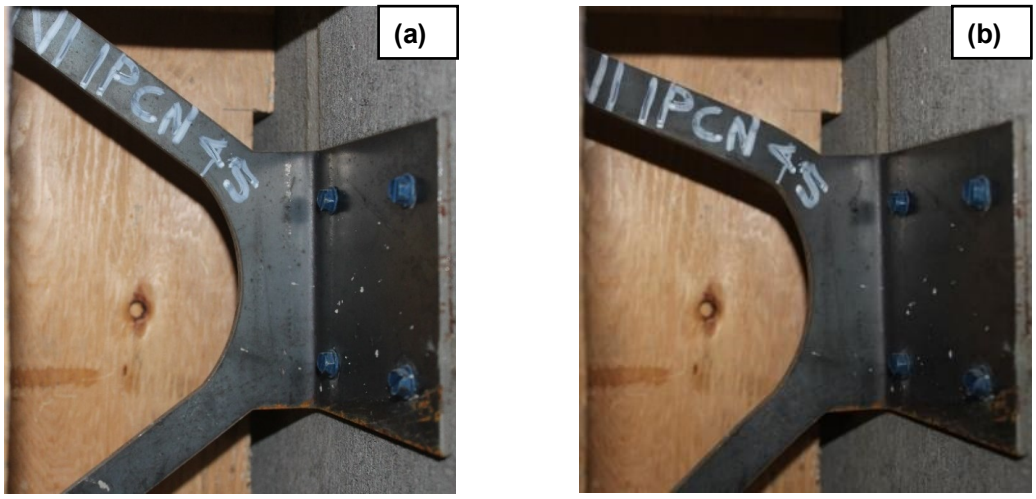

Figure 4-22. Failure process of NC tie (45 mm embedment): a) connector before the test, and b) deformation of the tie after the test.

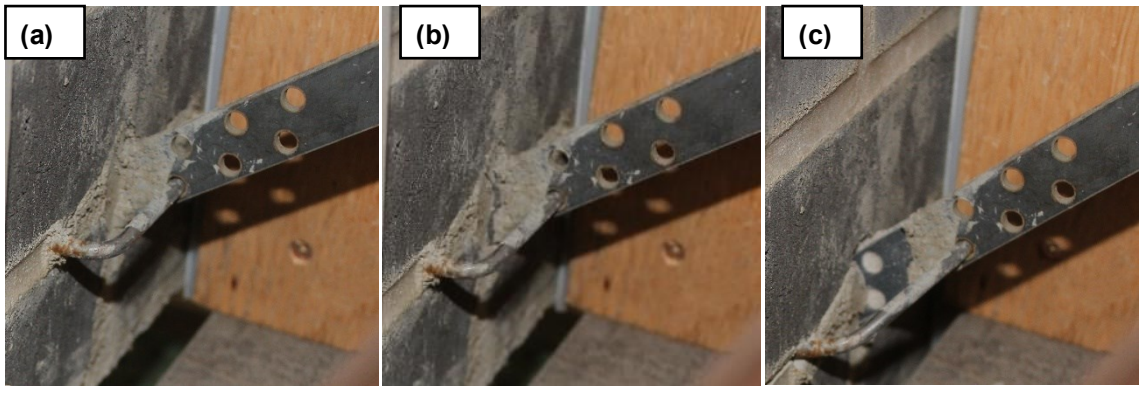

Figure 4-23. Bottom plate of NC tie (60 mm embedment): a) specimen before the test, b) formation of cracks and pull out of the bottom plate, and c) deformation after the test.

4.10 Discussion of Results

4.10.1 Effect of Connector Type

Three tie configurations were used in the specimens: conventional tie horizontally placed (HC), conventional tie vertically placed (VC), and the novel tie (NC). The influence of the tie configuration on the shear strength and initial shear stiffness is discussed.

The VC specimens exhibited a larger peak load than the VC specimens. This is due to the position of the connector about the direction of the applied load. The moment of inertia acting against the applied load is larger for the VC. This resulted in an increase in peak load of 1.7 times for the VC specimens compared with the HC tie specimens.

The resistance of the specimens with NC connectors was the largest, it reached 6.7 and 2.5 times the peak load of the HC and VC specimens, respectively. This is due to a better utilization of the geometry of the connector. This can be explained as discussed in Section 2.6.3., the inclined geometry of the novel tie allows to achieve truss action, leading to larger shear resistance compared with the conventional ties perpendicularly placed about the applied load (Tomlinson et al., 2016). The truss geometry allowed the top member to act in compression and the bottom member in tension, with the latter fastened to an embedded bar that provided additional resistance. This is consistent with the literature that shows that the geometry of the connector has a significant influence on the shear strength of the wall (Zisi and Bennett, 2011).

The initial stiffness of the NC ties was the largest, it was 2.1 and 1.5 times the stiffness exhibited by the HC and VC ties, respectively. The VC ties displayed 1.1 times the stiffness of the HC ties. As composite action can be expressed in terms of strength and stiffness, comparing the three tie configurations using the same arrangement, the novel tie will exhibit a larger composite action compared with the horizontally and vertically placed conventional ties.

4.10.2 Effect of Tie Embedment Length

Three embedment lengths of the round bent bars embedded on the veneer were studied: 45, 60, and 75 mm. The effect of the embedment length on the shear strength and initial shear stiffness is discussed.

On average, increasing the embedment length led to larger shear strength. The shear strength of the ties using embedment lengths of 45, 60, and 75 mm was 1.72, 1.71, and 1.79 kN for the VC tie and 4.22, 4.36, and 4.44 kN for the NC tie. Increasing the embedment length from 60 to 75 mm increased the peak load 1.04 times for the VC tie and 1.05 times for the NC tie. The results of this study are consistent with previous research that showed that increasing the embedment length of the round bent bars in the veneer increased the axial strength of the ties (Choi and LaFave, 2004; Arslan et al., 2021). The results of this study show that the embedment length influences the shear strength of the ties. Larger embedment lengths in general displayed higher shear strength. This can be explained as a larger embedment length will provide more development length between the bar and the mortar embedding it, increasing the tensile resistance of the tie assembly.

No influence of the embedment length was observed on the initial shear stiffness of the ties. The initial stiffness using embedment lengths of 45, 60, and 75 mm was 0.49, 0.43, and 0.49 kN/mm for the VC tie and 0.94, 0.51, and 0.62 for the NC tie.

4.10.3 Effect of Type of Brick

Two types of bricks were used for the construction of the veneer: clay and concrete bricks. The influence of the type of brick on the shear strength and initial shear stiffness of the ties is discussed.

Specimens with concrete brick displayed larger shear strength than those with clay brick. The shear strength for clay and concrete brick specimens was 1.67 and 1.81 kN for VC ties, and 4.22 and 4.47 kN for NC ties, respectively. The shear strength was 1.1 times larger for concrete brick specimens compared with clay brick, for both VC and NC ties. Additionally, the stiffness was also larger for concrete brick specimens than clay specimens. The shear strength for clay and concrete brick specimens was 0.45 and 0.49 kN/mm for VC ties, and 0.70 and 0.72 kN/mm for NC ties.

Previous research showed that using concrete bricks instead of clay bricks in the veneer increased the axial strength of the tie assembly in wider cavities (Romero and Tomlinson, 2023). The findings from this study align with the results of previous

research. This can be attributed to the higher bond strength developed from the deeper and wider frogs in concrete bricks (Rao et al., 1996).

4.11 General Considerations

Including the novel tie in the construction of cavity walls will increase the shear strength and shear stiffness of the connection between the wythes. However, some implications may be considered. Having a stiffer connection in cavity walls subjected to large bowing deformations can induce more cracks in the brick veneer. This should be considered in the design of cavity walls. Using the embedded bars, it is possible to allow different ranges of vertical slip between the wythes according to the exposure of the specific wall. Additionally, expansion joints can be provided to mitigate the effect of shrinkage in the inner and outer wythe.

Some limitations of the test performed in this study are presented in the following:

- It is recommended to perform small-scale shear tests using typical cavity walls of 100 mm to compare the shear strength of the studied novel and conventional ties in typical cavity widths compared with the presented wider cavity wall specimens.
- The use of the wood spacer was a solution to restrain the rotation of the veneer to produce the shear load on the ties. Due to the scarcity of full-scale tests on these wider cavity walls using larger ties, it is recommended to test full-scale cavity walls using these larger ties and including the typical wall elements such as the insulation material and subject the wall to out-of-plane loading. This is to verify the assumption that the rotation of the veneer about the CMU wythe is not significant under the studied loads.
- Shear and axial forces are often working at the same time as the tie may be under tension from suction on the wall as well as shear caused by that suction. Therefore, the interaction response between the axial and shear strength should be investigated.
- The material comprising all the ties was galvanized steel and is allowed by CSA A370-14 for level 1 of environment exposure. This was the only material used as it is widely used for masonry ties.

- Testing full-scale walls subjected to out-of-plane loading with these larger novel and conventional ties can be compared to typical walls with cavity widths of 100 mm. This is to compare the out-of-plane strength and stiffness of wider cavity walls, which is expected to comply the meet the increasing energy requirements.
- Testing the novel ties in full-scale cavity walls requires careful considerations for the analysis and experimental testing. Firstly, analytical expressions are needed to determine the degree of composite action achievable with the novel ties. The Masonry Research group at the University of Alberta, specifically the Ph.D. candidate Benedict Egbon, is currently working on developing such expressions for full-scale walls. Secondly, to experimentally assess the level of composite action in wide cavity walls using the novel ties, the following testing scheme is suggested. Compare the out-of-plane response of a control wall with ties offering only axial resistance and another wall with the same characteristics but incorporating the novel ties. The non-composite wall is represented by the first, and the additional out-of-plane strength observed in the second serves as a measure of the composite action achieved by introducing the novel tie. The tie placement, wall height, loading, and support conditions of these two specimens are shown in Fig 4-24.

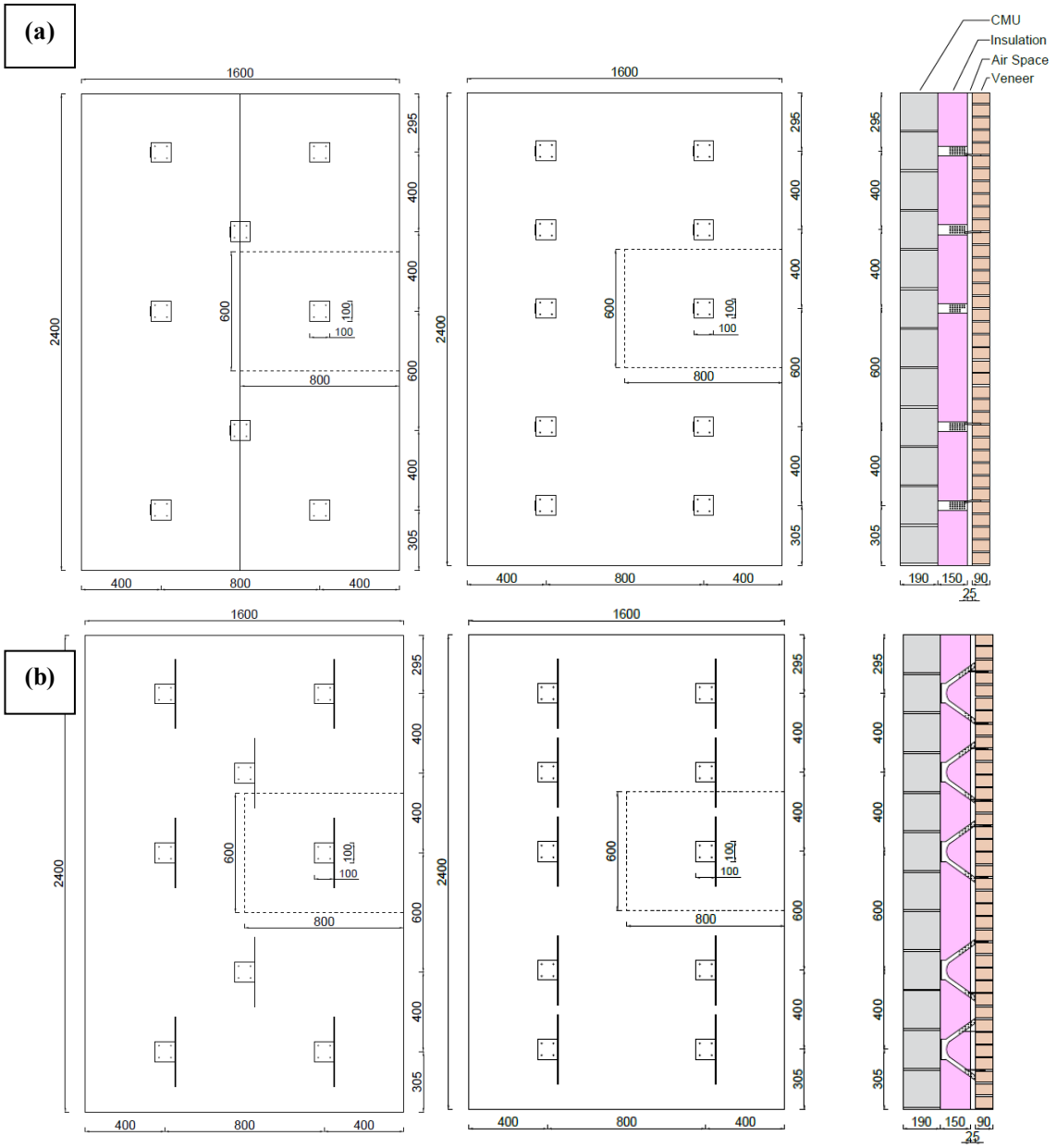

Figure 4-24. Suggested full-scale specimens under out-of-plane load: dimensions and tie arrangements with: a) conventional tie, and b) novel tie.

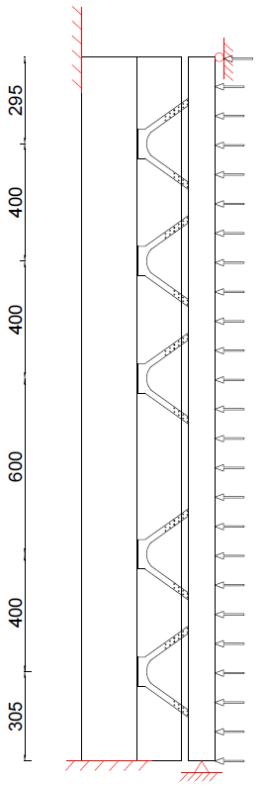

Figure 4-25. Suggested full-scale specimens under out-of-plane load: loading and support conditions (novel tie shown).

4.12 Conclusions

In this chapter, the performance of a novel tie is compared to existing plate ties, through longitudinal shear testing. The influence of embedment length and veneer type on the strength and failure mode are discussed.

- In the concrete brick samples, the formation of cracks occurred in the later stages of deformation, whereas clay brick samples exhibited early crack propagation. Additionally, the shear strength and initial shear stiffness were larger for specimens with concrete bricks than those with clay bricks in the veneer.
- Better utilization of the tie material properties allowed the novel inclined connector to attain larger strength than the conventional plate tie, while the

vertical plate tie attained larger strength than the horizontal plate tie due to a larger moment of inertia from placement.

- In general, increasing the embedment length led to larger shear strength. For the VC tie, the shear strength was increased 1.04 times comparing the 75 mm to 60 mm. For the NC tie, the shear strength was increased to 1.03 and 1.05 comparing the 75 mm with 45 and 60 mm, respectively. No influence of the embedment length was observed on the initial shear stiffness of the ties. It is recommended that embedment lengths lesser than 45 mm be tested to study the optimal amount of embedment needed to prevent the pullout of the tie.
- The larger strength of the inclined connector enables it to be used with wider spacing in full-scale walls. In addition, since the inclined tie is stiffer than other tie types, expansion joints should be provided to mitigate the effect of shrinkage in the inner and outer wythe.

5 THERMAL RESISTANCE OF CAVITY WALLS WITH NOVEL AND CONVENTIONAL TIES

5.1 Introduction

With the advent of newer, more stringent thermal and energy requirements in building envelopes, current masonry construction techniques and modelling strategies need to be revamped and modernized to remain competitive. In the 2017 version of the National Energy Code of Canada for Buildings (NECB), there was a 25% increase in the minimum thermal resistance (R-values) required for envelope components compared with the 2015 NECB. Calculation of the R-value in the 2015 NECB permitted the exclusion of structural and other thermally conductive elements that penetrated the envelopes if they comprised less than 2% of the total wall area. However, starting in 2017 the NECB requires that all of these elements are included in the calculation of R-value. This change was motivated by the recognition that thermal bridging elements, such as masonry connectors, reduce the R-value of a building envelope significantly. While ties in a cavity wall often comprise a small percentage of the total wall area, these highly conductive elements are among the most substantial contributors to thermal bridging in concrete masonry walls (Roppel et al., 2012; Liu, 2019).

As discussed in Chapter 3, the NECB (2022) provides the maximum overall thermal transmittance (U-value) for the building envelope elements. Therefore, the minimum R-value for walls can be calculated as the inverse of the U-value, as shown in Table 5-1. The table mentions an example of a city located in each climate zone. Figure 5-1 shows the minimum R-value for walls for the different climatic zones of Canada. Typical thermal design in cavity masonry walls makes use of the space between the wythes to fit the required amount of insulation that would result in a target R-value. With more demanding energy requirements in cold regions of Canada in recent years, the resulting insulation thickness in typical designs has increased significantly (Bennett et al., 2017), requiring larger cavities. This requires the use of custom-made, expensive tie systems, for which there are scarce structural and thermal test data or rational design guidelines. As a consequence, in the energy/thermal side, this opens up an opportunity to investigate the

performance of conventional and innovative tie designs, and evaluate advantages and limitations for masonry wall systems with large cavities.

Table 5-1. Maximum U-value and maximum R-value for walls for different climate zones in Canada (NECB, 2022).

Wall	Zone	U-value, W/m2K	R-value, m2K/U	City
Zone 4	4	0.29	3.4	Victoria
Zone 5	5	0.265	3.8	Toronto
Zone 6	6	0.24	4.2	Ottawa
Zone 7A	7	0.215	4.7	Edmonton
Zone 7B	7	0.19	5.3	Whitehorse
Zone 8	8	0.165	6.1	Yellowknife

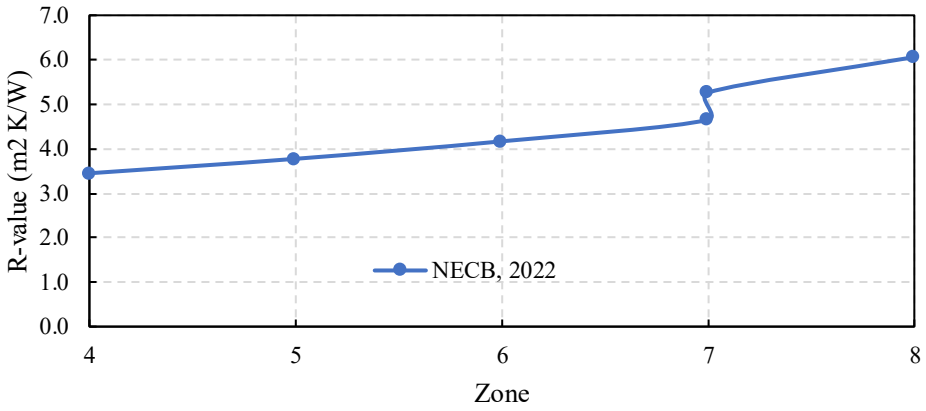

Figure 5-1. Minimum R-value for different climatic zones of Canada according to the NECB (2022).

There is previous evidence of Energy standards that increased the minimum R-value and the masonry design standards had to allow the construction of wider cavity walls, as shown in Fig. 5-2 (Raouf and Al-Ghamdi, 2019). The figure shows the minimum R-value required by three different versions of the ASHRAE and the cavity thickness allowed by the masonry standards to reach the increased R-value for 7 different insulation materials: Cellulose Fiber Insulation (CFI), Expanded Polystyrene (EPS), Stone Wool (RW), Glass Wool (GW), Polyurethane (PUR), Extruded Polystyrene (XPS) and Polyisocyanurate (PIR). Therefore, is expected that the future versions of the Energy codes require an increased minimum R-value, and an approach to reach that value could be to increase the cavity width (Jacob et al., 2023).

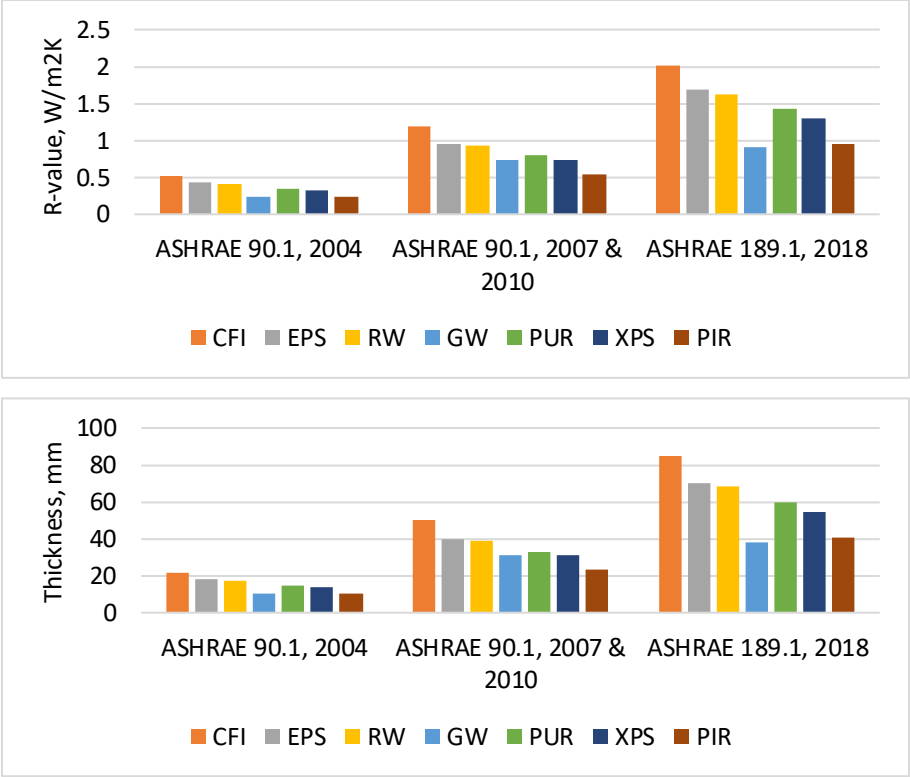

Figure 5-2. Insulation thickness and R-value adopted to comply with different codes (Raouf and Al-Ghamdi, 2019).

Additionally, another factor that affects the thermal resistance of the walls are the thermal bridging effects produced by highly thermal conductive elements that pierce the insulation layer, such as the masonry ties. Therefore, current research on the thermal performance of ties aims to improve their impact on the R-value. Some thermal improvements include drilling holes in ties to reduce cross-sectional area, which leads to less thermal conductance (Wilson, 2013). Also, the use of tie materials with lower thermal conductivity. Some researchers (Shao, 2021; Woltman et al., 2017; Ismaiel, 2022) have verified that the thermal resistance of wall assemblies can be improved by using ties made of less conductive materials such as stainless steel and glass fibre reinforced polymers (GFRP).

5.2 Thermal Principles

The thermal performance of a wall is primarily determined by the thermal conductivity (k) and geometry of the materials used in the assembly. Two means to summarize the

thermal behaviour of an element are the thermal resistance (R-value) and thermal transmission (U-value). These and other relevant thermal concepts were defined in Section 2.4.2. The R-value and U-value can be calculated experimentally or obtained by theoretical calculations or computer simulations, as discussed in Section 2.4.5.

The thermal resistance (R-value) of a wall assembly is the capacity of the system to resist heat flow, and can be determined in steady state or dynamic state conditions. The steady-state condition consists in performing an experimental test or theoretical calculation under constant temperatures in the internal and external faces of the assembly as stated in ASTM C1363 (ASTM, 2019). In contrast, a dynamic state condition takes into account variable temperatures in the internal and external faces of the assembly to simulate temperature changes experienced by a structure during the day. Typically, steady state heat transfer condition is used for the calculation of the R-value as it requires less time and is easier than the dynamic test.

The thermal resistance (R-value) in steady state conditions is calculated as the thickness of the material over the thermal conductivity of the respective material, or in terms of the total heat flux (Q), as the difference in temperature between the internal and external surfaces divided in the average flux density of the studied element, as shown in Equation 5-1. The first form is used when addressing a single material, while the second form is used to calculate the R-value using the total heat flux (Q) obtained using software.

$$R = \frac{t}{k} \; or \; R = \frac{\Delta T}{Q} \qquad \textbf{(5-1)}$$

Where R is the thermal resistance (R-value) ($\mathrm{m^2K/W}$), t is the thickness of the material (m), k is the thermal conductivity of the addressed material ($\mathrm{W/mK}$), ΔT is the difference in temperature between the internal and external surfaces (ºC), and Q is the heat flux density of the addressed wall ($\mathrm{W/m^2}$).

When the system is comprised of complex geometries or if there are thermal bridging elements, the calculation of the heat flux density becomes complex. In those situations, the calculation can be obtained using computer simulations. Finite Element (FE) programs can be used to calculate the temperature distribution along the assembly and

the total heat flux of the assembly. In this study, the 3D FE software program ANSYS was used. The formulation of the equation used by the FE software is elaborated as follows.

In a steady state heat transfer condition, the governing equation Fourier's law of heat conduction is expressed in the differential form as expressed in Equation 5-2.

$$\dot{Q}_n = -kA\frac{\partial T}{\partial n} \quad \textbf{(5-2)}$$

Where n is the normal direction of the isothermal surface at the specific point, $\dot{Q}_n$ is the rate of conduction heat flow at the specific point (W), k is the thermal conductivity of the material (W/mK), A represents the surface area perpendicular to the direction under consideration (m^2), and $\frac{\partial T}{\partial n}$ is the temperature gradient (ºC).

The general heat conduction equation is established using rectangular coordinates and considers a small rectangular element with dimensions Δx in length, Δy in width, and Δz in height, as shown in Fig. 5-3. Assuming that the density of the body is represented by ρ and its specific heat by c, an energy balance for this element over a time interval Δt can be expressed as shown in Equation 5-3 (Ã-zisik and Özışık, 1993).

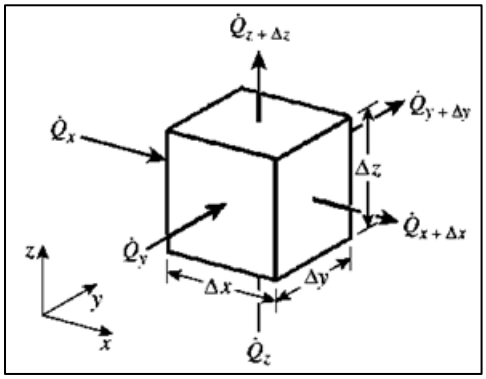

Figure 5-3. Three-dimension rectangular element used in heat conduction (Ismaiel, 2022).

$$\dot{Q}_x + \dot{Q}_y + \dot{Q}_z - \dot{Q}_{x+\Delta x} - \dot{Q}_{y+\Delta y} - \dot{Q}_{z+\Delta z} + \dot{E}_{gen} = \frac{\Delta E_e}{\Delta t} \quad \textbf{(5-3)}$$

Where $\dot{Q}_x$, $\dot{Q}_y$, $\dot{Q}_z$ represent rates of heat conduction at x, y, z (energy added); $\dot{Q}_{x+\Delta x}$, $\dot{Q}_{y+\Delta y}$, $\dot{Q}_{z+\Delta z}$ are the rate of heat conduction at $x+\Delta x$, $y+\Delta y$, $z+\Delta z$ (energy removed);

$\dot{E}_{gen}$ is the rate of energy generation within the element; and $\frac{\Delta E_e}{\Delta t}$ is the rate of energy change occurring within the element. The volume of the element is expressed in Equation 5-4.

$$V_e = \Delta x \Delta y \Delta z \quad \textbf{(5-4)}$$

Equations 5-5 and 5-6 show the rate of heat generation in the addressed element and the change in the energy content.

$$\Delta E_e = E_{t+\Delta t} - E_t = mc(T_{t+\Delta t} - T_t) = pc\Delta x \Delta y \Delta z\ (T_{t+\Delta t} - T_t) \quad \textbf{(5-5)}$$

$$\dot{E}_{gen} = \dot{e}_{gen} V_e = \dot{e}_{gen} \Delta x \Delta y \Delta z \quad \textbf{(5-6)}$$

The general balance equation is expressed in Equation 5-7.

$$-\frac{1}{\Delta y \Delta z}\frac{\dot{Q}_{x+\Delta x} - \dot{Q}_x}{\Delta x} - \frac{1}{\Delta x \Delta z}\frac{\dot{Q}_{y+\Delta y} - \dot{Q}_y}{\Delta y} - \frac{1}{\Delta x \Delta y}\frac{\dot{Q}_{z+\Delta z} - \dot{Q}_z}{\Delta z} + \dot{e_{gen}} = \rho c\ \frac{T_{t+\Delta t} - T_t}{\Delta t} \quad \textbf{(5-7)}$$

Taking into account the heat transfer areas of the element under consideration in the x, y, and z directions as $A_x = \Delta y \Delta z$, $A_y = \Delta x \Delta z$ and $A_z = \Delta x \Delta y$, and considering the limit as Δx, Δy, Δz and Δt tends to zero, the general heat conduction equation in rectangular coordinates for constant thermal conductivity is simplified to Equation 5-8.

$$\frac{\partial^2 T}{\partial x^2} + \frac{\partial^2 T}{\partial y^2} + \frac{\partial^2 T}{\partial z^2} + \frac{\dot{e}_{gen}}{K} = \frac{1}{\alpha}\frac{\partial T}{\partial t} \quad \text{Where: } \alpha = \frac{k}{\rho c} \quad \textbf{(5-8)}$$

Where α is the thermal diffusivity of the material. Considering the steady state condition with no heat generation, Equation 5-9 is obtained, which is the Laplace equation.

$$\frac{\partial^2 T}{\partial x^2} + \frac{\partial^2 T}{\partial y^2} + \frac{\partial^2 T}{\partial z^2} = 0 \quad \textbf{(5-9)}$$

In this chapter, a FE model was developed to assess the thermal resistance of cavity wall assemblies using both the novel and conventional ties in wide (175 mm cavity width) cavity walls.

5.3 Finite-Element Analysis

5.3.1 Model description

In this chapter, a FEA model was developed to assess the thermal resistance of cavity wall assemblies using both the novel and conventional ties and the cavity width of 175 mm (as used in Chapter 4). To obtain the R-value of the assemblies, the three-dimensional FE modelling program ANSYS was used. Finite-element analysis is considered to be a reliable numerical method for thermal analysis (Zieukiewicz and Taylor, 1991; Xie, 2012) and has been validated abundantly with experimental tests.

All the components of the wall assemblies were modeled in ANSYS using the element SOLID70. This element possesses three-dimensional thermal conduction capabilities. It consists of eight nodes, with a single degree of freedom (temperature) at each node. This element is suitable for conducting three-dimensional analyses, both in steady-state and transient thermal scenarios (Ismaiel, 2022). Moreover, it can account for heat flow due to mass transport from a constant velocity field.

To simulate the wall assembly, each material was created as a single layer. Figure 5-4 shows one of the wall assemblies without a tie used in this study. The assembly is comprised of the following layers: CMU, insulation, air space, veneer, interior and exterior films. Table 5-2 shows the material properties used in the examined wall assemblies, obtained from the ASHRAE Handbook and literature (ASHRAE, 2019; Morrison Hershfield, 2022a; Di Placido et al., 2019; Anderson and Kosmina, 2019; Shao, 2021; Hassan, et al. 2021). The dimensions of all the assemblies, including height, width, and thickness ($800 \times 800 \times 475$ mm, respectively), were constant. The cavity width was set to 175 mm as used in specimens for the tests in Chapter 4. The insulation in all assemblies was mineral wool insulation.

As mentioned in Chapter 2, the thermal conductivity of the materials depends on the temperature gradient. However, the FE models developed in this study were analyzed

under steady-state conditions as established in ASHRAE ISO 6946 and NECB. Therefore, the values of thermal conductivity shown in Table 5-2 are constant for each material under the internal and external temperatures of 22 ºC and -18 ºC.

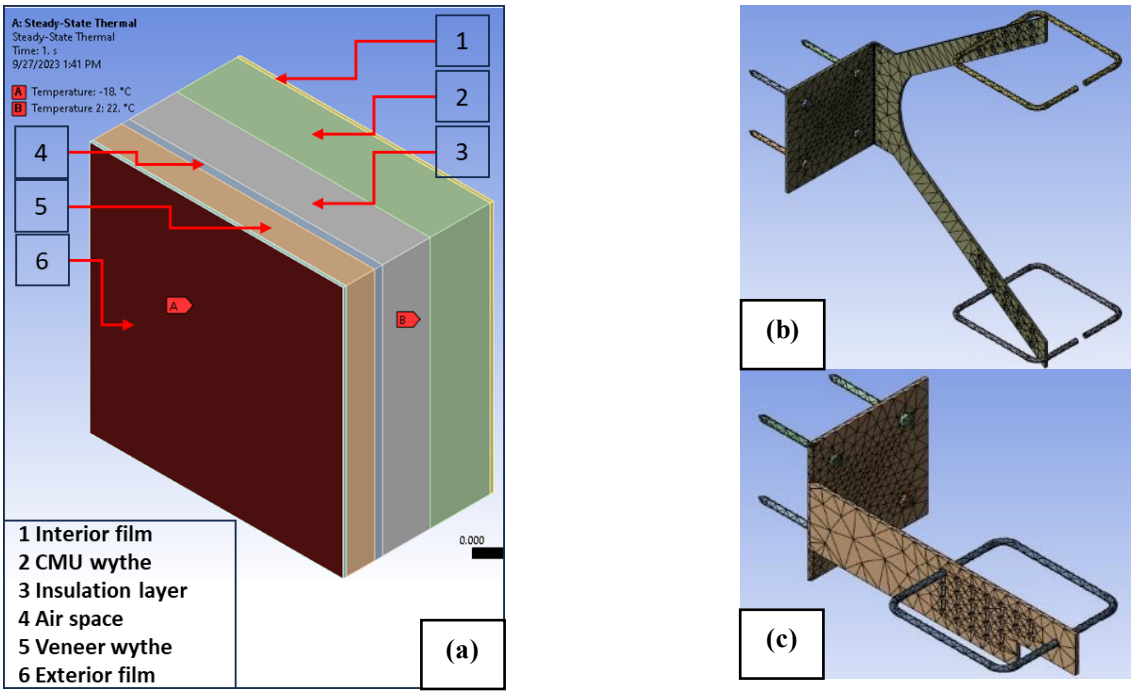

Figure 5-4. Wall assembly example in ANSYS: a) temperature loads and materials, b) NC tie, and c) VC tie.

Table 5-2. Material thickness and properties used in the studied assemblies.

Component	Thickness, mm	Conductivity, W/mK	Source
Veneer	90	0.80	ASHRAE 2017
CMU	190	0.72	Hassan, et al. 2021
Mineral wool insulation	Various	0.036	ASHRAE 2017
Exterior film	10	0.0333	Morrison Hershfield, 2018
Interior film	10	0.00833	Morrison Hershfield, 2018
Air space	Various	0.18	Anderson and Kosmina, 2019; Shao, 2021
Galvanized Steel	3	45.30	ASHRAE 2017
Stainless steel	3	17.00	Shao, 2021
GFRP	3	0.20	Shao, 2021

The CMU and veneer wythes were simulated as two homogeneous layers. The thermal conductivity of those layers represents the combined thermal conductivity between the

masonry units, grouting, and mortar, as obtained from literature and previous studies. The CMU wythe was simulated as a single layer with the thermal properties of the concrete block obtained from the ASHRAE Handbook (ASHRAE, 2017). The relevant properties of the materials are reported in Table 5-1. The veneer wythe was simulated as a single layer with the properties of the brick veneer used by BC HYDRO (2021) in the "Building Envelope Thermal Bridging Guide". This guide shows examples of typical wall assemblies with the respective R-value and thermal conductivity of the materials comprising the wall.

The insulation material was simulated as a single wythe using the thermal properties of mineral wool which is a typical insulation material used in cavity walls. The thermal conductivity was obtained according to the ASHRAE Handbook (ASHRAE, 2017).

The ties, round bent bar attached to the tie, and the screws (Fig. 5-3bc) were simulated using a 3D object for each of them with the thermal conductivities of the steel, which is the typical material used in these elements. The thermal conductivity was used according to the ASHRAE Handbook (ASHRAE, 2017).

To simulate the internal and external faces of the wall assembly in contact with the interior and exterior air conditions, a "film" layer is created on each surface (Fig. 5-3a). These films represent the surface resistance to the edge of the materials in contact with the interior and exterior spaces (ASTM, 2015; NECB, 2022; Shao, 2021). In the models used in this study, the exterior and interior films have a thickness of 10 mm and thermal conductivities of 0.0333 and 0.00833 W/mK, respectively (ASHRAE, 2017; Morrison Hershfield, 2018).

The air space within the gap between the insulation layer and the brick veneer is typically ventilated through weep holes located at the upper and lower sections of the brick veneer (Ibañez-Puy et al., 2017). Weep holes serve as pathways for draining moisture from the wall assembly (Sanjuan et al., 2011). To simulate the air space in the assembly, ISO 6946 (2017b) suggests treating the air gap as a thermally homogeneous layer. Consequently, when calculating the thermal resistance of the wall assembly, the air gap can be seen as an equivalent building layer with the effective thermal resistance of the air, which can be obtained from different standards and codes. For instance, the

thermal resistances for air proposed by different authors in m^2K/W are: 0.18 for ISO 6946 (2017), 0.22 for ASHRAE (2017), 0.16 for Morrison Hershfield (2018) and 0.17 for CLEAR (2004). In the simulations conducted in this study, it was assumed that the air space between the insulation is ventilated. Modelling convection and radiation within a cavity is challenging and time-consuming. For computational efficiency and following the ISO 6946 (2017b) guidelines, the air layer was represented as a uniform solid layer with a thermal conductivity approximately equal to the combined effect of all heat transfer mechanisms in the cavity. The thermal conductivity of the air space was set to 0.180 W/mK, consistent with prior research (ISO, 2017b; Anderson and Kosmina, 2019; Shao, 2021).

All FE models were studied under steady-state thermal analysis, and air leakage from the cavity to the interior of the building was not taken into account as this condition is typically prevented using a vapour barrier. Contact resistance was excluded from the models because it has a minimal impact on the thermal resistance of concrete-block masonry walls. This is primarily due to the limited occurrence of highly conductive contact surfaces between concrete and steel (Roppel et al., 2011).

Because the heat conduction equation does not contain any time-dependent terms in steady-state conditions, there is no requirement to define initial conditions, such as temperature changes. However, during the modelling process, three types of boundary conditions were considered, as outlined by ASHRAE, ISO 6946, and NECB for steady-state conditions. First, two thermal loads were applied on the internal and external surfaces, where the specified temperatures were constant, with an interior temperature of 22°C and an exterior temperature of -18°C (Fig. 5-3a). Second, the remaining four sides of the wall were assumed to have adiabatic boundary conditions, which means that there is no heat transfer through those faces. It is not necessary to assign this boundary condition in ANSYS, as surfaces without temperature load are considered adiabatic by default. Third, interface boundary conditions, which means that there is heat transfer between the contact surfaces of the materials of the assembly. This refers to the contact between the individual layer of each material in contact with another layer. Those surfaces

in contact are automatically defined in ANSYS according to the thermal resistance of the layers in contact.

5.3.2 Sensitivity analysis

A series of mesh convergence tests were conducted to find the balance between accuracy and computational efficiency for assemblies with both conventional and novel ties. In these tests, the convergence study focused on mesh size and its effect on heat flux as the number of mesh nodes varied. The results showed that a mesh size of 10 mm, equivalent to 418,332 nodes for conventional tie models and 543,340 nodes for novel tie models, was suitable in terms of achieving accuracy while maintaining computational efficiency for all configurations. Figure 5-5 illustrates the convergence of the R-values for the analyzed configurations as a function of the number of nodes used in the mesh for both conventional and novel tie configurations.

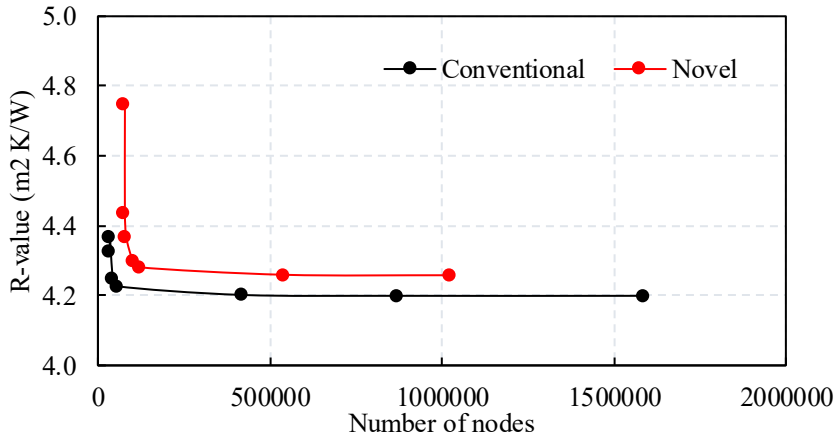

Figure 5-5. Convergence of the R-value of the addressed configurations versus the number of nodes used in the mesh for conventional and novel tie assemblies.

5.3.3 Model Setup

In this chapter, three distinct configurations of external concrete-block masonry cavity walls are investigated: 1) a cavity wall with no ties, 2) a cavity wall with a conventional tie, and 3) a cavity wall with an innovative, inclined tie, as depicted in Fig. 5-6.

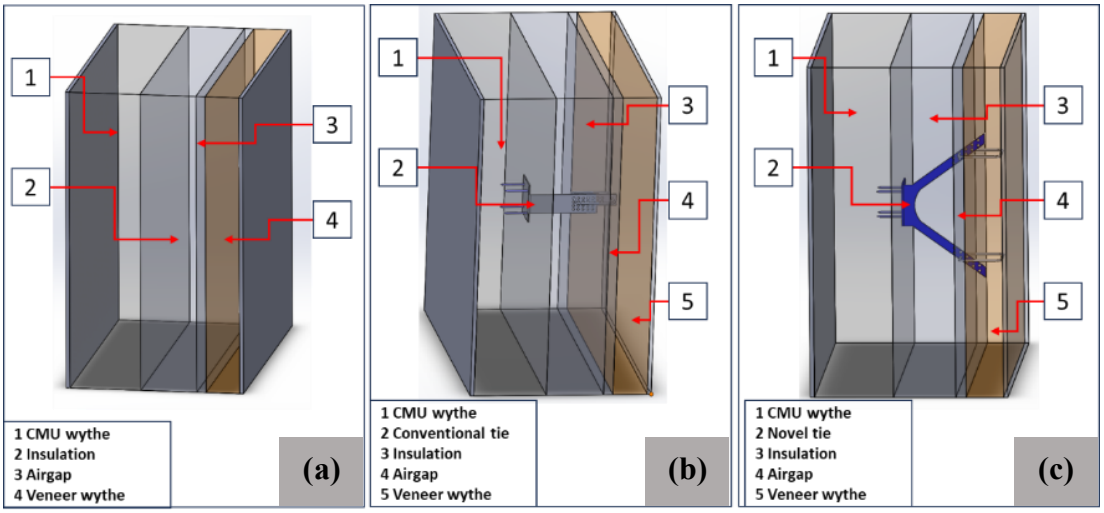

Figure 5-6. Wall assemblies used in this study a) no tie assembly, b) conventional tie assembly, and c) novel tie assembly.

5.3.4 Validation

The FEA approach used in this study was verified with previous research. In those studies (Santos, et al., 2021; Santos and Mateus, 2020), the authors performed guarded hot box tests and FEA to assess the R-values of two wall systems, as shown in Fig. 5-7. These wall assemblies contained steel studs that penetrated insulation layers producing thermal bridging effects. The same FEA approach was used to calculate the R-value of these wall assemblies using ANSYS and the error obtained was 1% and 6%. These results show that the R-value calculations agree with the R-values obtained in the experiments. Table 5-3 shows the R-values obtained by the authors and the FE calculation obtained in this study.

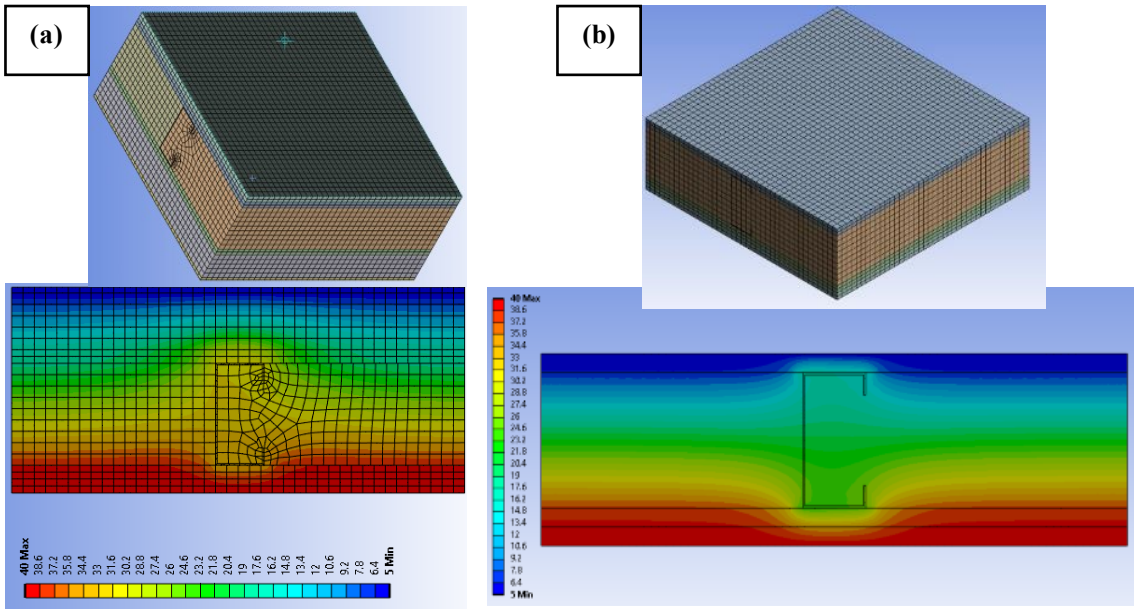

Figure 5-7. Validation of literature models: a) Santos, et al. (2021) and b) Santos and Mateus (2020).

Table 5-3. Results of the validation of literature models.

Reference	R-value, m^2K/W			%Error
	Previous results		Current study	
	Experimental	FE	ANSYS	
Santos, et al. (2021)	3.2	3.203	3.164	1%
Santos and Mateus (2020)	1.558	1.594	1.462	6%

5.4 Parametric Analysis

To compare the thermal resistance of cavity wall assemblies using the novel and conventional ties used in Chapter 4, parametric studies were conducted to evaluate the impact of these ties on the thermal resistance of the assembly using wider cavities. The parameters of this study are classified as fixed, independent, and dependent, which are described as follows.

5.4.1 Fixed Parameters

The fixed parameters were not changed in the study and were constant for all the R-value calculations. For a direct comparison of the effect of both ties, the same thicknesses of CMU wythe, veneer wythe, cavity width, and interior and exterior films were used. The

cavity width used in this chapter is the same as used in Chapter 4. The values of the fixed parameters above were set to those used for typical wall construction in Canada. The fixed parameters are summarized in Table 5-4.

Table 5-4. Fixed parameters summary.

Parameter	Value	Units
CMU thickness	190	mm
Veneer thickness	90	mm
Cavity width	175	mm
Interior temperature	22	°C
Exterior temperature	-18	°C

5.4.2 Independent Parameters

The study explored the effects of three independent parameters on dependent parameters. These independent parameters include the type of tie in the wall assembly, insulation thickness, and the material of the tie. The variation in insulation thickness aims to assess its influence on wider cavity walls utilizing two types of ties. Meanwhile, the variation in tie material aims to evaluate the impact of ties made from three materials with distinct thermal conductivities: galvanized steel, GFRP, and stainless steel. The geometry of the conventional and novel ties was fixed, and only the material properties were modified for this parameter. Stainless steel is chosen to represent the conventional material used in masonry ties, GFRP is known for its exceptionally low thermal conductivity, and previous studies have employed it in PCSW and masonry systems (Wotman et al., 2013; Kim et al., 2015; Shao, 2021; Ismaiel, 2022). Finally, stainless steel is a contemporary option for masonry ties, having a thermal conductivity value between the aforementioned materials.

Analyzing materials with different thermal conductivities allows for studying the impact of tie material on thermal bridge effects. The summary of independent parameters is presented in Table 5-5, and the thermal conductivities of these materials are provided in Table 5-2.

Table 5-5. Independent parameters summary.

Parameter	Value Range
Tie type	No tie, conventional tie, and novel tie (same used in Chapter 4)
Insulation thickness	100, 125 and 150 mm.
Tie Thermal conductivity (W/mK)	Galvanized steel (45.3), stainless steel (17), and GFRP (0.2).

A total of 43 assemblies with different configurations underwent thermal analysis, encompassing 3 tie configurations, 3 insulation thicknesses, and 3 tie materials. Additionally, the thermal resistance of an assembly without ties was calculated, considering a cavity width of 175 mm.

To assess the impact of insulation thickness on the R-value of the wall assembly, the R-value of a wall without ties was computed for 10 different insulation thickness values ranging from 0 to 175 mm in a wall with a cavity width of 175 mm.

The following modelling assumptions were considered in this study: the analysis was conducted under steady-state conditions, assuming a ventilated cavity where air circulation is typical in actual cavity walls. Moreover, it was assumed that there is no air and water leakage into the interior of the building, as the vapor barrier prevents such occurrences.

5.4.3 Dependent Parameters

The dependent parameter is the thermal resistance (R-value) of the wall assemblies. The R-values are presented in metric system units (RSI) (m^2 K/W).

5.5 Results and Observations

The thermal analysis using the FE model was developed and the results are shown. First, it was compared an assembly without tie using 10 insulation thicknesses (0, 20, 40, 60, 80, 100, 120, 140, 160, 175 mm) to observe the influence of the insulation thickness in the R-value without thermal bridge effects. Secondly, the assemblies with three tie configurations (no tie, novel, and conventional tie) were compared using three insulation thicknesses (100, 125, and 150 mm) and three tie materials (galvanized steel, stainless steel, and GFRP) to observe the effect of both parameters in the R-value. The results are shown in graphs of R-value vs insulation thickness with a separate graph per tie material.

All the graphs show the minimum R-value for Edmonton according to NECB (2022) and with a control wall assembly that represents the current typical cavity wall assembly, which cavity is comprised of 100 mm of insulation and 25 mm of air space, shown as "Control 125".

5.5.1 Assembly Without Tie

Table 5-6 shows the R-value of the wall assembly without ties calculated for ten insulation thicknesses using ANSYS and the theoretical approach described below. The R-value is shown in m^2K/W units. Figure 5-8 shows the linear correlation between the R-value and the insulation thickness.

Table 5-6. R-value for 10 insulation thicknesses in no tie assembly.

N	Thickness, mm		R-value, m^2K/W		
	Insulation	Air space	ANSYS	Theoretical	Error
1	0	175	2.9	2.8	0.02%
2	20	155	3.3	3.3	0.03%
3	40	135	3.7	3.7	0.00%
4	60	115	4.2	4.2	0.03%
5	80	95	4.6	4.6	0.05%
6	100	75	5.1	5.1	0.04%
7	120	55	5.5	5.5	0.02%
8	140	35	6.0	6.0	0.01%
9	160	15	6.4	6.4	0.08%
10	175	0	6.7	6.7	0.01%
11	100	25	4.8	4.8	0.05%

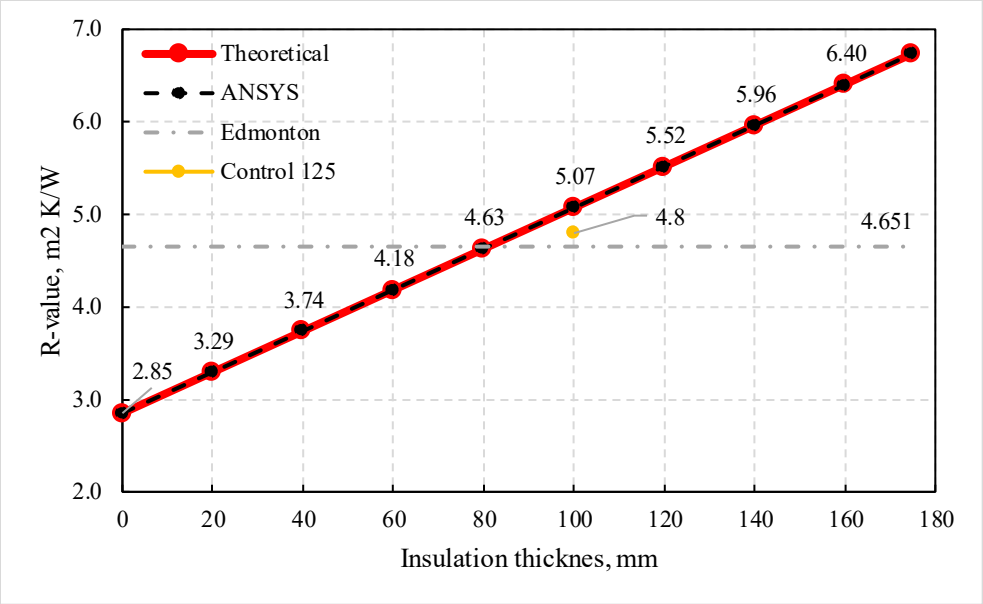

Figure 5-8. R-value vs insulation thickness for the assembly without a tie.

Figure 5-8 shows that there is a linear relationship between the insulation thickness and the R-value in the assembly without a tie and cavity width of 175 mm. The results show that increasing insulation thickness by 20 mm leads to an average increase in the R-value of 11%. The error between the theoretical R-value and the results from ANSYS is less than 1%.

Figure 5-8 shows the maximum R-value for walls required for Edmonton according to NECB (NECB, 2022) to compare the results of the studied assemblies. The graph shows that both walls with 125 mm and 175 mm of cavity width comply with the minimum R-value using insulation of 100 mm. However, the wall with a cavity width of 175 mm permits to accommodate up to 150 mm of insulation increasing the R-value by 29% compared with the wall with a typical cavity width of 125 mm.

Additionally, the graph shows the R-value of the assembly with a typical configuration of 100 mm insulation thickness and 25 mm air space, shown as “Control 125”. It can be observed that due to the increase in cavity width, the R-value of the assembly with an insulation thickness of 100 mm is 5% larger than that of the control assembly, even having the same insulation thickness. This is due to the thicker air space in the wall with a cavity width of 175 mm. Having a cavity width of 175 mm allows placement of up to 150 mm

of insulation reaching a larger R-value. The R-value of the assembly with 150 mm of insulation is 30% larger than the control wall.

The theoretical calculation process is shown using Assembly 2 from Table 5-5, as an example. As the assembly is comprised of various layers with different thermal conductivities, the overall R-value is calculated as the sum of the R-value of each layer.

$$\mathrm{R-value} = \frac{t_{CMU}}{k_{CMU}} + \frac{t_{ven}}{k_{ven}} + \frac{t_{ins}}{k_{ins}} + \frac{t_{air}}{k_{air}} + \frac{t_{int}}{k_{int}} + \frac{t_{ext}}{k_{ext}}$$

The values are replaced using the thermal conductivities from Table 5-1 and the thickness of each material shown in Table 5-4, as follows:

$$\mathrm{R-value} = \frac{0.19}{0.72} + \frac{0.09}{0.8} + \frac{0.02}{0.036} + \frac{0.155}{0.18} + \frac{0.01}{0.16} + \frac{0.01}{0.129}$$

$$\mathrm{R-value} = 1.93\ \mathrm{m^2K/W}$$

5.5.2 Assemblies With Ties

The R-values of wall assemblies featuring three tie configurations (no tie, conventional tie, and novel tie) were calculated for insulation thicknesses of 100, 125, and 150 mm, considering three tie materials (galvanized steel, stainless steel, and GFRP). The FE software ANSYS was utilized for the calculations, and the results are presented in Table 5-7. The last column of the table depicts the ratio of the R-value for each assembly with a tie to the corresponding assembly without a tie but with the same insulation thickness. This ratio signifies the reduction in R-value attributed to the inclusion of the specific tie (novel or conventional), considering insulation thickness and tie material. The relationship between R-value and insulation thickness is illustrated in three separate graphs for each tie material: Fig. 5-9 depicts the relationship for galvanized steel, Fig. 5-10 shows the graph for stainless steel, and Fig. 5-11 illustrates the relationship for GFRP ties.

Table 5-7. R-value for three tie configurations, insulation thickness of 100, 125, and 150 mm, and three tie materials.

N	Tie	Tie material	Thickness, mm		R-value, m^2K/W	Tie/NoTie
			Insulation	Air space		
1	No tie	-	100	75	5.1	-
2		-	125	50	5.6	-
3		-	150	25	6.2	-
4	Conventional	Galvanized Steel	100	75	4.7	92.6%
5			125	50	5.1	91.3%
6			150	25	5.6	90.1%
7		Stainless steel	100	75	4.9	96.1%
8			125	50	5.3	95.0%
9			150	25	5.9	94.8%
10		GFRP	100	75	5.1	99.9%
11			125	50	5.6	99.8%
12			150	25	6.2	99.8%
13	Novel	Galvanized Steel	100	75	4.7	93.0%
14			125	50	5.2	91.8%
15			150	25	5.6	90.9%
16		Stainless steel	100	75	4.9	96.5%
17			125	50	5.4	96.1%
18			150	25	5.9	95.6%
19		GFRP	100	75	5.1	99.8%
20			125	50	5.6	99.9%
21			150	25	6.2	99.8%

The average difference in R-value of the assemblies with galvanized steel, stainless steel, and GFRP ties compared with the assembly without ties are 91.6%, 95.7%, and 99.8%, respectively. The assemblies with the GFRP ties have the largest R-value among the compared materials, reaching the R-value of the respective assembly without a tie, with an average difference of less than 1%. This is to be expected, due to the very low thermal conductivity of the GFRP that almost eliminates the thermal bridge in the assembly. The stainless-steel ties reached a larger R-value of about 5% compared with the conventional galvanized steel ties. This larger R-value was expected as the stainless steel has a lower thermal conductivity compared with the galvanized steel.

Figure 5-9 shows the linear relationship between the R-value and the insulation thickness of the wall assemblies with the three tie configurations (no tie, novel, and

conventional tie). The "control 125" assembly is shown as a yellow dot. The minimum R-value for Edmonton is shown as the gray segmented line to compare with the results.

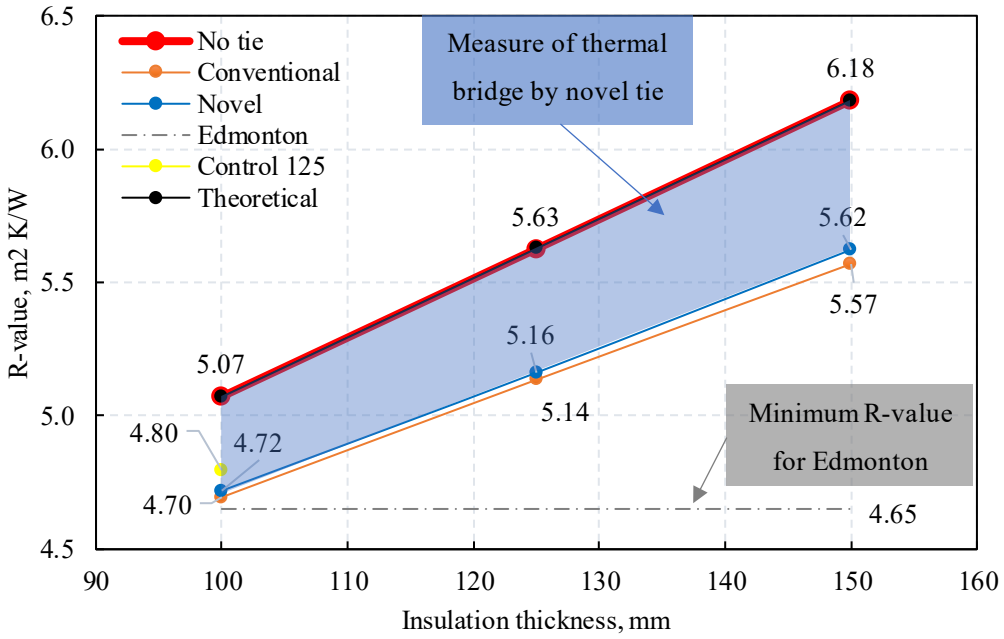

Figure 5-9. R-value vs insulation thickness for 3 types of tie configurations with galvanized steel ties.

The graph shows that the assembly with the novel tie provides nearly the same thermal resistance as the assembly with the conventional tie with an average difference of about 1% larger for the novel tie assembly. Increasing the insulation thickness from 100 to 150 mm increased the R-value by 22%, 19%, and 19% for the no tie, conventional, and novel tie assemblies, respectively.

Compared with the minimum R-value required for Edmonton, all the assemblies comply with that value. The R-value of the assemblies with conventional and novel ties is 20% and 21% larger than the minimum R-value for Edmonton and 16% and 17% larger than the R-value of the assembly without a tie and typical cavity width of 125 mm (control 125), respectively. The area shown between the no tie and the novel tie lines can be observed as the measure of the thermal bridge effect produced by the novel tie.

Fig. 5-10 shows the linear relationship between the R-value and the insulation thickness of the wall assemblies with the three tie configurations with stainless steel ties. The "control 125" assembly and the minimum R-value for Edmonton are shown.

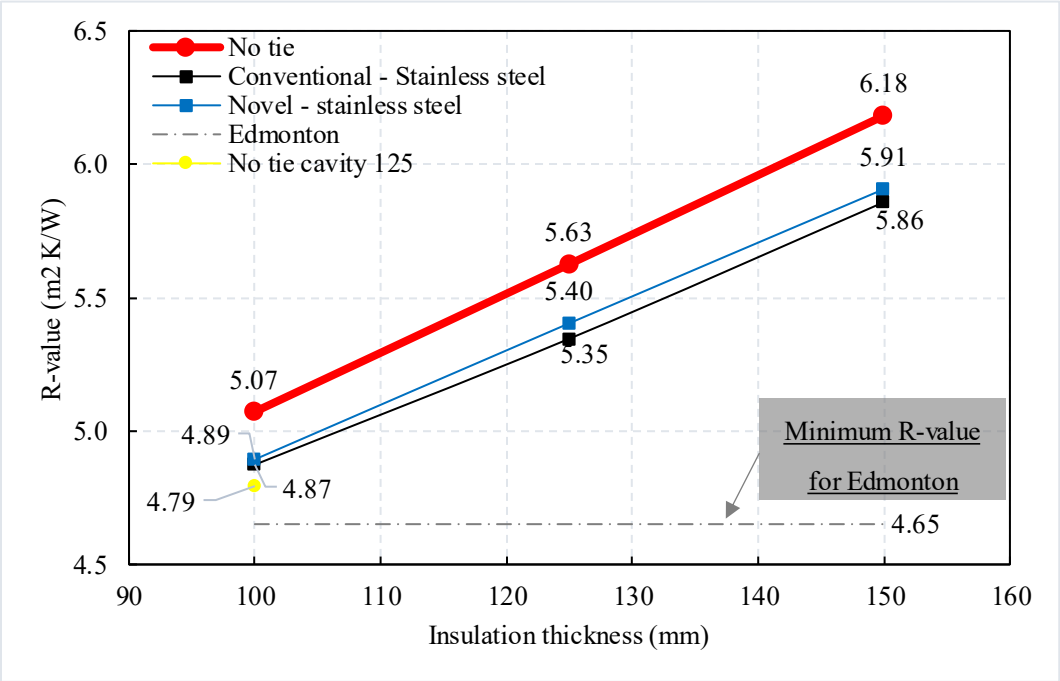

Figure 5-10. R-value vs insulation thickness for 3 types of tie configurations with stainless-steel ties.

The graph shows the R-value of the assemblies with stainless steel ties. It can be observed that assemblies with stainless steel ties reached a larger R-value than those using galvanized steel ties, reducing the thermal bridging effects. These larger R-values are expected due to the lower thermal conductivity of the stainless steel compared with the galvanized steel.

Fig. 5-11 shows the linear relationship between the R-value and the insulation thickness of the wall assemblies with the three tie configurations with GFRP ties. The "control 125" assembly and the minimum R-value for Edmonton are shown.

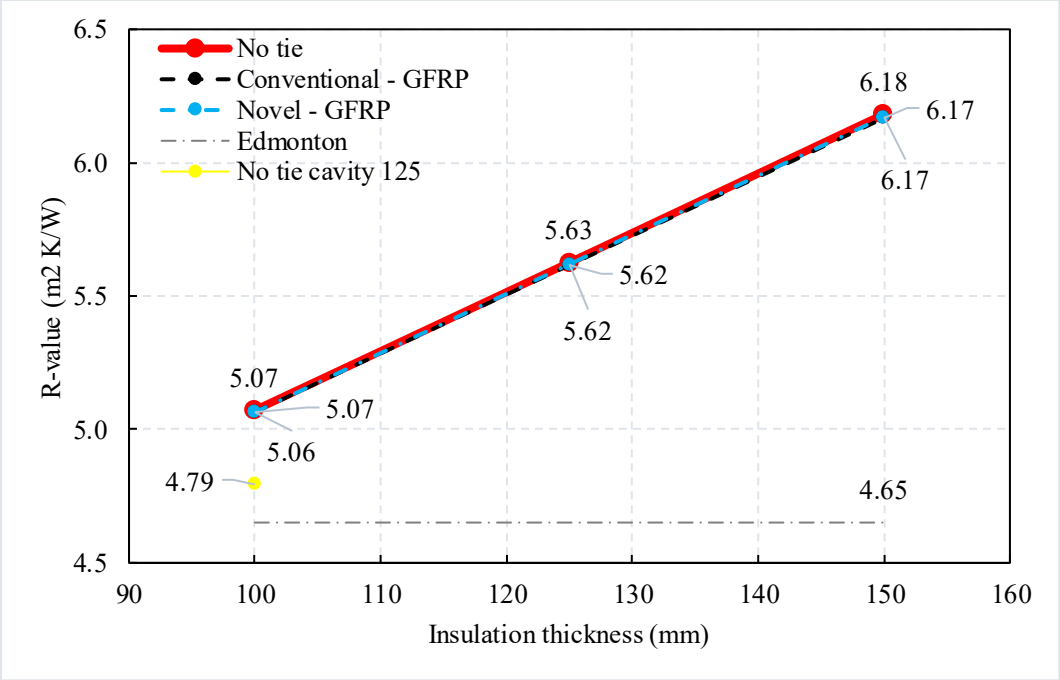

Figure 5-11. R-value vs insulation thickness for 3 types of tie configurations with GFRP ties.

The graph shows that the assemblies with GFRP ties achieve almost the same R-value as the assemblies without ties, this means that using this material neglects the thermal bridging effects due to the very low thermal conductivity of the material. The assemblies with GFRP ties achieved the largest R-value among the tie materials used.

5.5.3 Thermal Bridge Effect

To illustrate the thermal bridge effects in the wall assemblies, the simulations provide the temperature distribution and heat flux distribution on the wall assemblies. The temperature distribution consists of a graphic representation with a colour scale along the assembly showing the distribution of the temperature from the hot temperature ($22°C$) in the interior face represented by the red color, to the cold temperature ($-18°C$) in the exterior face represented by the dark blue colour. The heat flux distribution consists of a graphic representation of the exterior face of the wall, showing the temperature that penetrates the assembly through the wall due to the presence of thermal bridging elements, such as ties for this study.

Figure 5-10 shows the temperature distribution and heat flux distribution of the wall assembly with three tie configurations (no tie, conventional tie, and novel tie) and three insulation thicknesses (100, 125, and 150 mm). The first row shows the assembly without tie, the temperature distribution of this assembly is uniform as there is no presence of thermal bridge elements, only the layers of the materials comprising the wall. The heat flux distribution shows that the exterior face of the wall has a constant cold temperature equal to the boundary condition applied to that surface ($-18°C$).

The second row shows the assembly with the conventional tie. The temperature distribution shows the discontinuity produced in the area surrounding the tie due to the low thermal conductivity of the material, this shows the thermal bridge effect along the wall. The heat flux distribution shows the heat that flows from the interior face to the exterior face through the conventional tie, this shows the thermal bridge effect in the exterior face. The hottest temperature in the external face is concentrated in the center of the tie and is dissipated in the surrounding area as shown by the colour scale.

Finally, the third row shows the assembly with a novel tie. The temperature distribution shows the effect of the presence of the tie in the area surrounding the tie. The heat flux distribution shows the heat that flows from the interior face to the exterior face through the novel tie. The hottest temperature in the external face is concentrated in two regions, in the center of the top and bottom plates, and is dissipated in the area surrounding it.

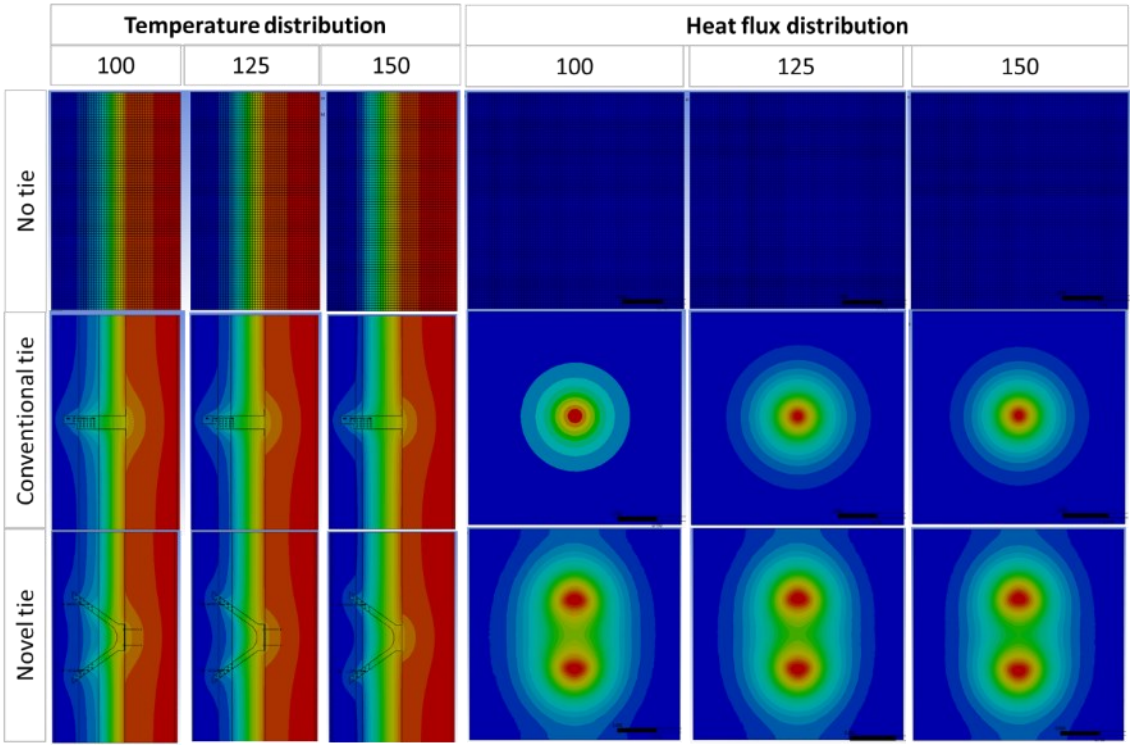

Figure 5-12. Thermal distribution and heat flux for three tie configurations and insulation thickness of 100, 125, and 150 mm.

Similarly, Fig. 5-11 shows the comparison between the assemblies with the two ties (conventional and novel ties), three insulation thicknesses (100, 125, and 150 mm), and three tie materials (steel, stainless steel, and GFRP) showing the thermal distribution and heat flux. Increasing the insulation thickness reduced the thermal bridge effect in the assembly, as observed in the temperature distribution figures. This is due that thicker insulation thickness increases the R-value in the assembly. The GFRP ties exhibited almost negligible thermal bridge due to the low thermal conductivity of the material, as observed in the temperature distribution and total heat flux figures. For those specimens with GFRP ties, the temperature distribution is almost as uniform as in the no tie assembly. This agrees with the calculated R-values, as GFRP assemblies reached almost the same value as the no tie assemblies.

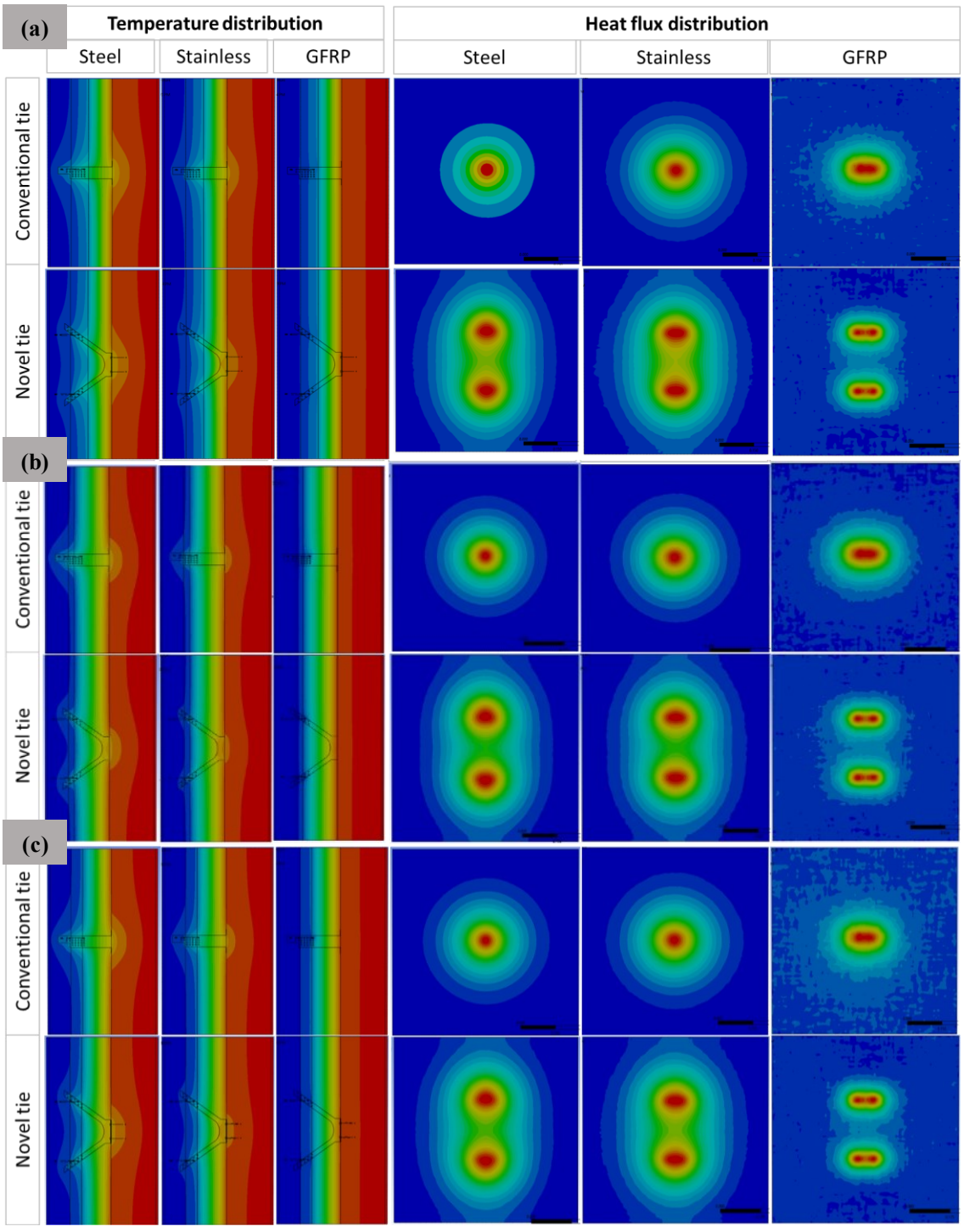

Figure 5-13. Thermal distribution and heat flux for three tie materials and three insulation thicknesses: a) 100 mm, b) 125 mm, and c) 150 mm.

5.6 Discussion of Results

5.6.1 Effect of Tie Type

The R-value of cavity wall assemblies was calculated for three tie configurations. First, assemblies without ties were analyzed to determine the R-value of the assembly without the thermal reduction (thermal bridge) caused by the inclusion of ties. Subsequently, a comparison was made between assemblies using conventional ties and those using novel ties. This comparison illustrated the thermal bridge effect resulting from the inclusion of ties in the assembly. The reduction in the R-value, measured as the difference between the R-value of the assembly without ties and the respective assembly with ties, is evident in Fig. 5-9. The graphical representation in Fig. 5-12 illustrates that the inclusion of ties distorts the temperature distribution throughout the assembly, allowing heat to flow to the exterior face of the assembly.

The R-values of assemblies using novel and conventional ties exhibited similar magnitudes, with a slight advantage for the novel tie assemblies (1% larger). This similarity can be attributed to the comparable height, thickness, and cross-sectional area of the ties.

5.6.2 Effect of Insulation Thickness

The investigation into the impact of insulation material thickness on the R-value of cavity wall assemblies considered three different thicknesses: 100, 125, and 150 mm. These variations were used while maintaining a constant cavity width of 175 mm. The objective was to assess how increasing insulation thickness within wider cavities influences the R-value.

The results revealed that insulation thickness had a significant impact on the R-value magnitude of the wall assemblies. A linear relationship was observed between insulation thickness and R-value. This correlation is logical, as thicker insulation material enhances the thermal break effect in the assembly, thereby increasing thermal resistance. Figures 5-9, 5-10, and 5-11 visually represent this linear relationship.

5.6.3 Effect of Tie Material

To investigate the impact of tie material on thermal performance, three materials were compared: galvanized steel, stainless steel, and GFRP. These materials were chosen due to their distinct thermal conductivities and suitability for use, as established in prior research. The tie geometries were the same for all the materials used, and only the material properties were modified in the FE assemblies.

The results reveal a linear relationship between the thermal conductivity of tie materials and the corresponding R-value of wall assemblies. The use of ties with lower thermal conductivity led to increased R-values in the wall assemblies. GFRP ties achieved the highest R-value and nearly matched the R-value of assemblies without ties. This indicates that there are no significant thermal bridge effects in GFRP tie assemblies. However, a comprehensive assessment of both thermal and mechanical characteristics is essential when choosing tie materials. Tension, compression, and longitudinal shear tests must be conducted on wider cavity walls connected with GFRP ties to determine their mechanical resistance, ensuring compliance with structural requirements and enabling comparison with the galvanized steel ties used in Chapter 4.

5.7 General Considerations

Limitations of this study are the presented in following:

The CMU and veneer wythes were simulated as homogeneous layers with combined thermal conductivity between the blocks, the grout, and the mortar as obtained from literature and previous studies. However, it is recommended to perform simulations separating each material as a different object with the respective thermal conductivity to get a better understanding of the interaction of the different materials under thermal analysis.

To compare the obtained R-value for all the assemblies with the thermal requirements in Canada, the R-values were compared with the minimum R-value required by the NECB (2022) for Edmonton, which is a strict example. This maximum R-value was shown in the plots, Additionally, the results were compared with a control cavity wall (Control 125) that represents a typical cavity wall comprised of the same materials and with 125 mm

cavity width to accommodate 100 mm of insulation and 25 mm of air space. This permits us to compare the improvement in R-value achieved by increasing the cavity width from a typical 125 mm to 175 mm to accommodate thicker insulation material.

Literature and previous studies show the thermal conductivity of the air space with a typical cavity width between 25-100 mm (ASTM, 2015; Shao, 2021). Limited studies have investigated the thermal resistance of the air space of masonry cavity walls with a cavity width of 175 mm. It is recommended to perform experimental studies such as like guarded box to determine the thermal resistance of the air space in such wider cavity walls.

In the analysis of the selection of tie material, several factors should be considered, including production cost, mechanical strength, and thermal resistance. The findings of Chapter 5 revealed that GFRP tie specimens exhibited the largest thermal resistance. However, further investigation is necessary to evaluate the cost and mechanical strength of these GFRP ties in comparison to other materials. The shear test conducted in Chapter 4 focused exclusively on galvanized steel ties, as a prior study demonstrated favourable tension and compression responses for the same ties utilized in this research. Due to the nature of GFRP material, its response will be significantly stronger when subjected to tension parallel to the fibers compared to other directions. Consequently, the shear response of GFRP ties may not meet the minimum requirements or could be considerably lower than that of steel ties. Therefore, it is recommended to conduct tests for tension, compression, and shear on GFRP ties to compare their performance against both the structural requirements and the galvanized ties used in this study.

Experimental investigations are required for verification purposes and improvements of the FE simulations.

5.8 Conclusions

The R-values for assemblies using both conventional and novel ties were nearly identical. On average, the thermal resistance of assemblies with conventional and novel ties reached about 91% and 92% of the R-value achieved by the assembly without ties, respectively.

This reduction in the R-value represents the thermal bridge effect caused by the inclusion of the ties in the wall assembly.

The comparison of the conventional and novel ties in terms of thermal resistance shows that both ties offer the same R-value with a difference of 1%. This is due to the same height and cross-section area, as well as the similar volume of material. However, another important factor to compare the ties is the mechanical behaviour. The tension, compression, and shear resistance of the ties need to be compared. This study presents the comparison of the shear resistance of the conventional and novel ties as shown in Chapter 4. The results show that the novel tie provides about 2.5 times greater shear resistance than the conventional tie.

The insulation thickness had the largest impact on the thermal resistance of the wall assemblies. On average, increasing insulation thickness from 100 to 150 mm increased the R-value by 22%, 19%, and 19% for the assemblies without tie, with conventional tie and novel tie, respectively. Constructing wider cavity walls permits to accommodate thicker insulation material leading to higher thermal resistance of the wall envelope.

The tie material had a significant influence on the thermal resistance of the studied wall assemblies. Three tie materials were compared (galvanized steel, stainless steel, and GFRP). The assemblies with stainless steel and GFRP as tie materials increased the R-value by 6% and 9% compared to conventional galvanized steel, respectively. The assemblies with galvanized steel, stainless steel, and GFRP ties reached 91.5%, 95.6%, and 99.8% of the R-value of the assembly without ties, respectively. That ratio represents the reduction of the R-value due to thermal bridge effects when including those ties in the wall assembly. Opting for a material with very low thermal conductivity (such as GFRP) can mitigate the substantial impact of thermal bridging caused by components that penetrate the insulation layer in cavity walls. However, as mentioned before, the mechanical behaviour of GFRP ties needs to be investigated to compare with the conventional steel ties and with the CSA requirements.

6 CONCLUSIONS AND RECOMMENDATIONS

6.1 Summary

Masonry cavity walls are used as exterior walls to reduce energy consumption and create a comfortable living environment in the building. One of the challenges that affects the thermal resistance of masonry cavity walls is thermal bridging. Thermal bridging in building envelopes occurs mostly in areas where structural components with high conductivity penetrate thermal insulation layers. An example of these thermal bridging elements are the masonry ties. Historically, energy standards have increased the energy requirements in buildings to increase energy efficiency. Therefore, upcoming codes are expected to increase the minimum thermal resistance of all the elements that comprise the building envelope. It is necessary to investigate alternatives to address these increasing requirements.

Additionally, masonry ties are a structural component used to transfer principally the out-of-plane loads between the exterior and interior wythes. According to the Canadian masonry codes, these wythes are designed to act together to resist out-of-plane loads, but no considerations are given to the wythes to act in composite action. Prior studies have demonstrated that wythes connected using ties with high shear strength enable the transmission of shear forces between the wythes, leading to the development of composite action within the system. This composite action enhances the overall resistance of the wall to out-of-plane forces when compared to systems connected by conventional ties. Consequently, there is a need for further investigation of composite action in cavity walls.

This study was part of a campaign at the University of Alberta and has two main objectives: conduct an experimental investigation on the longitudinal shear strength of cavity wall specimens using conventional ties and a novel tie within large cavities (175 mm) and develop computer simulations on finite element models to assess the thermal resistance (R-value) of cavity wall assemblies with both the conventional and novel ties in these wider cavity walls. Chapter 2 presented a literature review to understand the background of cavity walls, masonry ties, composite action, and thermal modelling on wall systems. Chapter 3 presented a background review of the structural and thermal requirements for masonry ties in cavity walls. Chapter 4 presented the experimental tests

on small-scale cavity wall specimens subjected to longitudinal shear load and the discussion of the results is presented. Chapter 5 presented finite element simulations to assess the thermal resistance (R-value) of wider cavity wall assemblies using both conventional and novel ties.

6.2 Conclusions

From Chapter 3, where the design background of masonry ties is presented:

- Canadian masonry standards allow for the design of cavity walls in which the wythes collaborate in resisting out-of-plane loads, but composite action is not accounted for. The standards stipulate that all ties must possess a minimum tensile and compressive resistance of 1 kN. Minimum shear strength is not specified.
- The Canadian masonry standards allow the design of cavity walls with the wythes sharing the out-of-plane loads but composite action is not taken into account. The standards also identify the use of ties with different characteristics in terms of shear strength with some ties permitting the vertical displacement between the wythes exhibiting low shear strength and others with high shear strength that restrict the vertical slip between the wythes.
- The standards indicate that all the ties need to have a minimum resistance in tension and compression of 1 kN. No minimum resistance is given for shear strength. The presence of ties with high shear strength can affect the crack propagation in the brick veneer as when vertical slip occurs, these shear ties will act to restrict that movement producing additional stresses in the brick veneer where the tie is embedded.

From Chapter 4, where an experimental program was presented to calculate the flexural stiffness and shear strength of the conventional and novel ties in wider cavity wall assemblies with varying embedment lengths of the attached round bent bars (45, 60, and 75 mm) and type of brick (concrete and clay):

- The inclined geometry of the tie allowed the novel tie to attain larger shear strength than the conventional plate tie. The truss action present in the novel tie was found to be more efficient in resisting shear load compared with the conventional ties

perpendicularly placed about the applied shear load. The vertical plate tie attained larger strength than the horizontal plate tie due to a larger moment of inertia from placement.

- The larger strength of the inclined tie enables it to be used with wider spacing in full-scale walls. In addition, since the inclined tie is stiffer than other tie types, expansion joints should be provided to mitigate the effect of shrinkage in the inner and outer wythe.
- In the concrete brick samples, the formation of cracks occurred in the later stages of deformation, whereas clay brick samples exhibited early crack propagation. Additionally, the shear strength and initial shear stiffness were larger for specimens with concrete bricks than those with clay bricks in the veneer.
- In general, increasing the embedment length of the bent bars into the veneer bed joint led to larger shear strength. For the VC tie, the shear strength was increased 1.04 times comparing the 75 mm to 60 mm. For the NC tie, the shear strength was increased to 1.03 and 1.05 comparing the 75 mm with 45 and 60 mm, respectively. No influence of the embedment length was observed on the initial shear stiffness of the ties. It is recommended that embedment lengths lesser than 45 mm be tested to study the optimal amount of embedment needed to prevent the pullout of the tie.

From Chapter 5, where the finite element model simulations were performed to calculate the thermal resistance of wider masonry cavity wall assemblies using both conventional and novel ties with varying insulation thickness (100, 125, and 150 mm) and tie material (steel, stainless steel, and GFRP):

- The comparison of the conventional and novel ties in terms of thermal resistance, shows that both ties offer the same R-value with a difference of 1%. This is due to the same height and cross-section area, as well as the similar volume of material. However, another important factor to compare the ties is the mechanical behaviour. The tension, compression, and shear resistance of the ties need to be compared.
- The R-value of wall assemblies using both conventional and novel ties were nearly identical. On average, the thermal resistance of assemblies with conventional and

novel ties reached about 91% and 92% of the R-value achieved by the assembly without ties, respectively. This reduction in the R-value represents the thermal bridge effect caused by the inclusion of the ties in the wall assembly.

- The insulation thickness had the largest impact on the thermal resistance of the wall assemblies. On average, increasing insulation thickness from 100 to 150 mm increased the R-value by 22%, 19%, and 19% for the assemblies without tie, with conventional tie and novel tie, respectively. Constructing wider cavity walls permits to accommodate thicker insulation material leading to higher thermal resistance of the wall envelope.
- The tie material had a significant influence on the thermal resistance of the studied wall assemblies. Three tie materials were compared (galvanized steel, stainless steel, and GFRP). Wall assemblies featuring stainless steel and GFRP ties exhibited a 6% and 9% increase in R-value, respectively, compared to assemblies with conventional galvanized steel ties. The R-values for assemblies with galvanized steel, stainless steel, and GFRP ties were 91.5%, 95.6%, and 99.8% compared with the R-value of the assembly without ties, respectively. This ratio indicates the reduction in R-value due to thermal bridge effects when incorporating these ties in the wall assembly.

6.3 Recommendations for Future Work

This thesis investigates the approach of designing wider cavity walls to accommodate thicker insulation material as a solution for the increasing energy requirements. The longitudinal shear strength and flexural strength of a novel and a conventional tie were compared. Additionally, the R-value of wall assemblies using these ties was determined. There are a series of recommendations for future work based on the outcomes of this study:

From Chapter 4:

- It is recommended to perform small-scale shear tests using typical cavity walls of 100 mm to compare the shear strength of the studied novel and conventional ties in typical cavity widths compared with the presented wider cavity wall specimens.

- The use of the wood spacer was a solution to restrain the rotation of the veneer to produce the shear load on the ties. Due to the scarcity of full-scale tests on these wider cavity walls using larger ties, it is recommended to test full-scale cavity walls using these larger ties and including the typical wall elements such as the insulation material and subject the wall to out-of-plane loading. This is to verify the assumption that the rotation of the veneer about the CMU wythe is not significant under the studied loads.
- Testing full-scale walls subjected to out-of-plane loading with these larger novel and conventional ties can be compared to typical walls with cavity widths of 100 mm. This is to compare the out-of-plane strength and stiffness of wider cavity walls, which is expected to comply the meet the increasing energy requirements. Shear and axial forces are often working at the same time as the tie may be under tension from suction on the wall as well as shear caused by that suction. Therefore, the interaction response between the axial and shear strength should be investigated.
- To test the novel ties in full-scale cavity walls, certain considerations must be taken into account. First, it is necessary to define analytical expressions to determine the degree of composite action that can be achieved with the novel ties. Such expressions for full-scale walls are in development by the Masonry Research group at the University of Alberta. Secondly, to experimentally determine the level of composite action of wide cavity walls connected using the novel ties, it is recommended to test a control wall with ties with only axial resistance, and a wall with the same characteristics but with the novel ties under out-of-plane load. The first wall will represent the non-composite wall and the additional out-of-plane strength reached by the second wall will be the measure of composite action achieved by the inclusion of the novel tie. The suggested dimensions and tie arrangement of such full-scale specimens are shown in Fig. 4-24 and the support and loading conditions are shown in Fig. 4-25.
- It is recommended to establish the level of composite action in the wall assembly based on the specific characteristics and demands of each project. High levels of

composite action may lead to cracks in the exterior wythe. To address this concern, some approaches include opting for lower levels of composite action, using ties with a mechanism to permit limited movement of the external wythe, incorporating expansion joints in the veneer, or providing longitudinal reinforcement in the external wythe are potential strategies to mitigate this issue.

From Chapter 5:

- It is recommended to perform simulations separating each material within the CMU and veneer wythes with their respective thermal conductivity to get a better understanding of the interaction of the different materials under thermal analysis.
- Results showed that ties made of materials with very low thermal conductivity, such as GFRP, reduce the thermal bridge effects. However, production cost, mechanical resistance, and thermal resistance need to be considered when comparing the appropriate material for the ties. Therefore, conducting tests for tension, compression, and shear on GFRP ties is recommended to compare their performance against both structural requirements and the galvanized ties used in this study.
- The thermal resistance of GFRP ties was significantly larger compared with ties with the same geometry made of galvanized steel and stainless steel. If shear tests were performed in GFRP ties, certain considerations must be taken into account. While GFRP ties may have larger tensile and compressive strength than steel, which can be advantageous, actual cavity walls experience a combination of loads resulting in diverse stress on the ties. Consequently, the anisotropic nature of GFRP may lead to lower shear resistance compared with steel ties. Additionally, the geometry of GFRP ties needs optimization due to the anisotropic characteristics of the material. Since the thermal bridging of these ties is almost negligible, increasing thickness can enhance the mechanical performance of such ties.
- It is recommended to perform experimental studies such as a guarded box to verify the simulations performed. Additionally, similar experimental studies are

recommended to determine the thermal resistance of the air space in such wider cavity walls.

- Transient state analysis is recommended to obtain the thermal response of wall assemblies with the influence of the temperature variations that are present in the real conditions. This also permits measuring the influence of the thermal mass of the clay brick veneer on the thermal resistance of the cavity walls.

REFERENCES

Abdou, O.A. and Murali, K.S. (1994). "The effect of air cells and mortar joints on the thermal resistance of concrete masonry walls." *Energy and Buildings*, 21(2): 111–119.

Adrien, Palermo, Dan, and Khan, Usman T.3. (2021). "Adapting CSA Masonry Standards to Climate Change: Part 1- Impacts on Masonry Materials, Design, And Construction Sparling." *14th Canadian Masonry Symposium*, Montreal, Canada. May 16th – May 20th, 2021.

Alterman, Dariusz, Page, Adrian W., Zhang, Congcong, and Moghtaderi, Behdad. (2017). "The Effect of Vertical and Horizontal Thermal Mass on The Thermal Performance of Australian Housing." *13th Canadian Masonry Symposium*, Halifax, Canada. June 4th – June 7th 2017.

Anand, Subhash C., and Rahman, Md. Ayubur. (1989) "Engineering Report Analytical Investigations of The Behavior and Failure of Composite Masonry Walls." Department of Civil Engineering Clemson University. A technical report submitted to the National Science Foundation. Clemson, South Carolina. 29634·0911. August, 1989.

ANSYS (2019). https://www.ansys.com/products/platform.

Arnold W. Hendry, (1981). "Structural Brickwork." MacMillan Press, 1st ed. London, 1981. DOI 10.1007/978-1-349-81439-8.

Arslan, Onura; Messali, Francesco; Smyrou, Eleni; Bal, Ihsan; and Rots, Jan. (2021). "Experimental characterization of the axial behavior of traditional masonry wall metal tie connections in cavity walls." *Construction and Building Materials Journal*, 266, 121141.

Arumala, Joseph O. (2007). "Brick Veneer Steel Stud Wall Systems: State-of-the-Art." *TMS Journal*, September, 2007.

ASHRAE. (1993). ASHRAE Handbook-Fundamentals, chapter 22. Atlanta. Ga.: American Society of Heating, Refrigerating and Air-Conditioning Engineers, Inc.

ASHRAE. (2017). 25.2.1.7 Series and Parallel Heat Flow Paths. 2017 ASHRAE® Handbook - Fundamentals (SI Edition). American Society of Heating, Refrigerating and Air-Conditioning Engineers, Inc. (ASHRAE), pp.7.

ASHRAE. (2017a). Chapter 27. Heat, Air, and Moisture Control in Building Assemblies — Examples, in: ASHRAE Handbook-Fundamentals. pp. 25.1-25.16.

ASHRAE. (2019). ASHRAE 90.1- Energy Standard for Buildings except Low-Rise Residential Buildings. Vol. Vol. 90 ASHRAE.

ASHRAE. (2021). Energy Standard for Buildings except Low-Rise Residential Buildings. Vol. 90 ASHRAE.

ASHRAE. (2021a). Series and Parallel Heat Flow Paths. 2021 ASHRAE® Handbook - Fundamentals (I-P Edition). American Society of Heating, Refrigerating and Air-Conditioning Engineers, Inc. (ASHRAE).

ASHRAE. (2021b). Steady-State Thermal Response. 2021 ASHRAE® Handbook - Fundamentals (I-P Edition). American Society of Heating, Refrigerating and Air-Conditioning Engineers, Inc. (ASHRAE).

ASTM. (2013). C1155 -95: Standard practice for determining thermal resistance of building envelope components from the in-situ data. ASTM International West Conshohocken, United States.

ASTM. (2015). C1058/C1058M-10: Standard Practice for Selecting Temperatures for Evaluating and Reporting Thermal Properties of Thermal Insulation. American Society for Testing and Materials. West Conshohocken, United States.

ASTM. (2019). C1363-19: Standard Test Method for Thermal Performance of Building Materials and Envelope Assemblies by Means of a Hot Box Apparatus. American Society for Testing and Materials. West Conshohocken, United States.

Banting, Bennett; Drysdale, Robert; El-Dakhakhni, Wael and Stubbs, David. (2017). "The New CSA S304-14 Design of Masonry Structures: Part 2 Discussion of Seismic Changes to the Standard." *13th Canadian Masonry Symposium*, Halifax, Canada. June 4th – June 7th 2017.

Bennett, R.M.; Pierson, D.L.; Dalrymple, G.A. and Samblanet, P.J. (2017a). The 2016 "TMS 402-602 Code Requirements & Specification: What to Expect and Why." *13th Canadian Masonry Symposium*, Halifax, Canada. June 4th – June 7th 2017.

Brown, R. and Elling, R. (1979). "Lateral Load Distribution in Cavity Walls." in Proceedings of the Fifth International Brick Masonry Conference. Washington, D.C., 1979, pp. 351-359

Brzev, Svetlana and Anderson, Donald. (2018) "Seismic Design Guide for Masonry Buildings." *Canadian Concrete Masonry Producers Association*, Second Edition, 2018.

Burnett, E.F.P., and Postma, M.A., (1995). "The pullout of ties from brick veneer." *7th Canadian Masonry Symposium*, Hamilton, Ontario, Canada.

Catani, Mario J.; Porter, Max L. and Banks, Kenneth G. (1995). "New Style Veneer Tie Answers the Need for Stiffness and Adjustability." *7th Canadian Masonry Symposium*, Hamilton, Ontario, Canada.

CCMPA. (2013). Canadian Concrete Masonry Producers' Association-Thermal Properties & Design Details. Technical Notes- Retrieved from: https://ccmpa.ca/download/metric-technical-manual/6-thermprop/.

Choi, Wonchang; Jang, Seok-Joon; and Yun, Hyun-Do. (2019). "Design properties of insulated precast concrete sandwich panels with composite shear connectors." *Composites*, Part B, 157 p. 36-42.

Choi, Young and LaFave, James. (2004). "Performance of corrugated metal tie for brick veneer wall systems." *Journal of Materials in Civil Engineering*, Volume 16, Issue 3, p. 202 – 211. DOI: 10.1061/(ASCE)0899-1561(2004)16:3(202)

Corrêa, M.R.S., Moreira, E.M.S., and Ramalho, M.A. (2009). "Experimental Small-Scale Analysis of The Connections Between Structural Clay Block Work Masonry Walls Submitted to Vertical Loads." *11th Canadian Masonry Symposium*, Toronto, Ontario. May 31- June 3, 2009.

CSA. (2014). CSA-A370-94. *Connectors for Masonry*. Canadian Standards Association. Rexdale, Ontario.

CSA. (2014a). CSA-S304-14 *Design of Masonry Structures*. Canadian Standards Association. Rexdale, Ontario.

Deconinck, An-Heleen and Roels, Staf. (2016). "Comparison of characterisation methods determining the thermal resistance of building components from onsite measurements." *Energy and Buildings Journal*, 130: 309-320. ISSN 0378-7788. https://doi.org/10.1016/j.enbuild.2016.08.061.

Del Coz Díaz, J.J., García Nieto, P.J., Rodríguez, A. Martín, Martínez-Luengas, A. Lozano and Betegón Biempica, C. (2006). "Non-linear thermal analysis of light concrete hollow brick walls by the finite element method and experimental validation." *Applied Thermal Engineering Journal*, 26 (8–9): 777-786. ISSN 1359-4311. DOI: https://doi.org/10.1016/j.applthermaleng.2005.10.012.

Desjarlais, A.O. and McGowan, A.G. (1997). "Comparison of experimental and analytical methods to evaluate thermal bridges in wall systems." *Insulation Materials: Testing and Applications*, 3.

Dey, Sandip. (2014). "Seismic performance of Composite Plate Shear Walls." Presented in Partial Fulfillment of the Requirements for the Degree of Master of Applied Science in Civil Engineering. Concordia University, Montreal, Quebec, Canada.

Dillon, Patrick B. (2017). "Towards A Consistent and Economical Design of Shelf Angles." *13th Canadian Masonry Symposium*, Halifax, Canada. June 4th – June 7th 2017.

Drysdale, R.G., and Banting, B.R. (2020). "Masonry Structures." 2nd Canadian Edition, Mississauga, Ontario, Canada, 2020.

Drysdale, R.G., and Hamid, A.A. (2005). "Masonry Structures - Behavior and Design," Canadian Edition, Canadian Masonry Design Center, Mississauga, Ontario, 2005.

Drysdale, R.G., and Wilson, M.J. (1989). "A Report on Behaviour of Brick Veneer/Steel Stud Tie Systems." Canada Mortgage and Housing Corporation. Hamilton, Ontario, Canada.

Drysdale, R.G.; Banting, B. and Stubbs, D. (2017). "The New CSA S304-14 Design of Masonry Structures: Part 1 Discussion of Non-Seismic Changes to The Standard." *13th Canadian Masonry Symposium*, Halifax, Canada. June 4th – June 7th 2017.

Egbon, B., and Tomlinson, D. (2021). "Experimental Investigation of Longitudinal Shear Transfer in Insulated Concrete Wall Panels with Notched Insulation," *Journal of Building Engineering*, 43 (2021), 103173.

FERO Corporation. (2023). FERO Thermal Tie TM - Slotted Rap-Tie. Masonry Connector. https://ferocorp.com/product/fero-thermal-slotted-rap-tie/

Finch G, Wilson M and Higgins J (2013) Thermal Bridging of Masonry Veneer Claddings & Energy Code Compliance. 12th Canadian Masonry Symposium, Vancouver, BC, June. 2-5.

Frankl, Bernard A.; Lucier, Gregory W.; Hassan, Tarek K.; and Rizkalla, Sami H. (2011). "Behavior of precast, prestressed concrete sandwich wall panels reinforced with CFRP shear grid." *PCI Journal*, Spring 2011, 42 -54.

Gleich, H. (2007). "New Carbon Fiber Reinforcement Advances Sandwich Wall Panels." *Structure Magazine* (April): 61–63.

Gombeda, Matthew, Trasborg, Patrick, Naito, Clay and Quiel, Spencer. (2017). "Simplified Model for Partially-Composite Precast Concrete Insulated Wall Panels Subjected to Lateral Loading." *Engineering Structures Journal*, 138: 367-380.

Gonzalez Mariscal, Rafael De Jesus. (2022). Study Of a Slender Masonry Wall Tested in An Innovative Device. A thesis submitted in partial fulfillment of the requirements for the degree of Master of Science. Department of Civil and Environmental Engineering, University of Alberta, Edmonton, Alberta, Canada.

Goyal, Ajay; Hatzinikolas, Michael A. and Warwaruk, Joseph. (1993). "Shear Connected Cavity Walls Under Vertical Loads." Structural Engineering Report No. 182, Department of Civil Engineering, University of Alberta, Edmonton, Alberta, Canada, 1993.

Gregory, Katherine, Moghtaderi, Behdad, Sugo, Heber and Page, Adrian. (2007). "Effect Of Thermal Mass on The Thermal Performance of Various Australian Residential Constructions Systems." *Energy and Buildings Journal*, 40 (4): 459-465.

Hamed, E. and Rabinovitch, O. (2008). "Masonry walls strengthened with composite materials – dynamic out-of-plane behavior." *European Journal of Mechanics*, A/Solids 27: 1037–1059.

Hassan, Dyaa; Shibani, Abdussalam; Agha, Araz and Al Sharqi, Said. (2021). "Performance of Sustainable Building Fabric to Replace the Traditional Cavity Wall Technique for New Housing Sector in the UK." *International Journal of Advanced Engineering Research and Science* (IJAERS), ISSN: 2349-6495(P), 2456-1908(O), 8 (3).

Hatzinikolas, M.A., and Warwaruk, J. (1994). "Connecting Cavity Walls." *Journal of the Masonry Society*, 1994.

Hatzinikolas, M.A., Longworth, J. and Warwaruk, J. (1982). "Ties In Large Cavity And Veneer Masonry Walls." *Alberta Masonry Institute*.

Helwig NE (2017) Data, Covariance, and Correlation Matrix. University of Minnesota (Twin Cities).

Hydro BC. (2021). Commercial new construction. Building envelope thermal bridging guide available at https://www.bchydro.com/content/dam/BCHydro/customer-portal/documents/power-smart/builders-developers/building-envelope-thermal-bridging-guide-v1-6.pdf.

Ibañez-Puy, M., Vidaurre-Arbizu, M., Sacristán-Fernández, J.A. and Martín-Gómez, C. (2017). "Opaque Ventilated Façades: Thermal and Energy Performance Review." *Renewable and Sustainable Energy Reviews*, 79: 180-191. ISSN 1364-0321. DOI: https://doi.org/10.1016/j.rser.2017.05.059.

International Masonry Institute. (2023). 01.030.0703: Shelf Angle Detail - Typ. face brick, term bar. URL: https://imiweb.org/01-030-0703-shelf-angle-detail-typ-face-brick-term-bar/

Ismaiel, Maysoun M. (2022). A Practical Method to Estimate the Effective Thermal Resistance of Exterior Masonry Walls. A thesis submitted in partial fulfillment of the requirements for the degree of Doctor of Philosophy. Civil and Environmental Engineering – Building Engineering, University of Alberta. Edmonton, AB, Canada.

ISO (2014). ISO 9869:2014. Thermal Insulation – Building Elements – In Situ Measurement of Thermal Resistance and Thermal Transmittance.

ISO (2017). 10211:2017 (E). Thermal bridges in building construction - Heat flows and surface temperatures - Detailed calculations. In: International Organization for Standardization (ISO).

ISO (2017a). ISO 14683:2017. Thermal bridges in building construction - Linear thermal transmittance - Simplified methods and default values

ISO (2017b). ISO 6946:2017. Building components and building elements - Thermal resistance and thermal transmittance - Calculation methods. Available Online: Https://Www.Iso.Org/Standard/65708.Html (Accessed on 20 December 2018).

Kazem, Hamid; Bunnb, William; Seliemc, Hatem; Rizkallaa, Sami and Gleich, Harry. (2015). "Durability And Long-Term Behavior Of FRP/Foam Shear Transfer Mechanism for Concrete Sandwich Panels." *Construction and Building Materials Journal*, 98: 722–734.

Kim, JunHee and You, Young-Chan. (2015). "Composite Behavior of a Novel Insulated Concrete Sandwich Wall Panel Reinforced with GFRP Shear Grids: Effects of Insulation Types." *Materials Journal*, 8: 899-913. doi:10.3390/ma8030899

Kontoleon, K.; Theodosiou, T.G. and Tsikaloudaki, K. (2013). "The Influence of Concrete Density and Conductivity on Walls' Thermal Inertia Parameters Under a Variety of Masonry and Insulation Placements." *Applied energy*, 112: 325-337.

LaFave, James M., and Reneckis, Dziugas. (2005). "Structural Behavior of Tie Connections for Residential Brick Veneer Construction." *TMS Journal*, December, 2005.

Lee, Byoung-Jun and Pessiki, Stephen. (2008). "Revised Zone Method R-Value Calculation for Precast Concrete Sandwich Panels Containing Metal Wythe Connectors." *PCI Journal*, September–October 2008. 53 (5): 86-100. DOI: https://doi.org/10.15554/pcij.09012008.86.100

Lohonyai, A. J., Korany, Y. and Trovato, N. (2015). "Analysis of Field-Measured Reversible Deformations in Masonry Cavity Walls." *TMS Journal*, December 2015.

Luebke, J., Pozo-Lora, F.F., Al-Rubaye, S. and Maguire, M. (2023). "Out-of-Plane Flexural Behavior of Insulated Wall Panels Constructed with Large Insulation Thicknesses." *Materials Journal,* 16, 4160.

Martins, A., Vasconcelos, G., and Costa, A.C. (2017). Experimental assessment of the mechanical behaviour of ties on brick veneers anchored to brick masonry infills. Construction and Building Materials, 156, 515–531. https://doi.org/10.1016/j.conbuildmat.2017.09.013

McGinley, W.M., Warwaruk, J., Longworth, J., and Hatzinikolas, M. “The Effect of Tie Type on Brick Veneer Walls.” University of Alberta, Edmonton, Alberta, Canada.

Messali, F., Skroumpelou, G. and Esposito, R. (2017). *Tests on existing wall ties: shear and axial tests*. Delft University of Technology.

Morrison Hershfield. (2018). Appendix a – Catalogue Material Data Sheets. Building Envelope Thermal Bridging Guide.

Morrison Hershfield. (2022) Building Envelope Thermal Bridging Guide, version 1.6. Hydro Power Smart. Vancouver, Canada.

Morrison Hershfield. (2022a). Thermal performance of building envelope details for mid- and high-rise buildings. ASHRAE Research Project RP-1365, Report.

Mullin, P. and O'Connor, O. (1987). "The Use of Steel Reinforcement Systems to Improve the Strength and Stiffness of Laterally Loaded Cavity Brick Walls", *Journal of Structural Engineering*, ASCE, Vol. 113, No.2, February 1987. pp 334-348.

NAIMA Canada. Codes and Standards. URL: https://www.naimacanada.ca/codes-standards

Naito, Clay; Hoemann, John; Beacraft, Mark and Bewick, Bryan. (2012). “Performance and Characterization of Shear Ties for Use in Insulated Precast Concrete Sandwich Wall Panels.” *Journal of Structural Engineering*, 138 (1).

Nave, R. (2000). HyperPhysics. “Thermal Conductivity”. Georgia State University. Available at: http://hyperphysics.phy-astr.gsu.edu/hbase/thermo/thercond.html#c1

NCMA. (2003). “TEK 5-1B, Concrete Masonry Veneer Details,” Virginia, USA.

NCMA. (2005). “TEK 16-01A Multiwythe Concrete Masonry Walls.”

NCMA. (2011). “TEK 12-01B Anchors and Ties for Masonry,”.

NCMA. (2012). “TEK 16-03B Reinforced Composite Concrete Masonry Walls,” Edmonton, Alberta, Canada.

NCMA. (2013) R-values of single-wythe concrete masonry walls.

NCMA. (2013). “TEK 06-01C R-Values of Multi-Wythe Concrete Masonry Walls,”.

NCMA. (2020). “TEK 16-04A Design of Concrete Masonry Noncomposite (Cavity) Walls,”.

NECB. (2015) National Energy Code of Canada for Buildings.

NECB. (2017). National Energy Code of Canada for Buildings.

NECB. (2020). National Energy Code of Canada for Buildings.

NECB. (2022). National Energy Code of Canada for Buildings 2020. Fifth edition. Canada.

Norris N, Lawton M and Roppel P (2012) The concept of linear and point transmittance and its value in dealing with thermal bridges in building enclosures. Building enclosure science & technology conference. 1-10.

Olsen, Jaiden Thomas. (2017). "Developing a General Methodology for Evaluating Composite Action in Insulated Wall Panels." URL: https://digitalcommons.usu.edu/etd/6548

Ortega, J., Mendes, N., Vasconcelos, G. (2022). "Numerical Simulation of the Tension–Compression Behavior of Tie Connections in Brick Masonry Walls." *CivilEng 2022*, 3: 441–455. DOI: https://doi.org/10.3390/civileng3020026

Pacholok, R.M., and Elwi, A.E. (1995). "Composite Walls." *7th Canadian Masonry Symposium*. Hamilton, Ontario, Canada.

Page, A.W., Simundic, G. and Masia, M. (2009). "A Study of Wall Tie Force Distribution in Veneer Wall Systems (Stage 1)." *11th Canadian Masonry Symposium*, Toronto, Ontario. May 31- June 3, 2009.

Papanikolas, K, Hatzinikolas, M and Warwaruk, J. (1990). "Behaviour of Shear Connected Cavity Walls," Structural Engineering Report No. 169. University of Alberta, Edmonton, Canada.

Papanikolas, P.K. (1990). "Behavior of Shear Connected Cavity Walls." MSc thesis Department of Civil Engineering, University of Alberta, Edmonton, Alberta, Canada.

Pessiki, Stephen, and Mlynarczyk, Alexandar. (2003). "Experimental Evaluation of the Composite Behaviour of Precast Concrete Sandwich Wall Panels," *PCI Journal*, March, 2003.

Pitoni, Beniamino. (1980) "Investigation of Cavity Wall Ties." A Report Submitted to the School of Graduate Studies in Partial Fulfilment of the Requirements for the Degree Master of Engineering. McMaster University. Hamilton, ON, Canada.

Precast/Prestressed Concrete Institute (1997). PCI committee. *State of the Art of Precast/Prestressed Concrete Sandwich Wall Panels*. PCI Committee Report.

Raouf, Ayman and Al-Ghamdi, Sami. (2019). "Effect of R-values changes in the baseline codes: Embodied energy and environmental life cycle impacts of building envelopes," 6th International Conference on Energy and Environment Research, ICEER 2019, 22–25 July, University of Aveiro, Portugal.

Ritchie, T. (1961). "Cavity Walls," NRC Publications Archive.

Rocky Mountain Masonry Institute. (2019). "Colorado Masonry Systems Design Guide."

Romero, Danny and Tomlinson, Douglas. (2023). "Tensile Response of Traditional and Contemporary Connectors in Masonry Cavity Walls with Thick Insulation." *CSCE Annual Conference*, Moncton, NB, Canada. May 24-27, 2023.

Roppel P, Hershfield M, Marif W, et al. (2011) Research Project Report RP-1365: Thermal Performance of Buildings Envelope Details for Mid and High-Rise Buildings. ASHRAE Inc. Report No. 5085243.01.

Roppel P, Lawton M and Norris N (2012) Thermal Performance of Building Envelope Details for Mid-and High-Rise Buildings. ASHRAE Transactions 118(2).

Sakr, K.M., and Neis, V.V. (2001). "Load-Deflection Analyses of Double Wythe Unreinforced Masonry Walls." *Journal of Structural Engineering*, September 2001, 1101-1108

Sanders, John; Carrier, Jerry; Clark Jr, Charles and Huygen, Nathaniel. (2017). "Dynamic Thermal Performance Measurements of Clay Brick Masonry." *The 3rd Canadian Masonry Symposium*, Halifax, Canada. June 4th to 7th, 2017.

Schumacher C, Straube J, Ober D, et al. (2013) Development of a new hot box apparatus to measure building enclosure thermal performance. Proceedings of Buildings XII. 1-19.

Shao, Yue. (2021). *Evaluating the Thermal Impacts of Different Masonry Wall Tie Designs Using FEM*. MSc Thesis. University of Alberta, Edmonton, AB, Canada.

Siveski, Zlatan. (1997). "Non-linear Structural Analysis of Shear Connected Cavity Walls Subject to Wind Load," Thesis submitted for the degree of Master of Science. University of Manitoba. Winnipeg, Manitoba, Canada.

Straka, Vera. (2001). "Composite Masonry Wall Ties," *Canadian Mortage and Housing Corporation*, Final Report. Ryerson University, Toronto, Ontario, Canada, 2001.

Tawil, H.; Tan, C.G.; Sulong, N.H.R.; Nazri, F.M.; Sherif, M.M. and El-Shafie, A. (2022). "Mechanical and Thermal Properties of Composite Precast Concrete Sandwich Panels: A Review." *Buildings Journal*, 12, 1429. DOI: https://doi.org/10.3390/buildings12091429.

The Brick Industry Association. (2003). *Tech Notes 44B - Wall Ties for Brick Masonry*.

The Masonry Standards Joint Committee. (2002). "Building Code Requirements for Masonry Structures," ACI 530/ASCE 5/ TMS 402, American Society of Civil Engineers, and The Masonry Society, Detroit, New York, and Boulder, 2002.

Tomlinson, Douglas and Fam, Amir. (2016). "Analytical approach to flexural response of partially composite insulated concrete sandwich walls used for cladding," *Journal of Engineering Structures*, 122: 251-266. DOI: https://doi.org/10.1016/j.engstruct.2016.04.059.

Tomlinson, Douglas. (2015). Behaviour of Partially Composite Precast Concrete Sandwich Panels Under Flexural and Axial Loads. PhD thesis. Queens University. Kingston, Ontario, Canada.

Tomlinson, Douglas; Teixeira, Nathan and Fam, Amir. (2016). "New Shear Connector Design for Insulated Concrete Sandwich Panels Using Basalt Fiber-Reinforced Polymer Bars." *Journal of Composites for Construction*, 20 (4).

Van, Geem, Fiorato, A. and Musser, D. (1982). Calibrated hot box tests of thermal performance of concrete walls. Proceedings of the ASHRAE/DOE Conference on Thermal Performance of the Exterior Envelopes of Buildings II, Las Vegas, NV.

Vermeltfoort, A.T. and Martens, D.R.W. (2015). "Composite Action in Masonry Walls Under Vertical In-Plane Loading: Experimental Results Compared with Predictions." *Canadian Journal of Civil Engineering*, 42: 449-462. DOI: https://doi.org/10.1139/cjce-2014-0098.

Wang, Ru; Elwi, Alaa E. and Hatzinikolas, Michael A. (1997). "Design of Slender Shear Connected Masonry Cavity Walls," Canadian Journal of Civil Engineering, 24: 808-818.

Wang, Ru; Elwi, Alaa E; Hatzinikolas, Michael A. and Warwaruk, Joseph. (1996). Behaviour of Masonry Cavity Walls Subjected to Vertical Eccentric Loads.

Williams C.R. and Hamid, A.A. (2005). "In-plane Stiffness and Strength of Adjustable Wall Ties." *10th Canadian Masonry Symposium*, Banff, Alberta.

Wilson M, Finch, G., Higgins, J. (2013) Masonry Design Support Details: Thermal Bridging. Proceedings from 12th Canadian Masonry Symposium. Vancouver, BC, Canada.

Wilson, M. and Higgins, J. (2019). FERO rap tie and fast system.

Woltman, Gregory; Noel, Martin and Fam, Amir. (2017). "Experimental And Numerical Investigations of Thermal Properties of Insulated Concrete Sandwich Panels with Fiberglass Shear Connectors." *Energy and Buildings Journal*, 145: 22-31.

Woltman, Gregory; Tomlinson, Douglas and Fam, Amir. (2013). "Investigation of Various GFRP Shear Connectors for Insulated Precast Concrete Sandwich Wall Panels." *Journal of Composites for Construction*, 17 (5): 575-752.

Xie, C. (2012). Interactive heat transfer simulations for everyone. The Physics Teacher 50(4): 237-240.

Zhang, Yumei, Ma, Guoyuan; Wu, Guoqiang; Liu, Shuailing and Gao, Lei. (2022). "Thermally Adaptive Walls for Buildings Applications: A State-of-The-Art Review." *Energy and Buildings Journal*, 271, 112314, ISSN 0378-7788. DOI: https://doi.org/10.1016/j.enbuild.2022.112314.

Zieukiewicz O and Taylor R (1991) The finite element method, 4-th Edition. Ed. Me Graw Hill.

Zisi, Nikola and Bennett, Richard. (2011). "Shear Behavior of Corrugated Tie Connections in Anchored Brick Veneer - Wood Frame Wall Systems." *Journal of Materials in Civil Engineering*, 23 (2). DOI: https://doi.org/10.1061/(ASCE)MT.1943-5533.0000143

Zorainy M, Ashour A and Galal K (2018) Comparing Canadian and American Standards Requirements for Evaluating Masonry Compressive Strength.

APPENDIX A: LOAD-DEFORMATION RESPONSE OF INDIVIDUAL SPECIMENS UNDER SHEAR LOAD

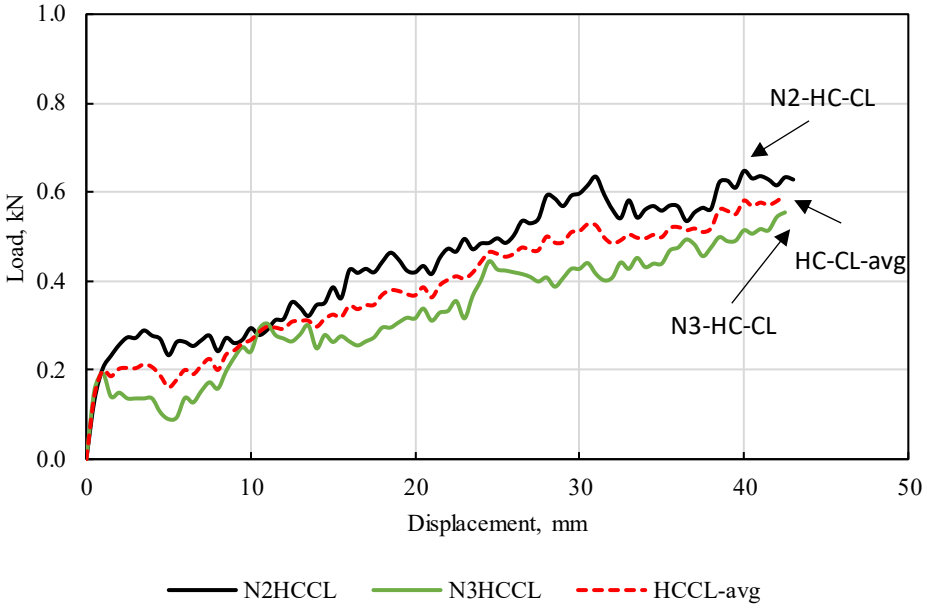

Figure A- 1. Shear response of specimens with HC tie and clay brick.

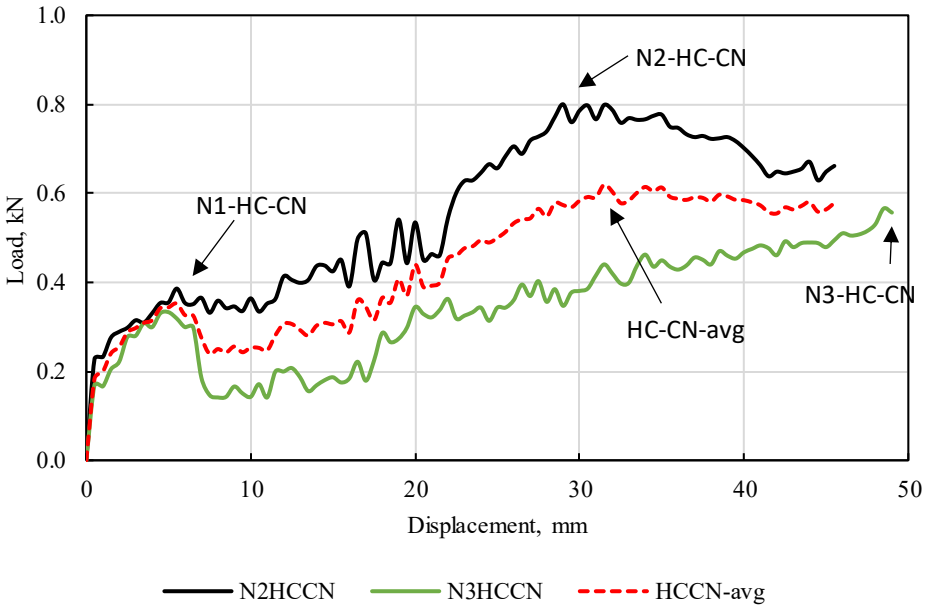

Figure A- 2. Shear response of specimens with HC tie and concrete brick.

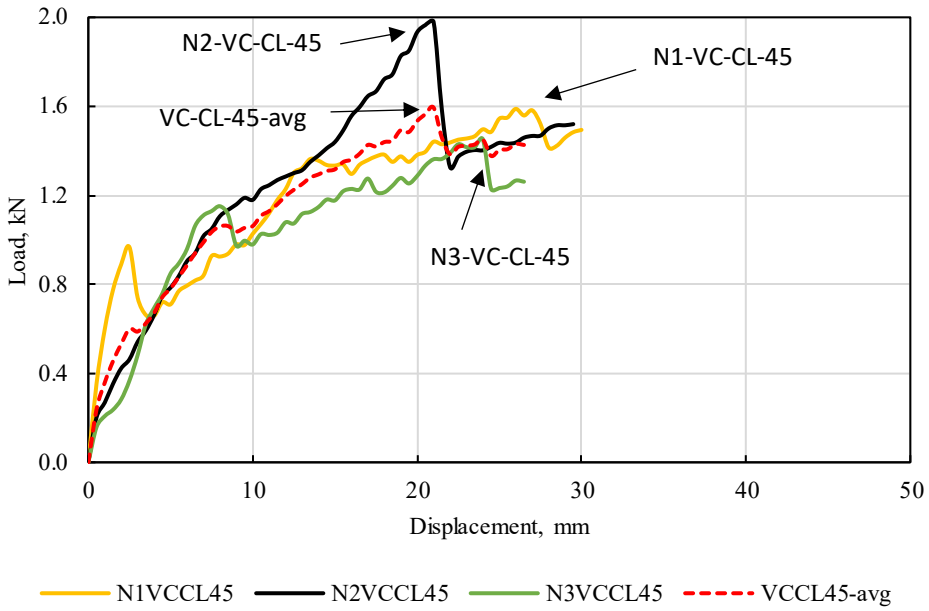

Figure A- 3. Shear response of VC ties, 45 mm embedment length and clay brick.

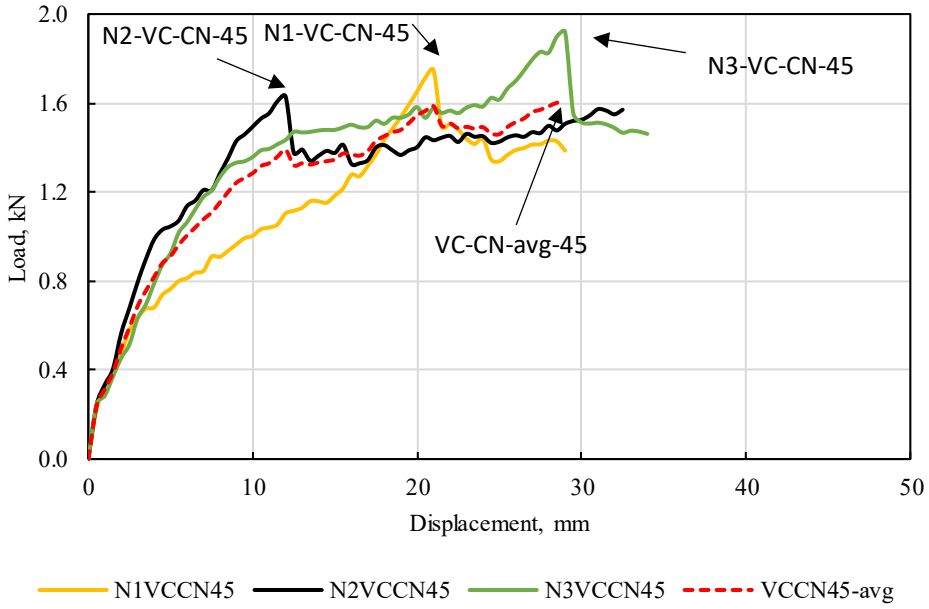

Figure A- 4. Shear response of VC ties, 45 mm embedment length and concrete brick.

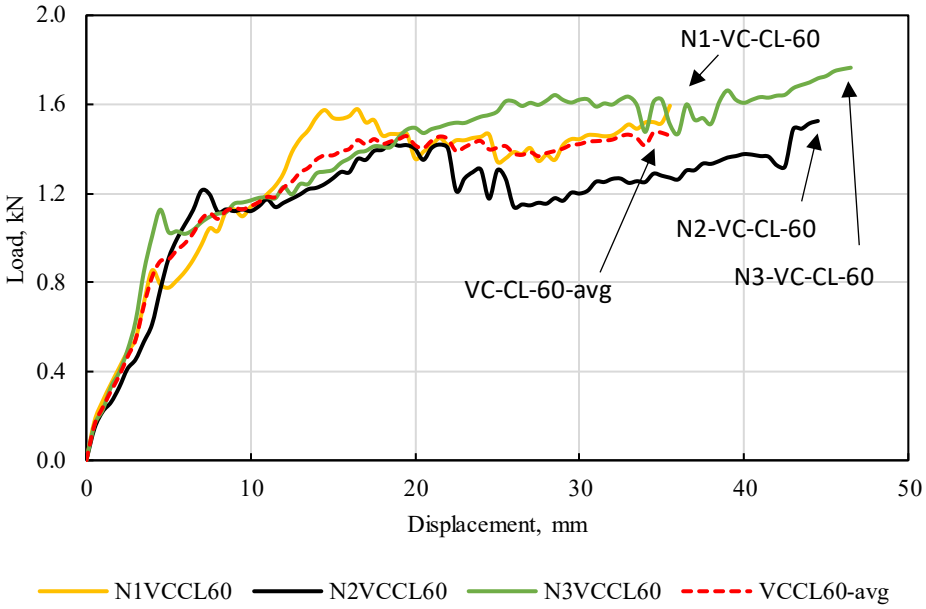

Figure A- 5. Shear response of VC ties, 60 mm embedment length and clay brick.

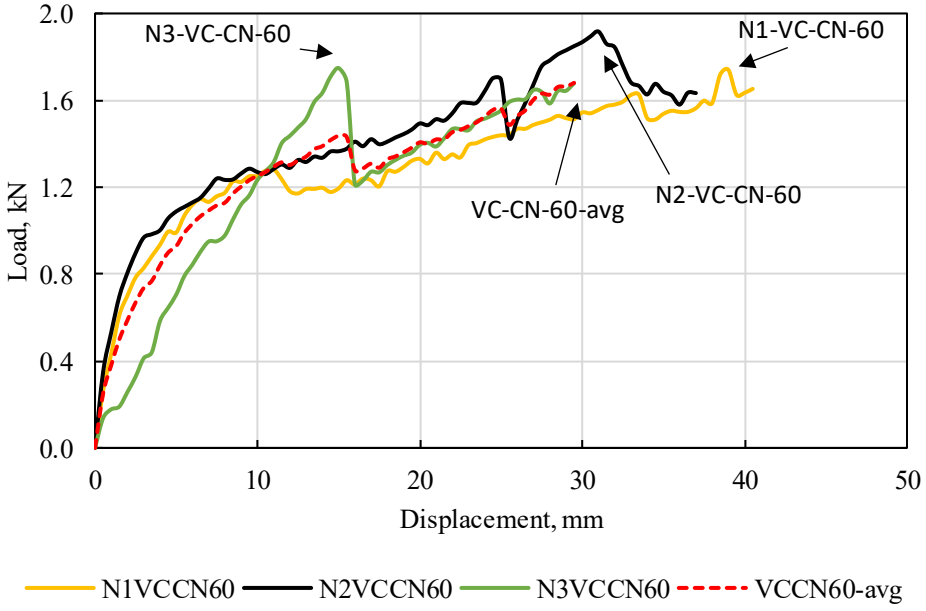

Figure A- 6. Shear response of VC ties, 60 mm embedment length and concrete brick.

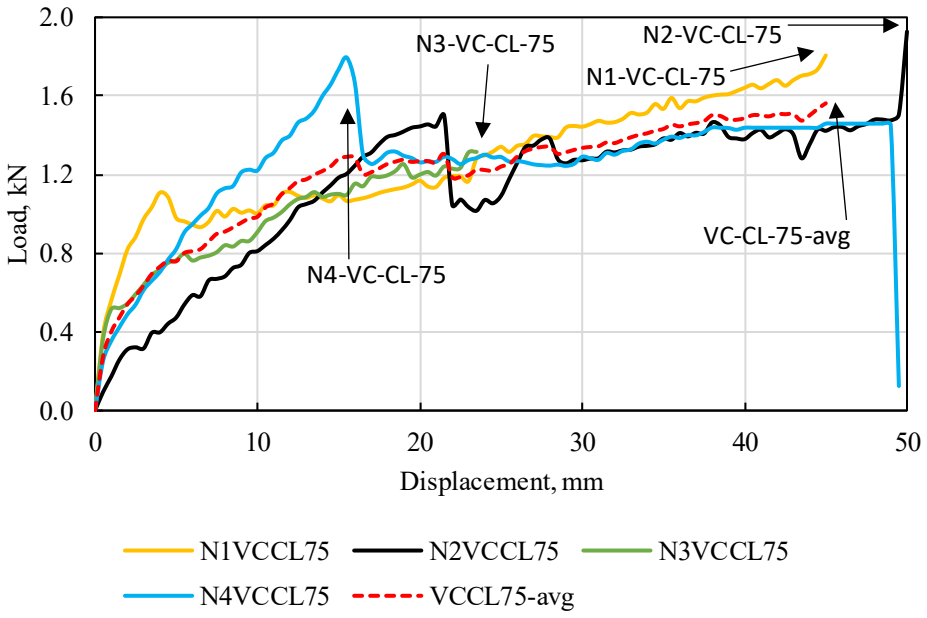

Figure A- 7. Shear response of VC ties, 75 mm embedment length, and clay brick.

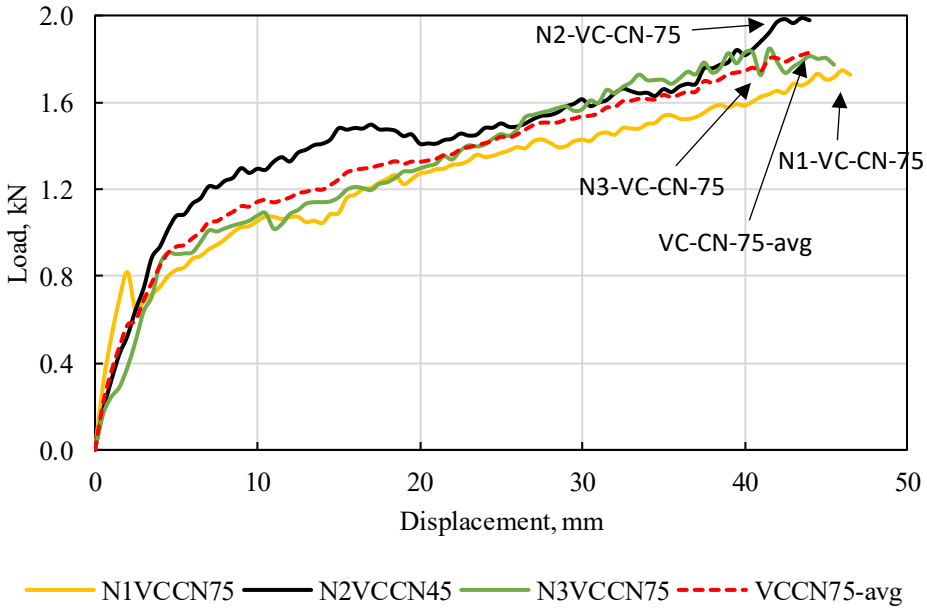

Figure A- 8. Shear response of VC ties, 75 mm embedment length and concrete brick.

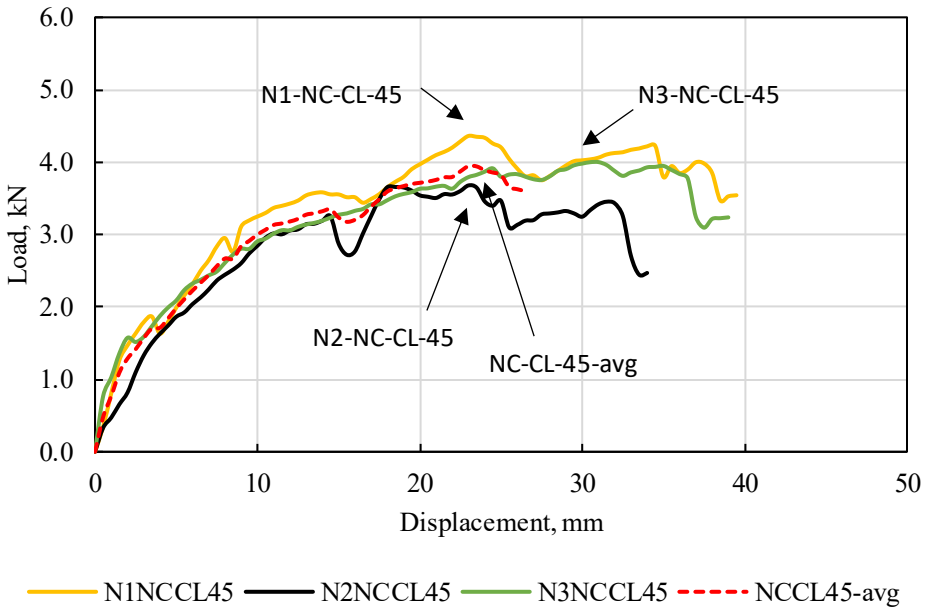

Figure A- 9. Shear response of NC ties, 45 mm embedment length, and clay brick.

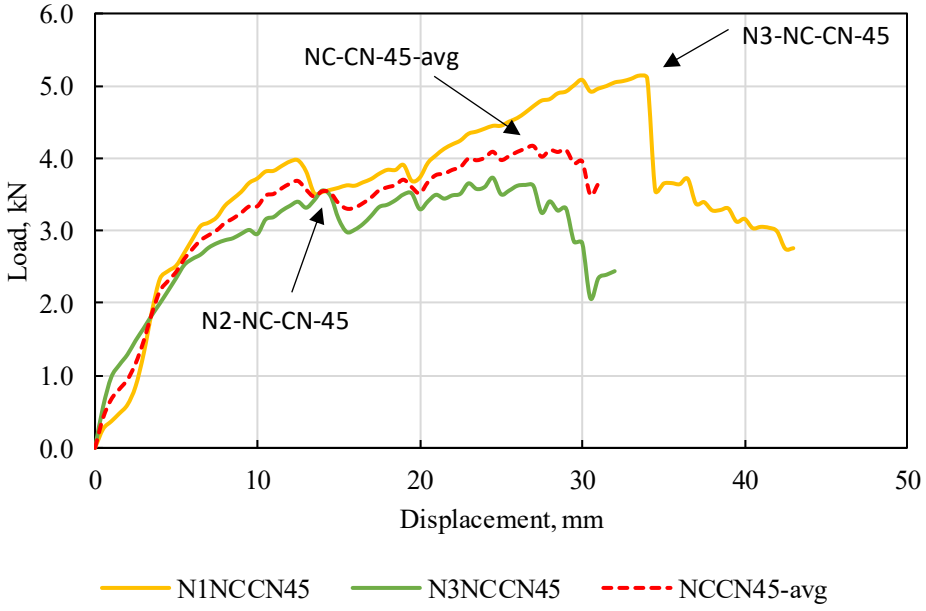

Figure A- 10. Shear response of NC ties, 45 mm embedment length, and concrete brick.

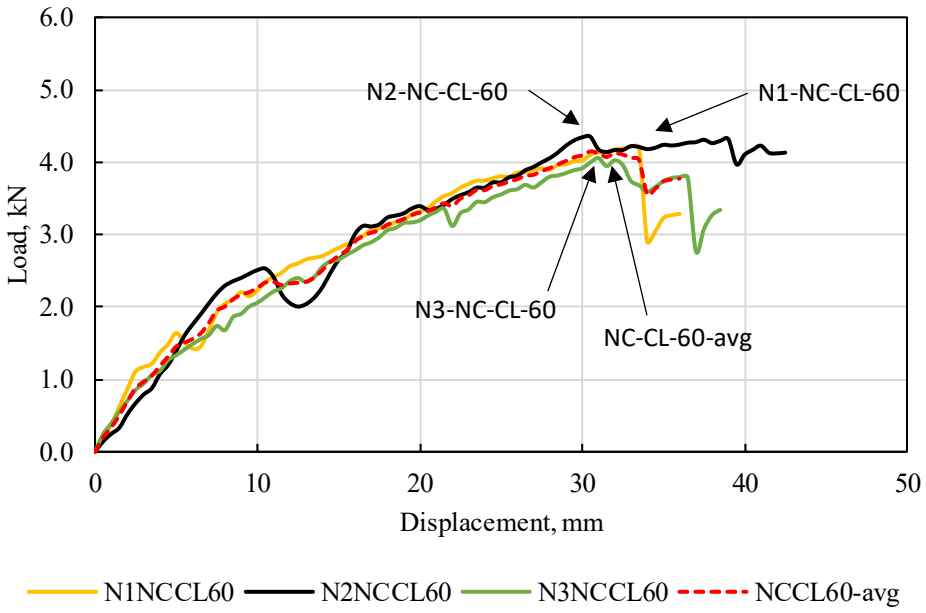

Figure A- 11. Shear response of NC ties, 60 mm embedment length, and clay brick.

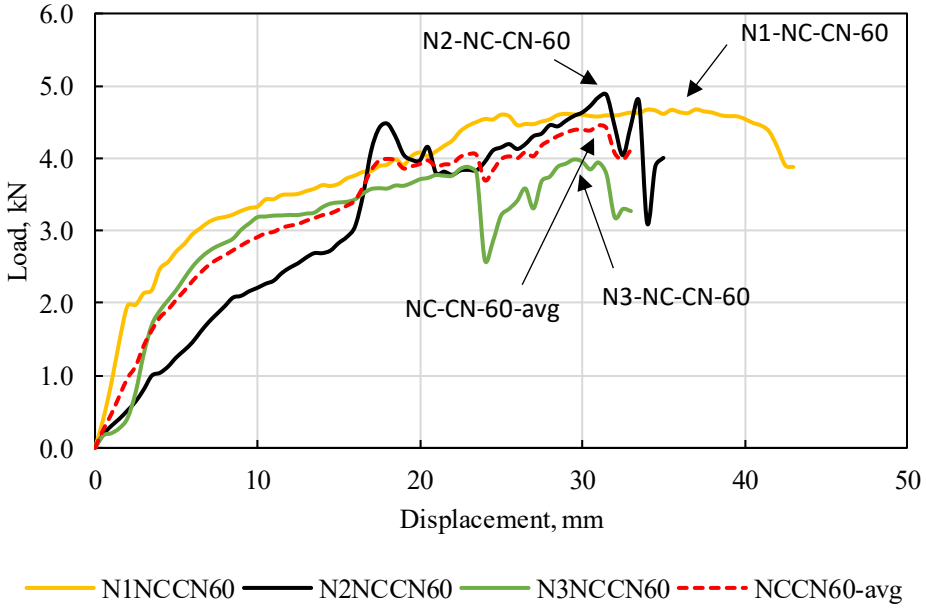

Figure A- 12. Shear response of NC ties, 60 mm embedment length, and concrete brick.

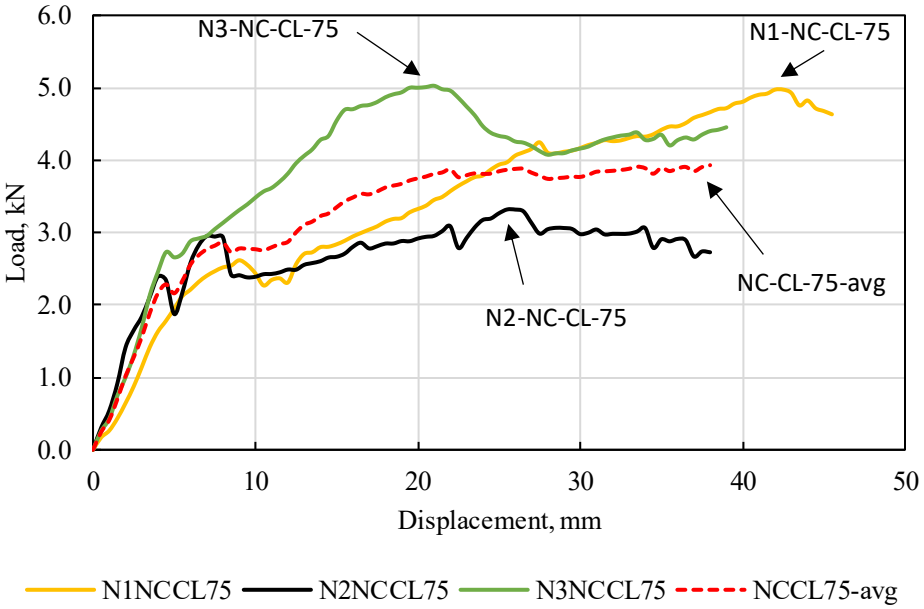

Figure A- 13. Shear response of NC ties, 75 mm embedment length, and clay brick.

APPENDIX B: GUIDE FOR THERMAL MODELLING

The steps to perform a steady-state thermal model simulation using ANSYS Workbench are presented below. The interface of ANSYS Workbench (version 2022 R2) is shown.

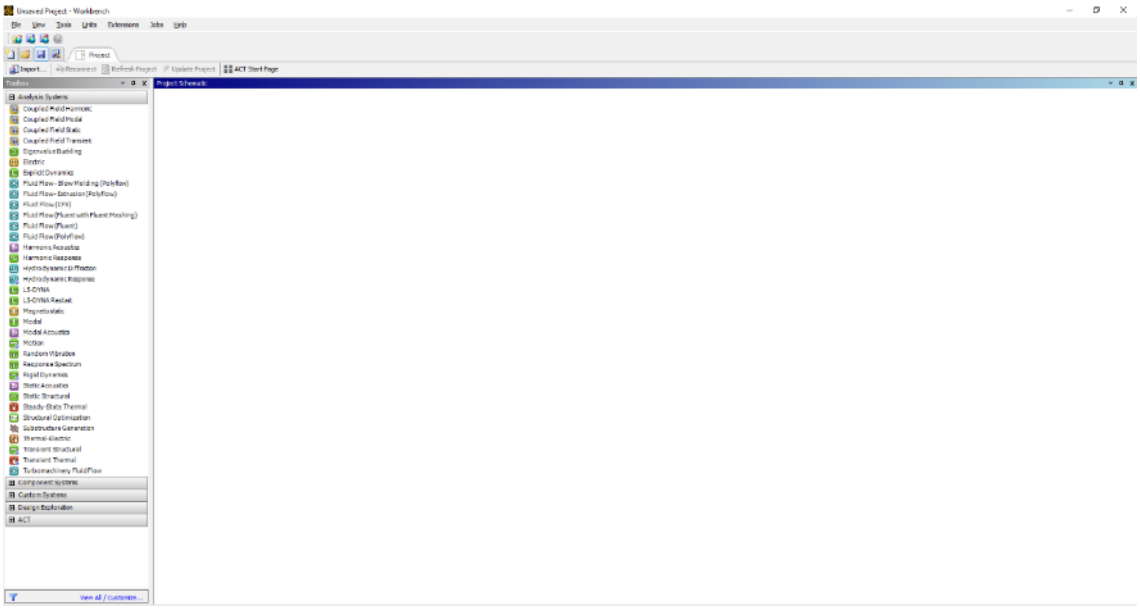

Figure B- 1. ANSYS Workbench 2022 R2 interface.

- Step 1: Create the steady-state thermal analysis.

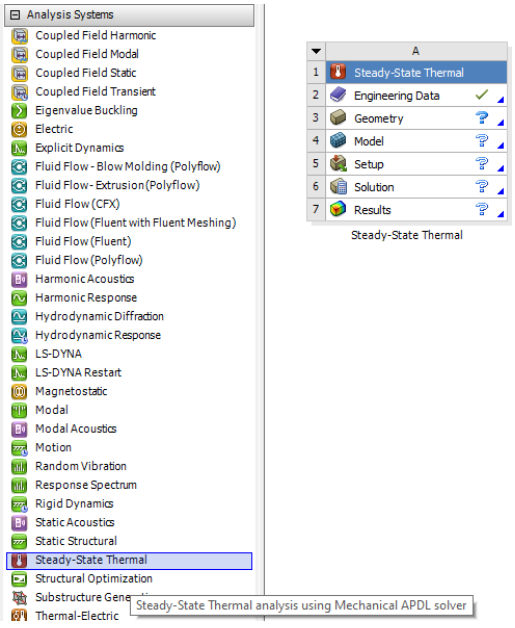

Figure B- 2. ANSYS Workbench steady state menu.

- Step 2: Draw the geometry of the object or assembly.

  The geometry can be drawn in one of the complementary drawing software included in ANSYS (SpaceClaim, DesignModeler, or Discovery). External drawing software can also be used to draw the assembly and then can be imported to the ANSYS file. If an external software is used, it is recommended to save the file as .igs file to avoid incompatibility issues.

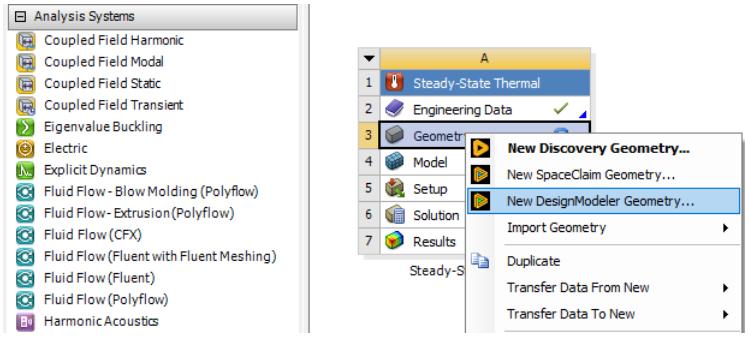

Figure B- 3. ANSYS Workbench geometry menu.

- Step 3: Define the engineering data

  The relevant material property for the steady-state thermal analysis is the thermal conductivity of the material (W/mK). In ANSYS this property is called Isotropic Thermal Conductivity and can be assigned the magnitude in the Engineering Data menu. It is recommended to use the ASHRAE Handbook and the Morrisons Hershfield catalogs to obtain the thermal conductivity of the materials.

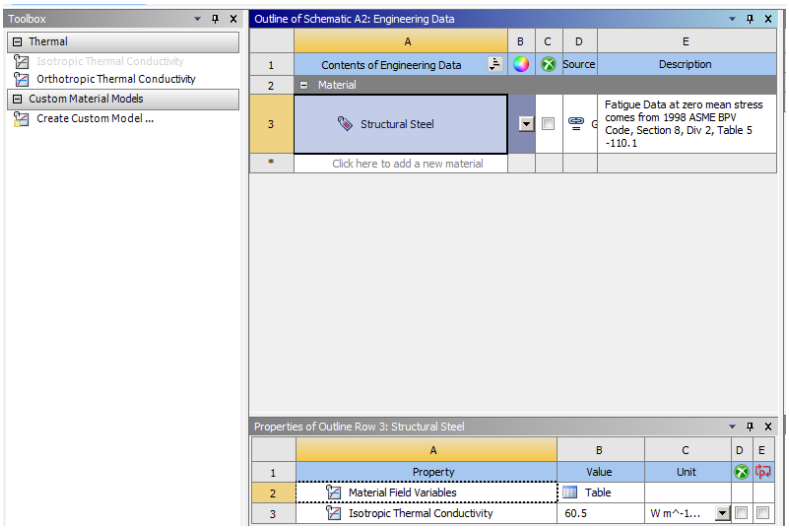

Figure B- 4. ANSYS Workbench Engineering Data menu.

- Step 4: Import or draw the geometry.
- Step 5: Assign the material properties to the geometries.

  It is necessary to access the menu Model and expand the tab Geometry. All the parts that comprise the assembly will be shown and you need to select each part and assign the corresponding material.

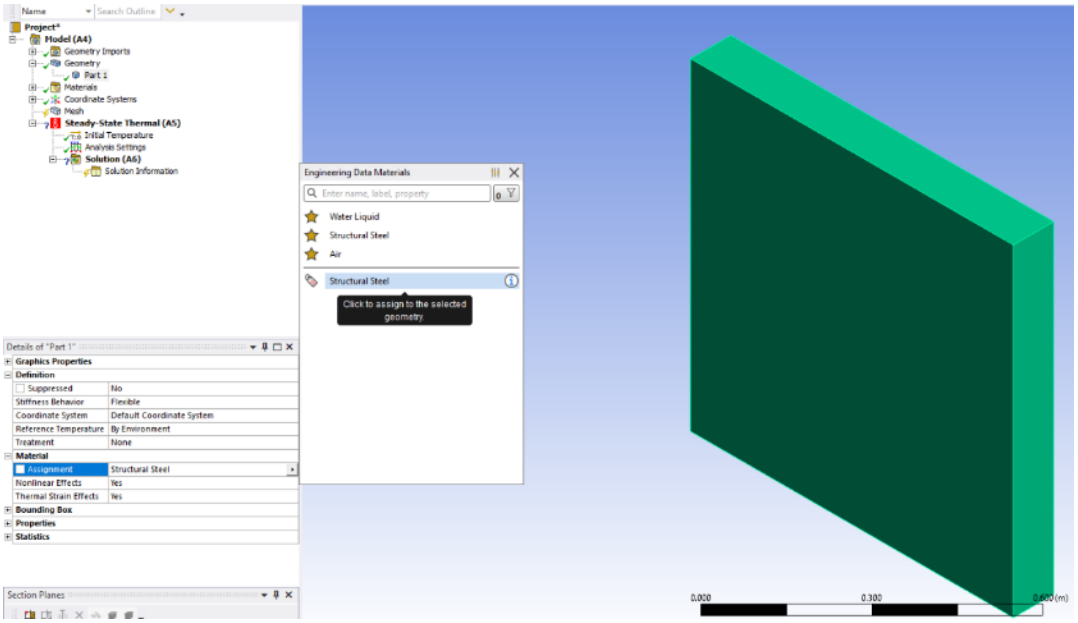

Figure B- 5. ANSYS Workbench Mechanical interface assigning material properties to the geometries.

- Step 6: Create the mesh.

  The mesh is created with a right click in the tab Mesh, then click in Generate Mesh. In the bottom you can edit the mesh properties, such as the size, type of physics and quality.

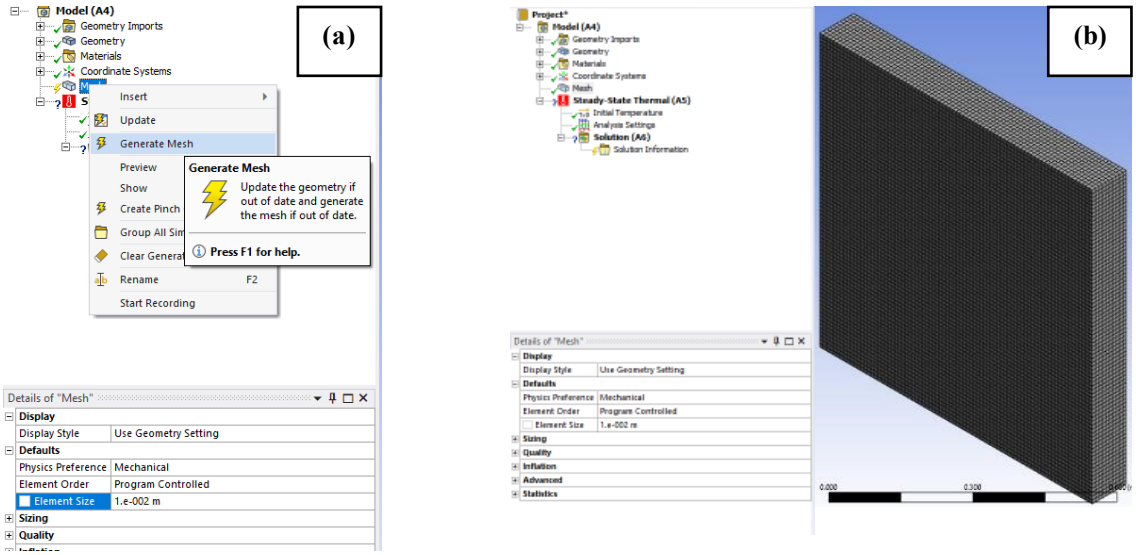

Figure B- 6. ANSYS Workbench Mechanical interface a) generation of mesh, and b) example of mesh.

- Step 7: Define the boundary conditions.

  To calculate the R-value of the assembly, two boundary conditions are applied. Two temperature loads in the internal and external faces of the assembly of 22 ºC and -18 ºC, respectively.

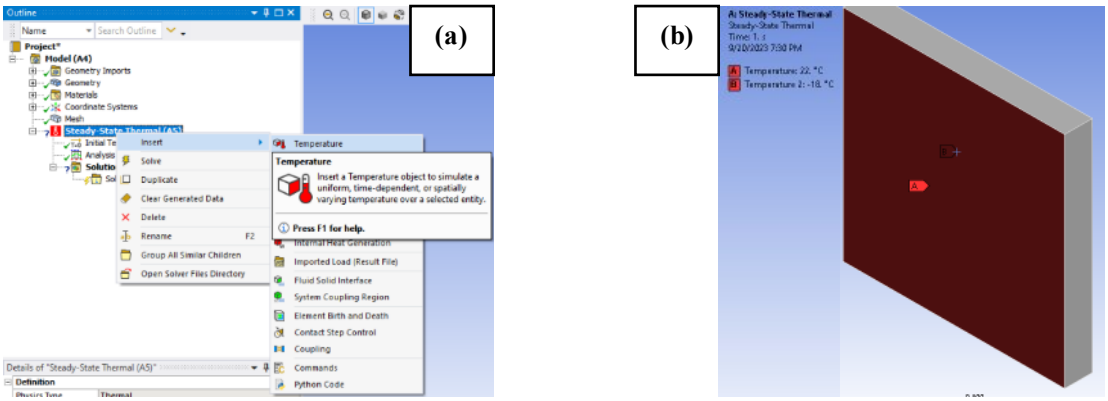

Figure B- 7. ANSYS Workbench Mechanical interface a) creation of temperature load, and b) example of loads applied in the object.

- Step 8: Create the solutions.

  We are interested in the Temperature solution to show the temperature distribution along the assembly. Additionally, we are interested in the Total Heat Flux solution to obtain the average total heat flux in the external face of the assembly.

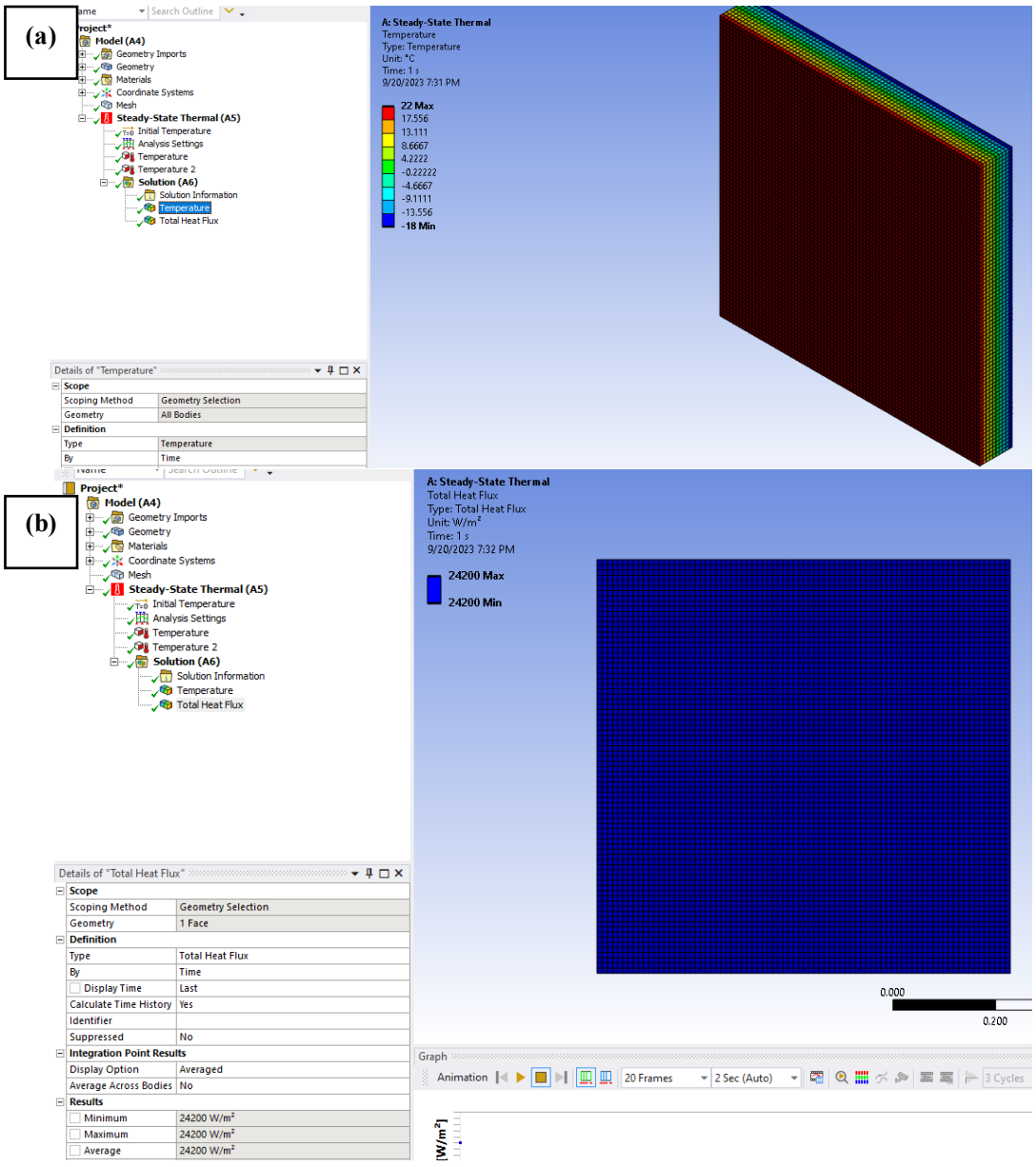

Figure B- 8. ANSYS Workbench Mechanical interface results: a) temperature distribution, and b) total heat flux.

- Step 9: Calculate the R-value.

  To calculate the R-value of the assembly the Equation 5-8 is used. R is the R-value (m^2K/W), ΔT is the difference in temperature across the specimen´s surface $[22-(-18)]$ (ºC), Q is the average total heat flux through the specimen´s area obtained by ANSYS (W/m^2).

Examples of R-value Calculation Using ANSYS:

a. R-value of a single element

The calculation of the R-value of the single layer of insulation material shown in Fig. 5-14 is shown bellow. The temperature loads are 22 and -18 °C, as shown in Fig. 5-18b. The heat flux density of the assembly (Q) obtained by ANSYS is 1.36 W/m^2. To calculate the R-value, the Equation 5-9 is used and the value obtained is 29,41 m^{2}K/W.

$$\Delta T = 22 - (-18)) = 40\ °\text{C}$$

$$Q = 1.36\ W/\text{m}^2$$

$$R = \frac{40}{1.36} = 29.41\ \text{m}^2 K/W$$

To validate this value, the theoretical calculation is presented. The material used is insulation with a thickness of 100 mm and the thermal conductivity is 0.0034 W/mK. The theoretical R-value is obtained as the thickness over the thermal difference betwe en obtained is 29,41 with an error of 0.0%, as shown bellow.

$$k = 0.0034\ W/\text{m}K$$

$$t = 0.1\ m$$

$$R = \frac{0.1}{0.0034} = 29.41\ \text{m}^2 K/W$$

$$Error\% = \frac{29.41 - 29.41}{29.41} = 0.00\%$$

b. R-value of an assembly comprised of multiple layers

In this example the R-value of an assembly comprised of the following materials: an exterior layer (10 mm), veneer layer (90 mm), air space (25 mm), insulation (150 mm), CMU layer (190 mm) and an interior layer (10 mm) with the thermal conductivities shown in Table 5-1. The same process is followed to calculate the R-valuse using ANSYS Workbench. First, create the objects, assign the thermal conductivities and then create the mesh (Fig. 5-18a). The boundary conditions are established by applying the thermal loads in the internal and external faces of 22 and -18 °C, respectively (Fig. 5-18b). Finally, the results of thermal distribution and total heat flux are created (Fig. 5-18cd).

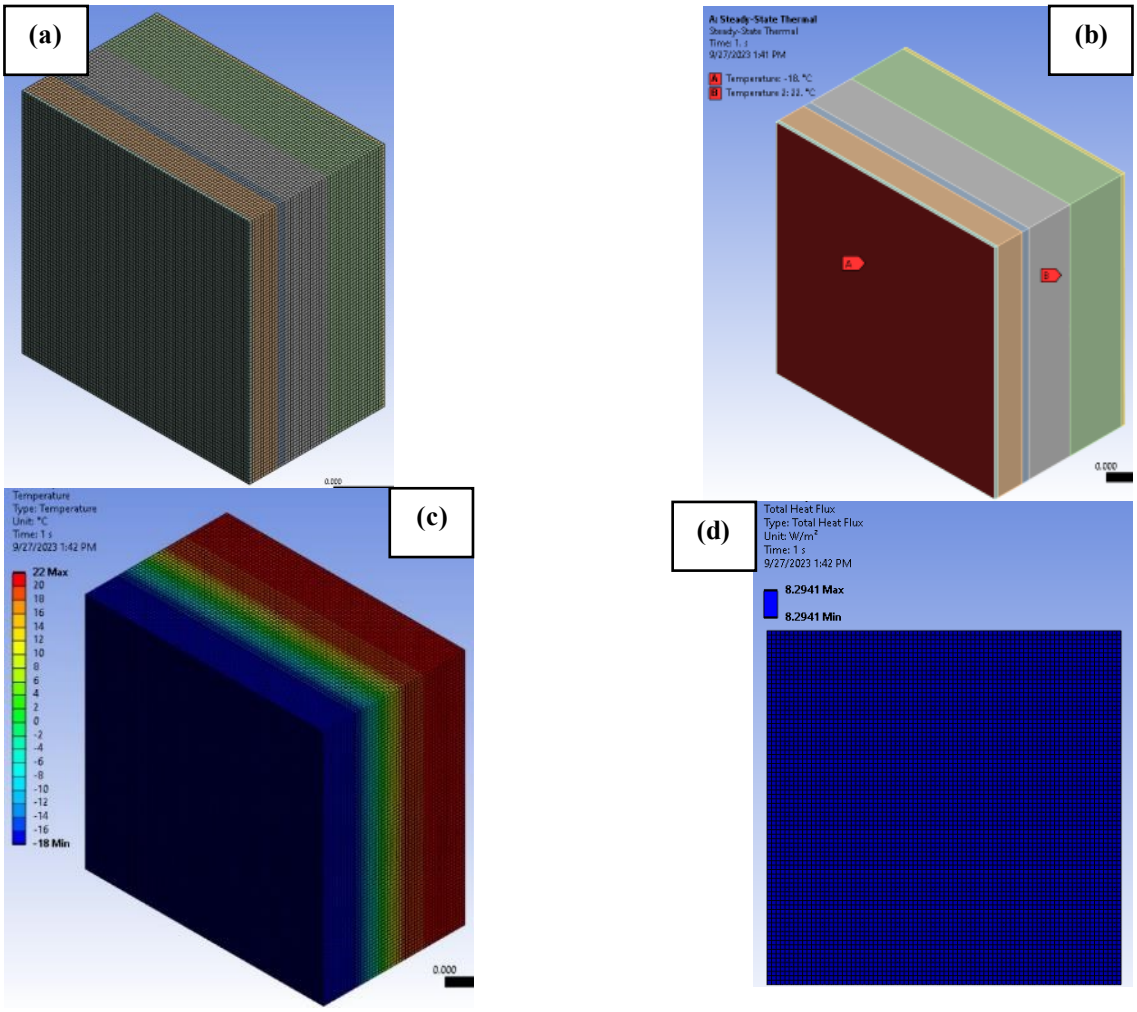

Figure B- 9. R-value calculation in multilayer assembly: a) mesh, b) boundary conditions, c) thermal distribution, and d) total heat flux in the external face.

The heat flux density of the assembly (Q) obtained by ANSYS is 8.29 W/m^2. To calculate the R-value, Equation 5-9 is used and the value obtained is 4.82 m^{2}K/W.

$$R = \frac{40}{8.29} = 4.82\ \mathrm{m}^2 K/W$$

To validate this value, the theoretical calculation is presented. The theoretical R-value is calculated as the sum of the thickness of each layer over the respective thermal conductivity of the layer. The theoretical R-value was 4.82 m$^2K/W$ with an error of 0.02%, as shown below.

$$R = \frac{0.01}{0.129} + \frac{0.09}{0.8} + \frac{0.025}{0.18} + \frac{0.15}{0.036} + \frac{0.19}{0.72} + \frac{0.01}{0.16} = 4.82 \text{ m}^2K/W$$

$$Error\% = \frac{4.82 - 4.82}{4.82} = 0.02\%$$